UC San Diego
UC San Diego Electronic Theses and Dissertations

Title

Probing Aerosol Mixing State and Composition via Direct Hygroscopicity Measurements of Highly-Representative, Laboratory-Generated Sea-Spray Aerosol

Permalink

https://escholarship.org/uc/item/08z7x48j

Author

Schill, Steven Robert

Publication Date

2017

Peer reviewed|Thesis/dissertation

UNIVERSITY OF CALIFORNIA, SAN DIEGO

Probing Aerosol Mixing State and Composition *via* Direct Hygroscopicity Measurements of
Highly-Representative, Laboratory-Generated Sea-Spray Aerosol

A dissertation submitted in partial satisfaction of the requirements for the degree of Doctor of
Philosophy

in

Chemistry

by

Steven Robert Schill

Committee in charge:

      Professor Nathan C. Gianneschi, Chair
      Professor Timothy H. Bertram, Co-Chair
      Professor Judy E. Kim
      Professor Katja Lindenberg
      Professor Lynn M. Russell

2017

The Dissertation of Steven Robert Schill is approved, and is acceptable in quality and form for publication on microfilm and electronically:

_____

_____

_____

_____

Co-Chair

_____

Chair

University of California, San Diego

2017

iii

DEDICATION

To my wife, Megan – thank you for your support, encouragement, and for teaching me what it

means to be loved unconditionally. This would never have happened without you.

EPIGRAPH

"Love must be sincere. Hate what is evil; cling to what is good. Be devoted to one another in love. Honor one another above yourselves. Never be lacking in zeal, but keep your spiritual fervor, serving the Lord. Be joyful in hope, patient in affliction, faithful in prayer. Share with the Lord's people who are in need. Practice hospitality.

Bless those who persecute you; bless and do not curse. Rejoice with those who rejoice; mourn with those who mourn. Live in harmony with one another. Do not be proud, but be willing to associate with people of low position. Do not be conceited.

Do not repay anyone evil for evil. Be careful to do what is right in the eyes of everyone. If it is possible, as far as it depends on you, live at peace with everyone. Do not take revenge, my dear friends, but leave room for God's wrath, for it is written: 'It is mine to avenge; I will repay,' says the Lord.

On the contrary: If your enemy is hungry, feed him; if he is thirsty, give him something to drink. In doing this, you will heap burning coals on his head. Do not be overcome by evil, but overcome evil with good."

Romans 12:9-21, NIV

TABLE OF CONTENTS

LIST OF FIGURES

LIST OF TABLES

ACKNOWLEDGEMENTS

I would like to thank Timothy Bertram, my research advisor, for all of his support, encouragement, and mentorship during my time in his group. I am particularly thankful for the opportunity to move to Madison and explore new and exciting places, and for the encouragement to work with NASA for multiple summers. These experiences will stay with me for the rest of my life.

I would also like to thank all of the members of the Bertram Group, both at UCSD (Olivia, Katy, Matt, Nicole, Timia, and Michelle) and at UW (James, Gordon, Sean, Michael, Avi, and Tom) for all of their help with lab mini-intensives and field campaigns, and for all of the laughs along the way. Graduate school would have been a very different experience without you all!

To my fellow CAICE graduate students (Sara, Holly, Elias, and Doug), collaborators (Chris Cappa, Alexei Tivanski, and Betsy Stone) and CAICE management (Kim Prather and Vicki Grassian), thank you for your invaluable expertise and support, and for pushing me to broaden and deepen my graduate school experience.

Thank you to Emily Schaller and NSRC for the chance to work with NASA SARP and all of the fantastic undergraduate research students they recruit. This truly unique program had a huge impact on my graduate studies and career path, and I genuinely enjoyed being a part of it.

To my Life Group, and the entire CM team at Blackhawk Church, thank you all for being so genuinely interested in what I do and for the much appreciated perspective on the bigger picture. I feel so lucky to have shared my time in Madison with you.

To my family and friends, thank you for the countless ways you have supported me by asking questions about my work, showing up to my presentations, and trying to convince your coworkers to read my papers. Your love and support have been the exact opposite of "nascent".

Lastly, to my wife, Megan, words cannot express how much I have truly loved sharing this experience with you. Your strength in encouraging me to keep going, confidence in moving across country with me (twice), and love in how you support me on a daily basis are shining testaments to the kind of woman you are. You are my favorite person, my best friend, and the only one I want to do life with. This accomplishment is just as much yours as it is mine. I love you.

Chapter 4, in full, is currently being prepared for submission of the material to *Environmental Science and Technology*: Steven R. Schill, Susannah M. Burrows, Elias S. Hasenecz, Elizabeth M. Stone, and Timothy H. Bertram. The dissertation author was the primary investigator and author of this material.

Chapter 5, in part, is a reformatted reprint of the material as it appears in *Atmospheric Measurement Techniques*: M. Dale Stokes, Grant Deane, Douglas B. Collins, Christopher Cappa, Timothy Bertram, Abigail Dommer, Steven Schill, Sara Forestieri, Mathew Survilo (2016) A miniature Marine Aerosol Reference Tank (miniMART) as a compact breaking wave analogue *Atmos. Meas. Tech.* 9, pp 4257-4267, doi: 10.5194/amt-9-4257-2016. The dissertation author was a co-author of this work. Also presented is unpublished, preliminary work concerning potential future directions for applications of SR-CCN measurements.

VITA

2009	Research Experience for Undergraduates Participant Department of Chemistry & Biochemistry California State University, Fullerton
2009 – 2011	Howard Hughes Medical Institute Undergraduate Research Scholar Department of Chemistry & Biochemistry California State University, Fullerton
2011	Undergraduate Research Assistant Department of Chemical and Biomolecular Engineering The Ohio State University
2011	Bachelor of Science, Chemistry & Mathematics Minor Cum Laude & University Honors California State University, Fullerton
2012	Teaching Assistant Department of Chemistry & Biochemistry California State University, Fullerton
2012 – 2015	Research Assistant Department of Chemistry & Biochemistry University of California, San Diego
2012 – 2013	Teaching Assistant Department of Chemistry & Biochemistry University of California, San Diego
2013 – 2014	San Diego Diversity Fellow Department of Chemistry & Biochemistry University of California, San Diego
2014	Master of Science, Chemistry University of California, San Diego
2014 – 2015	Graduate Student Mentor NASA Student Airborne Research Program
2015 – 2017	Research Intern Department of Chemistry University of Wisconsin, Madison
2017	Doctor of Philosophy, Chemistry University of California, San Diego

PUBLICATIONS

Schill, S. R. and Bertram, T. H. Introduction of a hygroscopicity basis set analysis to probe aerosol mixing state. *In preparation for submission to Atmos. Chem. Phys.* (2017)

Schill, S. R.; Burrows, S. M.; Hasenecz, E. S.; Stone, E. M.; Bertram, T. H. The impact of divalent cations on the enrichment of soluble saccharides in primary sea-spray aerosol. *In preparation for submission to Environ. Sci. Technol.* (2017)

Stokes, M. D.; Deane, G.; Collins, D. B.; Cappa, C.; Bertram, T.; Dommer, A.; Schill, S.; Forestieri, S.; Survilo, M. A miniature Marine Aerosol Reference Tank (miniMART) as a compact breaking wave analogue. *Atmos. Meas. Tech.*, 2016, 9, 4257–4267

Schill, S. R.; Collins, D. B.; Lee, C.; Morris, H. S.; Novak, G. A.; Prather, K. A.; Quinn, P. K.; Sultana, C. M.; Tivanski, A. V.; Zimmermann, K.; Cappa, C. D.; Bertram, T. H. The Impact of Aerosol Particle Mixing State on the Hygroscopicity of Sea Spray Aerosol. *ACS Cent. Sci.*, 2015, 1, 132-141

FIELDS OF STUDY

Major Field of Study: Chemistry (Atmospheric & Analytical Chemistry)

ABSTRACT OF THE DISSERTATION

Probing Aerosol Mixing State and Composition *via* Direct Hygroscopicity Measurements of
Highly-Representative, Laboratory-Generated Sea-Spray Aerosol

by

Steven Robert Schill

Doctor of Philosophy in Chemistry

University of California, San Diego, 2017

Professor Nathan Gianneschi, Chair

Professor Timothy Bertram, Co-Chair

Aerosol particles impact global climate in large part by acting as cloud condensation nuclei (CCN) and seeding cloud formation events in the atmosphere, which alters the Earth's albedo. The cloud formation ability of aerosol particles is determined by their water uptake tendencies, which is defined by their chemicophysical properties. Detailed composition information, such as the distribution of chemical components within the particles know as mixing

state, is therefore essential for assessing the impact of aerosols on climate. To date, such information remains elusive for small (< 50 nm) particles due to a paucity of high throughput analytical measurement techniques.

In this dissertation, I describe advances in the development and application of novel methodologies for probing aerosol mixing state and composition *via* direct hygroscopicity measurements of highly-representative, laboratory-generated sea-spray aerosol.

First, I developed a generalizable basis set analysis to establish direct measurements of aerosol hygroscopicity as a high-throughput and robust technique to extract mixing state information for small particles. Second, I constrained the basis set analysis with measurements of pure chemical mimics in a laboratory setting to probe the sensitivity and recovery efficiency of chemically diverse models, and then applied the analysis to complex laboratory and ambient field data to quantify the diversity in composition, according to hygroscopicity. Third, I utilized traditional SR-CCN measurements to validate a proposed mechanism by which soluble organics in the ocean are enhanced in resulting sea-spray aerosols (SSA).

Chapter 1   Introduction

1.1   Aerosol Particles in the Atmosphere

Aerosol particles, defined as any solid or liquid suspended in a gas phase, are present in Earth's atmosphere and impact the environment by altering visibility, air quality, and the radiation budget, which is important for global climate.[1] There are many different types of aerosols and they come from a variety of sources, including natural (e.g. biomass burning, dust storms, marine sea spray) and anthropogenic (e.g. fuel emissions, industrial processes) sources. Aerosols are removed from the atmosphere through dry (depositing onto a surface) or wet (inclusion into a cloud) deposition, and can also coagulate with other particles, react with trace gases, and take up water from their surroundings. The fate of aerosols in the atmosphere is determined by their chemicophysical properties, such as size, composition, and morphology, as these govern their ability to undergo a wide array of atmospheric processes.[2]

Primary aerosol are often emitted directly via a mechanical production mechanism, such as wave breaking in the ocean or mineral dust storms, whereas secondary aerosol are formed by gas-to-particle conversions, and are more common to areas characterized by high concentrations of volatile organic compounds.[3, 4] Both primary and secondary aerosol can vary significantly in composition and morphology, which impacts their chemical reactivity and water uptake properties, but their atmospheric lifetime is more directly affected by their size.

Particles can be categorized into four size modes, as shown in Fig. 1.1: nucleation (< 0.01 μm), Aitken ($0.01 - 0.10$ μm), accumulation ($0.10 - 2.5$ μm), and coarse (> 2.5 μm). Depending on the chemicophysical properties of the particles, as well as the meteorological conditions of their surroundings, aerosol lifetimes in the atmosphere can range from hours to weeks.[5, 6] Particles in the nucleation and Aitken modes grow via coagulation or water uptake on the order of seconds to minutes, with Aitken mode particles being particularly important to the formation of cloud droplets. Coarse mode particles are removed via deposition on the order of minutes to

hours, whereas particles in the accumulation mode are characterized by much longer lifetimes, on the order of days to weeks. These four classes are often referred to operationally as coarse (> 2.5 μm), and fine (< 2.5 μm) or ultrafine (< 0.10 μm) particles, particularly in the health sciences and environmental regulation communities.
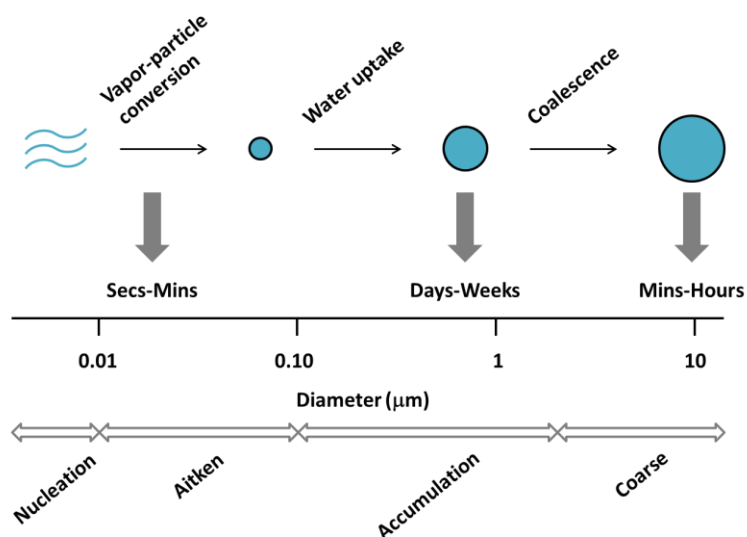
Figure 1.1: Atmospheric aerosol size regions, growth processes, and lifetimes.

1.1.1 Climate Impacts

Aerosols alter Earth's radiation budget by interacting with incoming solar radiation (direct effect) and by forming cloud droplets which alters Earth's albedo (indirect effect)[7], as shown in Fig 1.2.
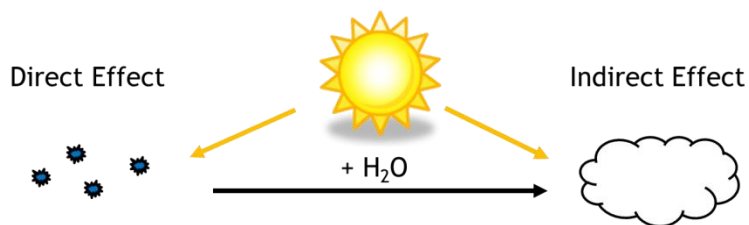
Figure 1.2: Schematic of direct and indirect effect of aerosols on climate.

Particles that seed cloud formation events are referred to as cloud condensation nuclei (CCN), and their efficiency as CCN is dependent on their water uptake properties and contributes to governing the microphysical and optical properties of clouds.[8-10] Although aerosol-cloud interactions are known to have a net cooling effect on global climate, these interactions are complex and are also associated with the largest amount of uncertainty[1] to the current understanding of the Earth's radiation budget. It is generally understood that the cloud forming potential of aerosols is related to their composition and size,[11] and a number of field studies have had success in characterizing these properties for particles in terrestrial,[12, 13] marine,[14-16] and urban environments.[11, 17, 18] What is more difficult to assess, and therefore remains unclear, is how the cloud forming potential of entire aerosol populations compares to that of the individual particles, particularly for populations with a large degree of chemical heterogeneity, and under what conditions particle-particle variability has a profound effect on the climate impacts of the entire population.

1.1.2   Aerosol Mixing State

Individual aerosols can be distinguished from the population at large based on how chemical components are distributed in the particles, which is called the aerosol mixing state. Aerosols are considered internally mixed if there is a single, representative composition, meaning that any one particle has the same composition as all others in the population. Conversely, externally mixed aerosols exhibit particle-particle variability, for example where some particles are more salt-like and others are enriched in organics. Many conventional techniques to measure aerosol composition utilize spectroscopy[14, 19-21] or mass spectrometry[22-25] to detect the presence of various chemical components, but it can be difficult to extract detailed information about the distribution of components within the particles. Studies that have extracted mixing state information typically utilize various microscopy methods[26-28] and require collection of particles

for offline analysis, often exposing particles to harsh environments, such as high-vacuum conditions. For these reasons, it can be exceedingly difficult to measure mixing state directly, and there remains a paucity of methods for obtaining mixing state information in real time.

1.2 Sea Spray Aerosols (SSA)

One of the largest and most chemically complex natural sources of primary aerosol to the atmosphere is the ocean systems which cover more than 70% of the Earth's surface.[29, 30] Wind-driven breaking waves at the surface of the ocean are responsible for producing sea-spray aerosol (SSA), which were historically thought to be comprised entirely of salt due to the high saline concentration (500 mM)[31, 32] of the ocean. Interestingly, SSA exhibit increasing organic content with decreasing particle size, in excess of 80% by volume for sub-40 nm aerosols,[33, 34] which is a result of the production mechanism by which they are generated. The identity of organic compounds within SSA is wide-ranging, including aliphatic compounds (lipids, esters) in the northeastern Atlantic,[35] hydrocarbons (alcohols, alkanes, amines) off the coast of California,[36] and functionalized organics (CHO, CHNO, CHOS) from the south Atlantic in the Angola Basin.[37, 38] The dissolved organic carbon (DOC) in the ocean is similarly diverse, containing saccharides, proteins, and lipids,[39, 40] which result in large part from biological activity. It is understood that organic compounds in the ocean, particularly those enriched at the surface in what is referred to as the sea surface micro layer (SSML),[41, 42] impact the composition of SSA, but the complexities of how these compounds are transferred from the bulk ocean and the SSML to the aerosol phase are poorly understood.

1.2.1 Production Mechanism

The production mechanism for SSA plays a critical role in SSA composition. Breaking waves are generated at the ocean surface with wind speeds above 5 m-s^{-1} and entrain large

volumes of air into the water column, which creates a distribution of bubble sizes beneath the surface.[43] These bubbles rise to the surface, scavenging organics based on their affinity for an air-liquid interface and transporting them to the surface of the ocean, where the bubbles burst and eject hundreds of film droplets ranging in size from nanometers to micrometers.[44, 45] The size of the bubble, and the corresponding bubble film cap before bursting, determines which compounds are ejected into the aerosol phase. Therefore, SSA composition is dependent on bubble size with, in general, smaller bubbles generating smaller film droplets more enriched in organic compounds, and larger bubbles generating larger jet droplets that contain inorganics (Fig. 1.3). This can also be altered by the presence of surfactants at the ocean surface which act to stabilize bubble film caps,[46] increasing their lifetime and impacting the bursting dynamics of adjacent bubbles. For this reason, the composition of the SSML has a direct impact on SSA production and composition.
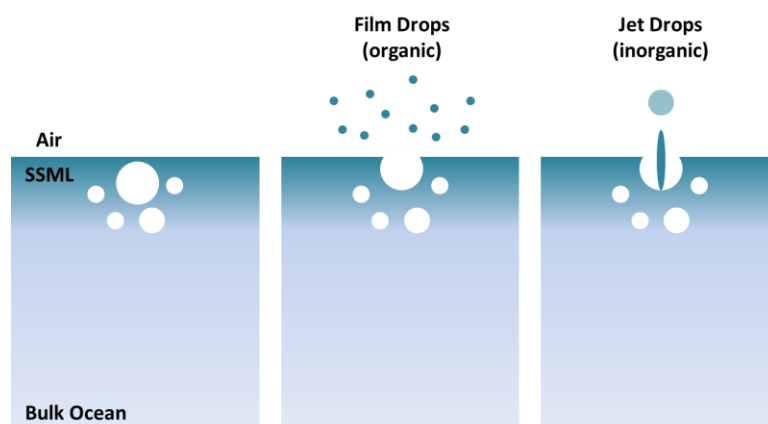
Figure 1.3: Generation of film vs. jet droplets via the bubble bursting production mechanism of marine SSA.

A major contributor to the surface organic pool is local biological activity, such as phytoplankton blooms, which is responsible for dramatic increases in organic carbon.[47] It is important to note, however, that the relationship between biological productivity and SSA

composition is complex, and a direct correlation between the two remains elusive. For example, one mesocosm experiment by Wang et al.[48] that sampled highly representative, laboratory-generated SSA from a wave channel in which a large-scale phytoplankton bloom was produced showed that changes in aerosol properties could be correlated to changes in biological activity. However, ambient field measurements by Quinn et al.[16] of aerosol cloud formation potential in the north Atlantic showed little variability between oligotrophic and biologically productive waters. This highlights the complexities of the production mechanism and the resulting SSA composition, and demonstrates the need for direct measurement of aerosol composition and mixing state to better understand the climate impacts.

1.2.2   Importance for Global Climate

Marine SSA are uniquely important for global climate because, in addition to their characteristic chemical complexity, they are naturally abundant at sizes ideal for CCN. Number-weighted size distribution measurements of marine SSA generated by wave breaking processes demonstrate that the dominant mode is centered at approximately 100 nm,[33] which suggests that the major component (by number) of SSA production are likely to impact climate via cloud formation. It should be noted that this interpretation is specifically for nascent or freshly emitted SSA, though ambient SSA are known to undergo atmospheric processing[28, 49] and serve as surfaces for heterogeneous reactions with an array of trace gases.[50-52]

The formation of optically thick clouds generally increases the albedo of the Earth and contributes to a net cooling effect of aerosols to global climate. For the specific case of SSA, this effect is enhanced, because increases in albedo over ocean systems (which absorb much of the incoming solar radiation to which they are exposed) are more dramatic relative to terrestrial regions where radiation is both absorbed and reflected. This highlights the potentially outsized impact of marine SSA on the Earth's radiation budget.

1.3   Hygroscopicity

The water uptake properties of atmospheric aerosols determine the phase state of the particle, which is important for reactivity, but also characterizes the ability of the aerosol to act as a CCN and grow into a cloud droplet. This water uptake capacity depends largely on particle size and composition, and the quantitative metric used to describe it is defined as hygroscopicity. Measurements of aerosol hygroscopicity are often difficult to make and interpret as they usually compare particle growth or water accommodation to some arbitrary reference state.[11] Additionally, while there are a variety of techniques used to measure hygroscopicity there is a lack of clarity in how to directly compare results from varying techniques.

1.3.1   Köhler Theory

One approach for quantitatively characterizing droplet growth due to water uptake is to use Köhler Theory,[53] which relates droplet radius (r) to the water vapor pressure of the surrounding environment (e/e$_s$), as shown in Equations 1.1-3, using the liquid-vapor surface tension (σ_{lv}), density (ρ_l), and molecular weight (M$_w$) of pure water, the universal gas constant (R), the system temperature (T), and the Van't Hoff factor (i) and number of moles (n$_s$) of solute in the original aerosol seed particle.

$$\frac{e(r,n_s)}{e_s} = \exp\left(\frac{a}{r}\right)\left(1 - \frac{b}{r^3}\right) \qquad \text{(E 1.1)}$$

$$a = \frac{\sigma_{lv}}{\rho_l RT} \qquad \text{(E 1.2)}$$

$$b = \frac{3iM_w n_s}{4\pi\rho_l} \qquad \text{(E 1.3)}$$

Köhler Theory combines two competing effects: the decrease in water accommodation due to increased surface tension in smaller droplets (Kelvin Effect), and the increase in water accommodation due to the presence of soluble material in the seed particle (Raoult Effect). The

resulting phenomenon is that below a critical water vapor pressure the droplet is in equilibrium with its surroundings, but upon reaching a critical supersaturation the droplet undergoes rapid, uncontrolled growth, as shown in Fig. 1.4. It is important to note that while the overall shape of the Köhler curve is the same for all compounds, the steepness of the curve and magnitude of the critical supersaturation are determined by the size and composition of the aerosol seed particle.
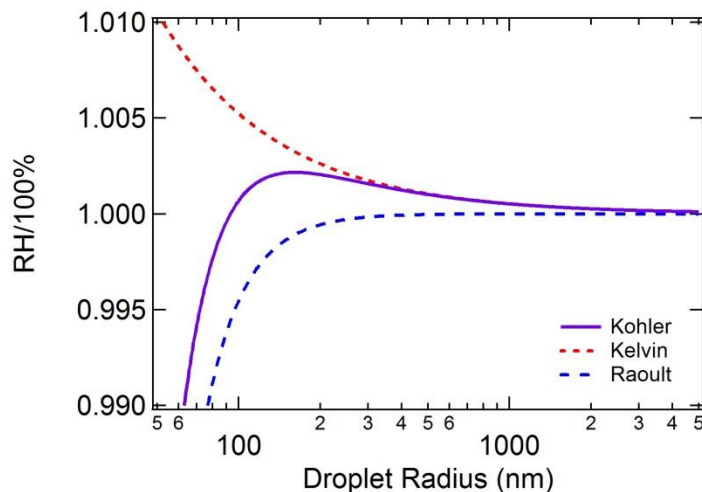
Figure 1.4: A typical Köhler curve for a 30 nm NaCl seed particle.

1.3.2   κ-Köhler Theory

The hygroscopicity of aerosol particles can also be characterized through direct measurements of their ability to activate into droplets, known as their activation efficiency. Such measurements are referred to as size-resolved cloud condensation nuclei (SR-CCN) measurements, and are the primary measurement technique for discussion in this dissertation. The activation efficiency (f_{CCN}) is defined as the fraction of particles of a given size that grow into droplets when exposed to a given water supersaturation (s), as shown in Equation 1.4.

$$f_{CCN}(s) = \frac{\# \, of \, CCN}{\# \, of \, Total \, Particles} \tag{E 1.4}$$

The more hygroscopic a particle is, the larger the activation efficiency at a given particle size and supersaturation. The activation efficiency for particles of fixed composition is also size-dependent, with larger particles having a larger $f_{CCN}(s)$ at a given s. Therefore, particle hygroscopicity is routinely quantitatively characterized by converting direct measurements of a selected particle diameter (D_p) and the critical supersaturation (s_{crit} – where 50% of the particle population has activated) to a single parameter, κ[54], where smaller κ-values correspond to less hygroscopic particles and vice versa. The so-called κ-Köhler theory is simply a reparameterization of Köhler Theory, shown in Equation 1.5, using the wet (D) and dry (D_d) particle diameters, and the liquid-vapor surface tension (σ_{lv}), density (ρ_w), and molecular weight (M_w) of pure water. This effectively separates the intrinsic hygroscopicity (composition-dependence) from the particle size dependence, thereby allowing for assessment of the influence of composition more specifically. Typical values of κ range between $0 - 1.4$, with lower values generally associated with less (or non-) soluble organic compounds, and higher values generally associated with soluble inorganic compounds.[54, 55]

$$S(D) = \frac{D^3 - D_d^3}{D^3 - D_d^3 (1-\kappa)} \exp\left(\frac{4\sigma_{lv}M_w}{RT\rho_w D}\right) \tag{E 1.5}$$

The hygroscopicity parameter of an internal mixture ($\kappa_{mix,int}$) can be estimated from volume-mixing rules, shown in Equation 1.6, where the predicted $\kappa_{mix,int}$ is a function of the volume fraction of the individual components (ε_i) and the κ-value of the pure compounds (κ_i).[54]

$$\kappa_{mix,int} = \sum \varepsilon_i \kappa_i \tag{E 1.6}$$

It is important to note that despite the inherent assumption of internal mixing that this volume mixing rule necessitates, it is commonly used to predict particle composition for externally mixed populations. This is due in large part to the absence of a standardized technique for appropriately accounting for external mixing, which is one area this dissertation will address in the chapters that follow.

1.3.3   Field and Laboratory Measurements

1.3.3.1   Field Measurements

Field studies have proven useful in characterizing water uptake properties for particles in terrestrial,[12, 13] marine,[14-16] and urban environments,[11, 17, 18] but most techniques rely on individual particle analysis, making them prohibitively time- and resource-intensive. More importantly, aerosol collection methods are often limited to characterizing either a broad size range of particles, or an average value over a large time scale. With respect to previous SR-CCN measurements, the current standard for estimating ambient particle composition utilizes the volume mixing rule (E 1.6) and assumes internal mixing, which for many ambient sources is known to be inaccurate. In general, hygroscopicity measurements of ambient aerosols provide constraints on population-average values and can detect changes over a period of days to weeks, but fail to adequately represent the known chemical complexity and particle-particle variability of many aerosols, and this is especially true for marine SSA.

1.3.3.2   Laboratory Measurements

There is an abundance of laboratory SR-CCN studies[54-57] that utilize internal mixtures with model systems of known composition to validate the mixing rule-predicted hygroscopicity (E 1.6). These studies have proven that SR-CCN measurements are effective at determining composition for small particles, assuming that they are internally mixed. However, little work has been done to assess the importance of external mixing or whether SR-CCN measurements can be used to detect it. A small number of previous studies[58, 59] have noted that the SR-CCN activation efficiency spectrum appears to have a different shape between pure model compounds and ambient field measurements, with some preliminary work focusing on the slope of the sigmoid activation curve. The extent to which this has been formalized is shown is Su et al.[59] where a

term known as the "extent of chemical heterogeneity" is defined, with the idea that pure compounds have less heterogeneity and ambient measurements appear to have more. It is important to note, however, that while this value can be provided in addition to a population-average κ-value there currently is no way to incorporate this into, for example, global climate models that currently propagate average κ -values over large geographic regions. There is an obvious need for the development of an analytical toolkit to assess external mixing in a quantitative and generalizable method, which is a major product of this dissertation and focus for the accompanying discussion.

1.4   Summary and Remaining Areas to Address

Aerosol particles play a critical role in determining global climate, particularly because of their ability to act as CCN and alter the Earth's albedo. While it is generally understood that aerosol-cloud interactions contribute a net cooling effect by reflecting incoming solar radiation, there remains great uncertainty surrounding the magnitude of this effect due to a wide range of varied particle sources, chemical complexity associated with particle production mechanisms, and difficulties in quantitatively assessing composition and mixing state of small particles. Despite an abundance of ambient field measurements and laboratory studies with model aerosol systems, aimed at characterizing population average hygroscopicity, critical areas remain to be addressed:

1) Is there additional information from SR-CCN measurements to give additional insight about particle composition, beyond a population-average hygroscopicity parameter? How do we better understand and utilize this data?

2) What is the impact of aerosol mixing state on their climate-relevant properties, namely their ability to act as CCN? Does the consideration of external mixing result in a significantly different interpretation of cloud-active aerosols than the internal mixing

assumption, and, if so, is this relevant to typical atmospheric conditions to which aerosols are exposed?

3) Given the inherent sensitivity of hygroscopicity to aerosol composition, can SR-CCN measurements be used to probe targeted, composition questions, such as details of aerosol production mechanisms?

1.5 Synopsis of Chapters

This dissertation demonstrates the usefulness of hygroscopicity measurements to extract aerosol composition information, including mixing state of small particles, by developing a novel analysis method for SR-CCN measurements of model systems and applying it to a variety of laboratory and field data sets. Specifically, this dissertation seeks to investigate the three unaddressed areas listed above.

Chapter 2 details the design and development of a basis set analysis to use direct measurements of aerosol hygroscopicity as a high-throughput and robust technique to extract mixing state information. This methodology provides a generalizable framework for the analysis of chemically complex systems, and provides additional insight for global climate modeling.

In Chapter 3, the hygroscopicity basis set analysis is applied to a range of model laboratory and ambient field studies to assess the climate impact of aerosol mixing state and the relative importance of this method compared to traditional analysis techniques that assume internal mixing state. It is shown that while accounting for external mixing is most important over a relatively narrow range of aerosol sources and atmospheric conditions, those conditions are responsible for a large fraction of cloud formation processes in the atmosphere.

Chapter 4 demonstrates the sensitivity of traditional SR-CCN measurements to changes in aerosol composition by generating highly representative marine SSA in a laboratory setting and identifying important chemical interactions related to the SSA production mechanism. These

experiments address the important question of how organic compounds can incorporate into marine SSA, and effectively demonstrate the high-throughput nature of the SR-CCN analysis method.

A summary of this dissertation work and a discussion of potential future applications are presented in Chapter 5.

1.6   References

1.   Boucher, O., D. Randall, P. Artaxo, C. Bretherton, G. Feingold, P. Forster, V.M. Kerminen, Y. Kondo, H. Liao, U. Lohmann, P. Rasch, S.K. Satheesh, S. Sherwood, B. Stevens and X.Y. Zhang, *Clouds and Aerosols*, in *Climate Change 2013: The Physical Science Basis. Contribution of Working Group I to the Fifth Assessment Report of the Intergovernmental Panel on Climate Change*. 2013: Cambridge, United Kingdom and New York, NY, USA.

2.   Farmer, D.K., C.D. Cappa, and S.M. Kreidenweis, *Atmospheric Processes and Their Controlling Influence on Cloud Condensation Nuclei Activity.* Chemical Reviews, 2015. **115**(10): p. 4199-4217.

3.   Poschl, U., *Atmospheric aerosols: Composition, transformation, climate and health effects.* Angewandte Chemie-International Edition, 2005. **44**(46): p. 7520-7540.

4.   Facchini, M.C., S. Decesari, M. Rinaldi, C. Carbone, E. Finessi, M. Mircea, S. Fuzzi, F. Moretti, E. Tagliavini, D. Ceburnis, and C.D. O'Dowd, *Important Source of Marine Secondary Organic Aerosol from Biogenic Amines.* Environmental Science & Technology, 2008. **42**(24): p. 9116-9121.

5.   Raes, F., R. Van Dingenen, E. Vignati, J. Wilson, J.P. Putaud, J.H. Seinfeld, and P. Adams, *Formation and cycling of aerosols in the global troposphere.* Atmospheric Environment, 2000. **34**(25): p. 4215-4240.

6.   Williams, J., M. de Reus, R. Krejci, H. Fischer, and J. Strom, *Application of the variability-size relationship to atmospheric aerosol studies: estimating aerosol lifetimes and ages.* Atmospheric Chemistry and Physics, 2002. **2**: p. 133-145.

7.   Aitken, J., *XII.—On Dust, Fogs, and Clouds.* Earth and Environmental Science Transactions of the Royal Society of Edinburgh, 1881. **30**(01): p. 337-368.

8.   Albrecht, B.A., *Aerosols, Cloud Microphysics, and Fractional Cloudiness.* Science, 1989. **245**(4923): p. 1227-1230.

9.   Baker, M.B., *Cloud microphysics and climate.* Science, 1997. **276**(5315): p. 1072-1078.

10.   Twomey, S., *Influence of Pollution on Shortwave Albedo of Clouds.* Journal of the Atmospheric Sciences, 1977. **34**(7): p. 1149-1152.

11.   Crosbie, E., J.S. Youn, B. Balch, A. Wonaschutz, T. Shingler, Z. Wang, W.C. Conant, E.A. Betterton, and A. Sorooshian, *On the competition among aerosol number, size and composition in predicting CCN variability: a multi-annual field study in an urbanized desert.* Atmospheric Chemistry and Physics, 2015. **15**(12): p. 6943-6958.

12.   Lathem, T.L., A.J. Beyersdorf, K.L. Thornhill, E.L. Winstead, M.J. Cubison, A. Hecobian, J.L. Jimenez, R.J. Weber, B.E. Anderson, and A. Nenes, *Analysis of CCN activity of Arctic aerosol and Canadian biomass burning during summer 2008.* Atmospheric Chemistry and Physics, 2013. **13**(5): p. 2735-2756.

13.   Gunthe, S.S., S.M. King, D. Rose, Q. Chen, P. Roldin, D.K. Farmer, J.L. Jimenez, P. Artaxo, M.O. Andreae, S.T. Martin, and U. Poschl, *Cloud condensation nuclei in pristine tropical rainforest air of Amazonia: size-resolved measurements and modeling of atmospheric aerosol composition and CCN activity.* Atmospheric Chemistry and Physics, 2009. **9**(19): p. 7551-7575.

14.   Frossard, A.A., L.M. Russell, S.M. Burrows, S.M. Elliott, T.S. Bates, and P.K. Quinn, *Sources and composition of submicron organic mass in marine aerosol particles.* Journal of Geophysical Research-Atmospheres, 2014. **119**(22): p. 12977-13003.

15.   Zhang, X.L., P. Massoli, P.K. Quinn, T.S. Bates, and C.D. Cappa, *Hygroscopic growth of submicron and supermicron aerosols in the marine boundary layer.* Journal of Geophysical Research-Atmospheres, 2014. **119**(13).

16.   Quinn, P.K., T.S. Bates, K.S. Schulz, D.J. Coffman, A.A. Frossard, L.M. Russell, W.C. Keene, and D.J. Kieber, *Contribution of sea surface carbon pool to organic matter enrichment in sea spray aerosol.* Nature Geoscience, 2014. **7**(3): p. 228-232.

17.   Lance, S., A. Nenes, C. Mazzoleni, M.K. Dubey, H. Gates, V. Varutbangkul, T.A. Rissman, S.M. Murphy, A. Sorooshian, R.C. Flagan, J.H. Seinfeld, G. Feingold, and H.H. Jonsson, *Cloud condensation nuclei activity, closure, and droplet growth kinetics of Houston aerosol during the Gulf of Mexico Atmospheric Composition and Climate Study (GoMACCS).* Journal of Geophysical Research-Atmospheres, 2009. **114**.

18.   Lance, S., T. Raatikainen, T.B. Onasch, D.R. Worsnop, X.Y. Yu, M.L. Alexander, M.R. Stolzenburg, P.H. McMurry, J.N. Smith, and A. Nenes, *Aerosol mixing state, hygroscopic growth and cloud activation efficiency during MIRAGE 2006.* Atmospheric Chemistry and Physics, 2013. **13**(9): p. 5049-5062.

19.   Frossard, A.A., L.M. Russell, P. Massoli, T.S. Bates, and P.K. Quinn, *Side-by-Side Comparison of Four Techniques Explains the Apparent Differences in the Organic Composition of Generated and Ambient Marine Aerosol Particles.* Aerosol Science and Technology, 2014. **48**(3): p. V-X.

20. Frossard, A.A., L.M. Russell, W.C. Keene, D.J. Kieber, P.K. Quinn, and T.S. Bates, *Regional Signatures in the Organic Composition of Marine Aerosol Particles.* Nucleation and Atmospheric Aerosols, 2013. **1527**: p. 543-546.

21. Russell, L.M., L.N. Hawkins, A.A. Frossard, P.K. Quinn, and T.S. Bates, *Carbohydrate-like composition of submicron atmospheric particles and their production from ocean bubble bursting.* Proceedings of the National Academy of Sciences of the United States of America, 2010. **107**(15): p. 6652-6657.

22. Slowik, J.G., D.J. Cziczo, and J.P.D. Abbatt, *Analysis of cloud condensation nuclei composition and growth kinetics using a pumped counterflow virtual impactor and aerosol mass spectrometer.* Atmospheric Measurement Techniques, 2011. **4**(8): p. 1677-1688.

23. Cahill, J.F., T.K. Darlington, C. Fitzgerald, N.G. Schoepp, J. Beld, M.D. Burkart, and K.A. Prather, *Online Analysis of Single Cyanobacteria and Algae Cells under Nitrogen-Limited Conditions Using Aerosol Time-of-Flight Mass Spectrometry.* Analytical Chemistry, 2015. **87**(16): p. 8039-8046.

24. Collins, D.B., D.F. Zhao, M.J. Ruppel, O. Laskina, J.R. Grandquist, R.L. Modini, M.D. Stokes, L.M. Russell, T.H. Bertram, V.H. Grassian, G.B. Deane, and K.A. Prather, *Direct aerosol chemical composition measurements to evaluate the physicochemical differences between controlled sea spray aerosol generation schemes.* Atmospheric Measurement Techniques, 2014. **7**(11): p. 3667-3683.

25. Guasco, T.L., L.A. Cuadra-Rodriguez, B.E. Pedler, A.P. Ault, D.B. Collins, D.F. Zhao, M.J. Kim, M.J. Ruppel, S.C. Wilson, R.S. Pomeroy, V.H. Grassian, F. Azam, T.H. Bertram, and K.A. Prather, *Transition Metal Associations with Primary Biological Particles in Sea Spray Aerosol Generated in a Wave Channel.* Environmental Science & Technology, 2014. **48**(2): p. 1324-1333.

26. Moffet, R.C., R. O'Brien, A.P. Ault, D.B. Collins, M.J. Ruppel, D.Q. Pham, V.H. Grassian, A. Laskin, M.K. Gilles, and K.A. Prather, *Spectromicroscopic observation of sea spray composition and aging.* Abstracts of Papers of the American Chemical Society, 2014. **248**.

27. Ault, A.P., T.L. Guasco, J. Baltrusaitis, O.S. Ryder, J.V. Trueblood, D.B. Collins, M.J. Ruppel, L.A. Cuadra-Rodriguez, K.A. Prather, and V.H. Grassian, *Heterogeneous Reactivity of Nitric Acid with Nascent Sea Spray Aerosol: Large Differences Observed between and within Individual Particles.* Journal of Physical Chemistry Letters, 2014. **5**(15): p. 2493-2500.

28. Ault, A.P., T.L. Guasco, O.S. Ryder, J. Baltrusaitis, L.A. Cuadra-Rodriguez, D.B. Collins, M.J. Ruppel, T.H. Bertram, K.A. Prather, and V.H. Grassian, *Inside versus Outside: Ion Redistribution in Nitric Acid Reacted Sea Spray Aerosol Particles as Determined by Single Particle Analysis.* Journal of the American Chemical Society, 2013. **135**(39): p. 14528-14531.

29.   Warneck, P., *Chemistry of the Natural Atmosphere*. 1988, San Diego, CA: Academic Press.

30.   Woodcock, A.H., *Note concerning human respiratory irritation associated with high concentrations of plankton and mass mortality of marine organisms.* J. Mar. Res., 1948. **7**: p. 56-62.

31.   Keene, W.C., H. Maring, J.R. Maben, D.J. Kieber, A.A.P. Pszenny, E.E. Dahl, M.A. Izaguirre, A.J. Davis, M.S. Long, X.L. Zhou, L. Smoydzin, and R. Sander, *Chemical and physical characteristics of nascent aerosols produced by bursting bubbles at a model air-sea interface.* Journal of Geophysical Research-Atmospheres, 2007. **112**(D21).

32.   Barker, D.R. and H. Zeitlin, *Metal-Ion Concentrations in Sea-Surface Microlayer and Size-Separated Atmospheric Aerosol Samples in Hawaii.* Journal of Geophysical Research, 1972. **77**(27): p. 5076-&.

33.   Prather, K.A., T.H. Bertram, V.H. Grassian, G.B. Deane, M.D. Stokes, P.J. DeMott, L.I. Aluwihare, B.P. Palenik, F. Azam, J.H. Seinfeld, R.C. Moffet, M.J. Molina, C.D. Cappa, F.M. Geiger, G.C. Roberts, L.M. Russell, A.P. Ault, J. Baltrusaitis, D.B. Collins, C.E. Corrigan, L.A. Cuadra-Rodriguez, C.J. Ebben, S.D. Forestieri, T.L. Guasco, S.P. Hersey, M.J. Kim, W.F. Lambert, R.L. Modini, W. Mui, B.E. Pedler, M.J. Ruppel, O.S. Ryder, N.G. Schoepp, R.C. Sullivan, and D.F. Zhao, *Bringing the ocean into the laboratory to probe the chemical complexity of sea spray aerosol.* Proceedings of the National Academy of Sciences of the United States of America, 2013. **110**(19): p. 7550-7555.

34.   Ault, A.P., R.C. Moffet, J. Baltrusaitis, D.B. Collins, M.J. Ruppel, L.A. Cuadra-Rodriguez, D.F. Zhao, T.L. Guasco, C.J. Ebben, F.M. Geiger, T.H. Bertram, K.A. Prather, and V.H. Grassian, *Size-Dependent Changes in Sea Spray Aerosol Composition and Properties with Different Seawater Conditions.* Environmental Science & Technology, 2013. **47**(11): p. 5603-5612.

35.   Facchini, M.C., M. Rinaldi, S. Decesari, C. Carbone, E. Finessi, M. Mircea, S. Fuzzi, D. Ceburnis, R. Flanagan, E.D. Nilsson, G. de Leeuw, M. Martino, J. Woeltjen, and C.D. O'Dowd, *Primary submicron marine aerosol dominated by insoluble organic colloids and aggregates.* Geophysical Research Letters, 2008. **35**(17).

36.   Bates, T.S., P.K. Quinn, A.A. Frossard, L.M. Russell, J. Hakala, T. Petaja, M. Kulmala, D.S. Covert, C.D. Cappa, S.M. Li, K.L. Hayden, I. Nuaaman, R. McLaren, P. Massoli, M.R. Canagaratna, T.B. Onasch, D. Sueper, D.R. Worsnop, and W.C. Keene, *Measurements of ocean derived aerosol off the coast of California.* Journal of Geophysical Research-Atmospheres, 2012. **117**.

37.   Schmitt-Kopplin, P., G. Liger-Belair, B.P. Koch, R. Flerus, G. Kattner, M. Harir, B. Kanawati, M. Lucio, D. Tziotis, N. Hertkorn, and I. Gebefugi, *Dissolved organic matter in sea spray: a transfer study from marine surface water to aerosols.* Biogeosciences, 2012. **9**(4): p. 1571-1582.

38.   Yang, G.P., S. Tsunogai, and S. Watanabe, *Biogeochemistry of dimethylsulfoniopropionate (DMSP) in the surface microlayer and subsurface seawater of Funka Bay, Japan.* Journal of Oceanography, 2005. **61**(1): p. 69-78.

39.   Verdugo, P., *Marine Microgels.* Annual Review of Marine Science, Vol 4, 2012. **4**: p. 375-400.

40.   Callaghan, A.H., G.B. Deane, and M.D. Stokes, *Two Regimes of Laboratory Whitecap Foam Decay: Bubble-Plume Controlled and Surfactant Stabilized.* Journal of Physical Oceanography, 2013. **43**(6): p. 1114-1126.

41.   Burrows, S.M., O. Ogunro, A.A. Frossard, L.M. Russell, P.J. Rasch, and S.M. Elliott, *A physically based framework for modeling the organic fractionation of sea spray aerosol from bubble film Langmuir equilibria.* Atmospheric Chemistry and Physics, 2014. **14**(24): p. 13601-13629.

42.   Cunliffe, M., A. Engel, S. Frka, B. Gasparovic, C. Guitart, J.C. Murrell, M. Salter, C. Stolle, R. Upstill-Goddard, and O. Wurl, *Sea surface microlayers: A unified physicochemical and biological perspective of the air-ocean interface.* Progress in Oceanography, 2013. **109**: p. 104-116.

43.   Quinn, P.K., D.B. Collins, V.H. Grassian, K.A. Prather, and T.S. Bates, *Chemistry and Related Properties of Freshly Emitted Sea Spray Aerosol.* Chemical Reviews, 2015. **115**(10): p. 4383-4399.

44.   Andreae, M.O. and D. Rosenfeld, *Aerosol-cloud-precipitation interactions. Part 1. The nature and sources of cloud-active aerosols.* Earth-Science Reviews, 2008. **89**(1-2): p. 13-41.

45.   Laskina, O., H.S. Morris, J.R. Grandquist, Z. Qiu, E.A. Stone, A.V. Tivanski, and V.H. Grassian, *Size Matters in the Water Uptake and Hygroscopic Growth of Atmospherically Relevant Multicomponent Aerosol Particles.* Journal of Physical Chemistry A, 2015. **119**(19): p. 4489-4497.

46.   Modini, R.L., L.M. Russell, G.B. Deane, and M.D. Stokes, *Effect of soluble surfactant on bubble persistence and bubble-produced aerosol particles.* Journal of Geophysical Research-Atmospheres, 2013. **118**(3): p. 1388-1400.

47.   Kirchman, D.L., Y. Suzuki, C. Garside, and H.W. Ducklow, *High Turnover Rates of Dissolved Organic-Carbon during a Spring Phytoplankton Bloom.* Nature, 1991. **352**(6336): p. 612-614.

48.   Wang, X.F., C.M. Sultana, J. Trueblood, T.C.J. Hill, F. Malfatti, C. Lee, O. Laskina, K.A. Moore, C.M. Beall, C.S. McCluskey, G.C. Cornwell, Y.Y. Zhou, J.L. Cox, M.A. Pendergraft, M.V. Santander, T.H. Bertram, C.D. Cappa, F. Azam, P.J. DeMott, V.H. Grassian, and K.A. Prather, *Microbial Control of Sea Spray Aerosol Composition: A Tale of Two Blooms.* Acs Central Science, 2015. **1**(3): p. 124-131.

49. Ault, A.P., T.L. Guasco, O.S. Ryder, J. Baltrusaitis, L.A. Cuadra-Rodriguez, D.B. Collins, M.J. Ruppel, D.F. Zhao, T.H. Bertram, K.A. Prather, and V.H. Grassian, *Heterogeneous reactions of nitric acid at the interface of nascent sea spray aerosol: Phase changes caused by anthropogenic contaminants.* Abstracts of Papers of the American Chemical Society, 2013. **246**.

50. Bertram, T.H., O.S. Ryder, J.A. Thornton, T.P. Riedel, E. Fitzgerald, and K.A. Prather, *Direct measurement of the heterogeneous reaction of N2O5 on ambient aerosol particles.* Abstracts of Papers of the American Chemical Society, 2010. **240**.

51. Ryder, O.S., N.R. Campbell, H. Morris, S. Forestieri, M.J. Ruppel, C. Cappa, A. Tivanski, K. Prather, and T.H. Bertram, *Role of Organic Coatings in Regulating N2O5 Reactive Uptake to Sea Spray Aerosol.* Journal of Physical Chemistry A, 2015. **119**(48): p. 11683-11692.

52. Ryder, O.S., N.R. Campbell, M. Shaloski, H. Al-Mashat, G.M. Nathanson, and T.H. Bertram, *Role of Organics in Regulating ClNO2 Production at the Air-Sea Interface.* Journal of Physical Chemistry A, 2015. **119**(31): p. 8519-8526.

53. Köhler, H., *The nucleus in and the growth of hygroscopic droplets.* Transactions of the Faraday Society, 1936. **32**: p. 1152.

54. Petters, M.D. and S.M. Kreidenweis, *A single parameter representation of hygroscopic growth and cloud condensation nucleus activity.* Atmospheric Chemistry and Physics, 2007. **7**(8): p. 1961-1971.

55. Petters, M.D. and S.M. Kreidenweis, *A single parameter representation of hygroscopic growth and cloud condensation nucleus activity - Part 2: Including solubility.* Atmospheric Chemistry and Physics, 2008. **8**(20): p. 6273-6279.

56. Bilde, M. and B. Svenningsson, *CCN activation of slightly soluble organics: the importance of small amounts of inorganic salt and particle phase.* Tellus Series B-Chemical and Physical Meteorology, 2004. **56**(2): p. 128-134.

57. Schill, S.R., D.B. Collins, C. Lee, H.S. Morris, G.A. Novak, K.A. Prather, P.K. Quinn, C.M. Sultana, A.V. Tivanski, K. Zimmermann, C.D. Cappa, and T.H. Bertram, *The Impact of Aerosol Particle Mixing State on the Hygroscopicity of Sea Spray Aerosol.* Acs Central Science, 2015. **1**(3): p. 132-141.

58. Cerully, K.M., T. Raatikainen, S. Lance, D. Tkacik, P. Tiitta, T. Petaja, M. Ehn, M. Kulmala, D.R. Worsnop, A. Laaksonen, J.N. Smith, and A. Nenes, *Aerosol hygroscopicity and CCN activation kinetics in a boreal forest environment during the 2007 EUCAARI campaign.* Atmospheric Chemistry and Physics, 2011. **11**(23): p. 12369-12386.

59. Su, H., D. Rose, Y.F. Cheng, S.S. Gunthe, A. Massling, M. Stock, A. Wiedensohler, M.O. Andreae, and U. Poschl, *Hygroscopicity distribution concept for measurement data analysis and modeling of aerosol particle mixing state with regard to hygroscopic growth and CCN activation.* Atmospheric Chemistry and Physics, 2010. **10**(15): p. 7489-7503.

Chapter 2   Introduction of a Hygroscopicity Basis Set Analysis to Probe Aerosol Mixing State

2.1   Abstract

Atmospheric aerosol particles exhibit wide-ranging variability in chemical composition, physical phase state, and morphology. Further, a population of aerosol particles can display wide particle-particle variability in these properties, commonly referred to as mixing state. Consideration of the mixing state of an aerosol population is required to relate measurements of either average or single particle chemical composition with measurements of population averaged particle hygroscopicity. To date, there remains a paucity of experimental methods available to assess how particle-particle variability in chemical composition translates to corresponding differences in hygroscopicity. Here, we describe an approach for the characterization of the distribution of aerosol supersaturated hygroscopicity within chemically complex populations of atmospheric particles, using existing observations of size-resolved cloud condensation nuclei measurements. This methodology, when applied to the interpretation of laboratory-generated model systems, atmospheric chamber experiments, and ambient aerosols, yields distributions in particle hygroscopicity that can be used to assess the role of particle mixing state in cloud formation.

2.2   Introduction

Atmospheric aerosol particles impact global climate directly through the scattering and absorption of solar radiation, and indirectly by acting as seed particles for cloud formation, altering Earth's radiation budget.[1] The ability of a population of aerosol particles to take up water from its surrounding environment and act as cloud seeds, or cloud condensation nuclei (CCN), is intimately linked to the particle size distribution, chemical composition, and mixing state.[2]

19

In the case of marine sea-spray aerosols (SSA), aerosol composition is dictated both by the chemistry and biology that occurs in the surface ocean which produce a wide array of organic compounds that can be transferred with high efficiency to SSA.[3, 4] Particle chemical composition measurements have demonstrated that the organic fraction of SSA increases with decreasing particle diameter, when considered either by mass[5-7] or by number.[8, 9] It follows that the hygroscopicity of SSA in the sub-micron size regime is also size dependent, due to the enrichment of organic material in smaller particles.[2, 10, 11] Beyond the observed enrichment in SSA organic content with decreasing particle diameter, nascent SSA particles have also been shown to be strongly externally mixed, displaying a wide diversity of individual particle types.[8, 9, 12-15] Such mixing state effects may influence the CCN behavior of a chemically complex aerosol population.

Despite this known complexity, typical analyses of ambient particle hygroscopicity assume that all particles of a given size have identical composition (i.e. are internally mixed). As just a few examples, the hygroscopicity parameter, κ,[16] has been reported under this assumption for pristine aerosols in the Amazonian rainforest,[17] aged aerosols in the highly polluted Chinese city of Guangzhou,[18] and nascent marine SSA from the WACS I cruise in the Atlantic Ocean.[10] Importantly, global models have suggested that aerosol mixing state can impact CCN concentrations by up to 20% in the case of marine SSA,[19, 20] indicating that improved constraints on aerosol mixing state and how this varies by source are still necessary for robust determination of CCN concentrations.

Direct measurements of CCN concentrations are often compared to volume mixing-based predictions from Köhler theory, where incorporation of size-dependent chemical composition results in model-measurement agreement to within 10-20%,[21-27] but these still do not deal with the inherent particle-particle compositional variability at a given size. Padró et al.[28] found that accounting for external mixing improved CCN number concentration predictions (within 10-20%

of measured), while the common internal mixing state assumption can have a significantly greater error associated with it (up to 100%), in agreement with prior studies focused on externally-mixed aerosols.[21, 22] Collins et al.[29] investigated the CCN activity of SSA generated from a large-scale mesocosm seawater experiment and found that the assumption that all particles were compositionally identical (internally mixed) was insufficient to explain the temporal changes in the SSA particle hygroscopicity. A model in which the SSA was assumed to contain a diversity of particles with distinct compositions (externally mixed) was needed to achieve model-measurement agreement.[29] A basic model introduced by Schill et al.[30] suggested that, assuming a given aerosol size and hygroscopicity distribution, the number of CCN predicted with an external mixing assumption is significantly less than that which is predicted with an internal mixing state assumption, the magnitude of which is dependent on the supersaturation of the particle environment. The apparent need for robust methods that can account for mixing state in the interpretation of CCN measurements is further supported by measurements of particle growth due to water uptake under subsaturated conditions, which often indicate the co-existence of particles with very different compositions and hygroscopicities.[31, 32]

Despite the evident utility for CCN-specific hygroscopicity analyses that routinely account for the actual diversity of particles, few CCN studies have considered implementing a distribution of hygroscopicity values, or how a distribution of hygroscopicity values may be detected using size-resolved cloud condensation nuclei (SR-CCN) measurements. A study by Cerully et al.[33] used supersaturated hygroscopicity measurements of aerosols in a boreal forest environment to describe the extent of chemical heterogeneity, which is related to the slope of a CCN activation efficiency spectrum. This methodology reports a dispersion value with the population average κ-value. Another study by Su et al.[34] used theoretical activation efficiency spectra to test a hygroscopicity distribution concept for assessing particle heterogeneity with similar supersaturated CCN measurements. This study suggested that the activation efficiency

spectrum likely contains mixing state information, and that this should likely influence how future CCN measurements are made.

Measurements of the molecular composition of individual aerosol particles in the CCN size regime (< 100 nm) are rare,[35] thus limiting our ability to connect heterogeneity in particle chemical composition with their ability to serve as CCN at a single particle level. Many conventional techniques to measure aerosol composition at these sizes utilize spectroscopy[36-39] or mass spectrometry[15, 40-42] to detect the presence of various chemical components, but it can be difficult to extract detailed information about the distribution of components within the particles. Studies that have extracted mixing state information typically utilize various microscopy methods[12, 13, 43] and require collection of particles for offline analysis, often exposing particles to harsh environments such as high-vacuum conditions. For these reasons it can be exceedingly difficult to measure aerosol mixing state directly, particularly at the size regime of interest for CCN-active aerosols.

This study builds upon the initial work of Cerully et al.[33] and Su et al.[34] and presents a mathematical framework developed to assess aerosol mixing state with high-resolution SR-CCN measurements in the form of a κ basis set analysis. Laboratory-generated model systems were used to constrain the ability of the technique to adequately identify varying particle types within a known population, and the application of the technique to real world systems will also be discussed. The κ basis set analysis is fully generalizable to a wide range of aerosol samples, highlighting SR-CCN hygroscopicity measurements as a robust, high-throughput technique for generating real-time mixing state information on small (50 - 100 nm) aerosol particles.

2.3   Methods

2.3.1   Overview of SR-CCN Measurements

The hygroscopicity of individual aerosol particles can be characterized through measurement of their ability to activate (or grow) into cloud droplets, which is also known as their activation efficiency. The activation efficiency is measured by the fraction of particles of a given size that grow into droplets when exposed to a specific water supersaturation (s), or $f_{CCN}(s)$, with more hygroscopic particles activating into cloud droplets at a lower water supersaturation. Measurement of the size and supersaturation dependent activation efficiency of a population of aerosol particles is referred to as a size-resolved CCN (SR-CCN) measurement.[16, 44] An SR-CCN measurement system consists of three stages: i) aerosol particle generation, ii) particle size selection, and iii) measurement of both the size resolved particle number concentration and the fraction that grow to droplet size (ca. $d_p > 1$ μm) at a specific water supersaturation.

Hygroscopicity values (κ) for the model systems used in this study were determined by aerosolizing compounds using a constant output atomizer (TSI model 3076). Nitrogen was used as an inert carrier gas to generate and transport aerosol particles from aqueous stock solutions, through silica gel diffusion dryers, to the SR-CCN system. Each solution was less than 1 L in volume, and the dissolved concentration of solute was selected so that monodisperse particle number concentrations were approximately $200 – 1000$ cm^{-1}. Monodisperse particles were selected from the polydisperse distribution according to their mobility diameters using a differential mobility analyzer (DMA, TSI model 3071) with a sheath:sample flow rate ratio of 10:1. The resulting aerosol stream was subsequently split between a condensation particle counter (CPC, TSI model 3787) measuring size selected particle concentrations, and a CCN counter (CCNc, DMT model CCN-100) for measurement of the fraction of particles that grow to droplet sizes (ca. $d_p > 1$ μm) as a function of water supersaturation. The ratio of the number concentration of particles that grow to droplet size (here referred to as cloud condensation nuclei (CCN), or

N_{CCN}) to the total particle concentration at that size (N_p) is measured as f_{CCN} (where f_{CCN} = N_{CCN}/N_p). In this study, the CCN activation efficiency spectra (f_{CCN} versus s), is reported for monodisperse particle populations.

2.3.2   Determination of κ-values

From the activation efficiency spectra, a hygroscopicity parameter (κ) is determined following Equations 2.1-2,[16] which include the liquid-vapor surface tension (σ_{lv}), density (ρ_w), and molecular weight (M_w) of pure water, the universal gas constant (R) and temperature (T), and two experimentally-measured values: the dry particle diameter (D_d) and the critical supersaturation (s_{crit}), operationally defined where 50% of the particle population has activated.

$$\kappa = \frac{4A^3}{27\, D_d^3\, ln^2(S_c)} \tag{E 2.1}$$

$$A = \frac{4\sigma_{lv}M_w}{RT\rho_w} \tag{E 2.2}$$

When the SR-CCN instrument is operated in scanning supersaturation mode, D_d is fixed at a constant known value, and s_{crit} is determined from fitting the activation efficiency spectrum and calculating the 50% activation point. All activation efficiency spectra in this study were fit using a four-parameter Boltzmann sigmoid, shown in Equation 2.3, where α is the fit maximum, β is the fit minimum, γ is the inflection point of the sigmoid halfway between α and β (50% activation point), and δ is the characteristic slope of the fit.

$$f_{CCN}(s) = \alpha + \frac{\beta - \alpha}{1 + \frac{\gamma - s}{\delta}} \tag{E 2.3}$$

The γ-value is typically taken as the s_{crit} and used with the particle size (D_d) to determine the κ-value for the compound, according to Equations 2.1-2. With this approach it is implicitly assumed that the 50% activation point for the entire population characterizes all particles in the sample. This is the same as saying there is one representative composition for the sample,

meaning it is either a pure model system or that it is internally mixed. For pure compounds the resulting κ-value is the hygroscopicity value for the compound, and for internal mixtures this observed κ-value is a linear combination of the pure κ-values and relative volume fractions (ε) of the individual components[16], as shown in Equation 2.4.

$$\kappa_{mix,int} = \sum \varepsilon_i \kappa_i \qquad \text{(E 2.4)}$$

It is important to note, however, that a population of aerosol particles can exhibit wide particle-particle variability in composition at a given size, particularly in urban areas. This is known as external mixing, and there is currently no standardized approach for accounting for these particles with SR-CCN hygroscopicity measurements. Developing a methodology for interpreting SR-CCN measurements for externally mixed populations is integral for extending the application of this high throughput technique to measure aerosol composition information for small particles in real time.

2.3.3   κ Basis Set Model

To date, the extent of interpreting SR-CCN measurements for externally mixed samples is the observation that chemical heterogeneity appears linked to the slope of the activation efficiency spectrum,[33, 34] which is related to the δ-value in the fit. In this study, we develop a mathematical framework to quantitatively assess the extent of chemical heterogeneity of an aerosol sample using the fitted activation efficiency spectrum, in the form of a κ basis set analysis.

This analysis begins with an activation efficiency spectrum in supersaturation space (f_{CCN} vs. s) that has been normalized and corrected for doubly charged particles, according to the method of Schill et al.[30] The activation efficiency spectrum is bracketed by the minimum and maximum supersaturation values, corresponding to the range of values for the entire activation efficiency spectrum, and a user-defined number of bins into which the data will be divided. The

resulting supersaturation bin width can be decreased or increased by dividing the experimental range of s into more or fewer bins in s, respectively. The activation efficiency spectrum is then integrated using a right edge-centered summation, and the relative abundance for each bin is tabulated. Lastly, the size of the particles used for analysis allows for conversion of the supersaturation bins into corresponding hygroscopicity bins, according to Equations 2.1-2, into which the relative abundance values for each bin are populated. This generates a hygroscopicity histogram, which represents the distribution of κ-values present within the aerosol sample.

It follows that if the measured activation efficiency spectrum has a steep sigmoid, the majority of particles should be sorted into a single hygroscopicity bin, in agreement with the interpretation that a steep activation curve represents a single, representative composition for the population. Notably, in the event that the activation efficiency spectrum is steep and the sample is either pure or internally mixed, traditional SR-CCN analysis provides more precision with a single value for κ, relative to the basis set analysis which, even when only one bin is populated, provides a range in κ. Conversely, if the measured activation efficiency spectrum is broad, the resulting hygroscopicity distribution should be similarly broad, providing quantitative constraints on the variability of hygroscopicities within the sample. Of course, the shape of the hygroscopicity distribution is dependent not only on the slope of the activation efficiency spectrum, but also on the width of the prescribed hygroscopicity bins. Sensitivity testing in Section 2.3.3 will discuss this further, but in general, the basis set analysis is meaningful for the comparison of multiple data sets, provided the same basis set resolution is used between experiments.

The full code for the κ basis set analysis is included in the supporting information (Sec. 2.7). Because the input for the κ basis set analysis is simply the CCN activation efficiency spectrum (f_{CCN} vs. s), for which the measurement technique has been extensively validated, the κ basis set analysis can be applied to any SR-CCN data set including previously collected data

provided the supersaturation resolution is sufficient. Moreover, this technique is fully generalizable and can be applied to a wide range of aerosol samples including those from urban environments, marine SSA, and others.

2.4 Results and Discussion

2.4.1 Single-Component Model System

A necessary first step in the validation of the κ basis set model was constraints imposed from a population of single-component aerosol particles. The CCN activation efficiency spectrum for 50 nm ammonium sulfate particles is characterized by an extremely sharp sigmoid, as shown in Fig. 2.1A, which is driven by the high precision in supersaturation control that is achievable by the CCNc, and the precision of the size selection achievable by the DMA. Variability in water content (s) and aerosol size (D_d) contribute to a broader activation efficiency spectrum, so knowing the characteristic spectrum slope for a pure compound is helpful in interpreting subsequent spectra. As discussed in Sec. 2.2.3, integration of the activation efficiency spectrum with the κ basis set analysis for a pure compound populates a single hygroscopicity bin, shown in Fig. 2.1B. For reference, the κ value for ammonium sulfate determined by traditional SR-CCN analysis was 0.6641 ± 0.0074 (3-trial average $\pm \sigma$).
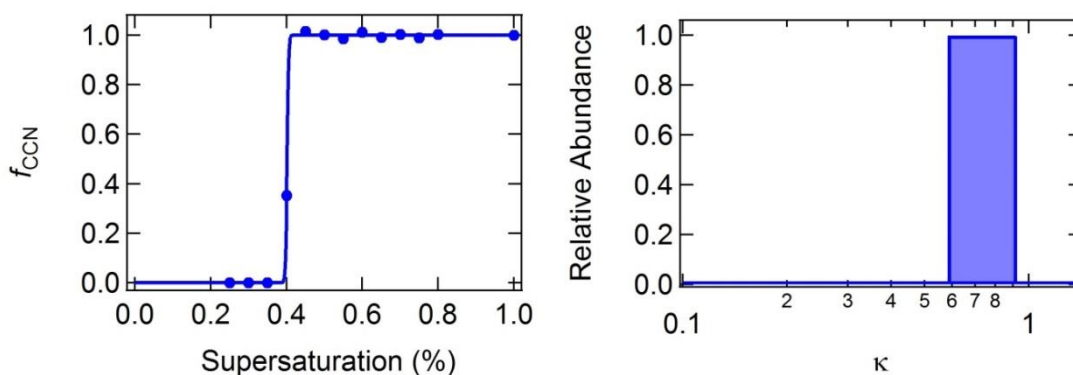
Figure 2.1: (left) CCN activation efficiency spectrum and (right) hygroscopicity distribution for 50 nm diameter ammonium sulfate particles.

2.4.2 Two-Component Model System

Next, a two-component, externally mixed model aerosol system was generated with sea salts and galactose in multiple atomizers, such that aerosol particles were generated separately and mixed prior to introduction to the SR-CCN inlet. The mixing time was kept at a minimum to avoid particle coagulation. As shown in Fig. 2.2A, high-resolution supersaturation scans observed two distinct activation curves, in addition to two doubly charged particle populations which were removed as described in section 2.3.1. The observation of two distinct populations within the activation efficiency spectrum demonstrates that the SR-CCN can differentiate between chemically distinct compounds within the same population with sufficiently high supersaturation resolution, where this information may be lost with lower resolution as shown by the modeled scan of the same population with typical resolution for traditional SR-CCN analysis. In the case of this model system, external mixing accounts for the difference between one broad activation curve and two sharp activation curves. Notably, the slope of the activation efficiency spectrum from traditional SR-CCN analysis serves as a first-order indication of whether accounting for external mixing may be required, with Boltzmann sigmoid slope parameters (δ) in this study on the order of 0.0021 and 0.1212, for pure or internally mixed systems and externally mixed

systems respectively. When the slope of the single sigmoid is sufficiently broad, the data set is divided, fit as individual activation curves, and combined to generate the activation efficiency spectrum.

The corresponding κ basis set hygroscopicity distributions are shown in Fig. 2.2B, with the traditional analysis suggesting a broad range of hygroscopicities, and the basis set analysis populating two distinct populations. This model system highlights the inconsistencies in retrieved hygroscopicity from the traditional analysis relative to the basis set analysis, and the utility of this analysis for interpretation of SR-CCN measurements of external aerosol mixtures.
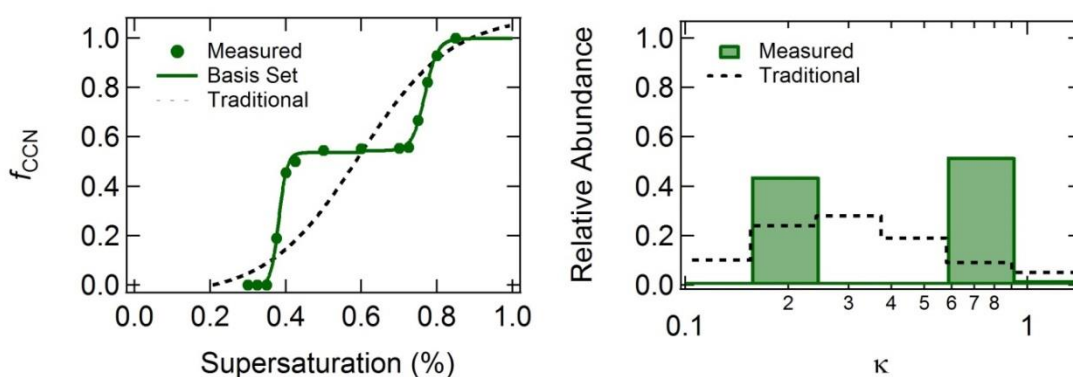
Figure 2.2: (left) CCN activation efficiency spectrum using the κ basis set (solid) and traditional (dashed) analysis, and (right) hygroscopicity distribution for 50 nm diameter externally mixed (1:1), sea salt and galactose particles.

2.4.3 Sensitivity Testing Using a Five-Component Mixture

The basis set analysis was extended to a five-component model mixture composed of internal mixtures with sea salt:galactose mass ratios of: 100:0, 43:57, 22:78, 9:91 and 0:100, with corresponding $\kappa_{int,mix}$ values of 0.83, 0.48, 0.34, 0.26 and 0.2 respectively. The relative number concentrations of the different particle types were 0.2, 0.12, 0.28, 0.10 and 0.3, and if all of the particle types were mixed together in these proportions, the overall $\kappa_{int,mix} = 0.40$ ($s_{crit,50nm} = 0.52\%$). Fig. 2.3 shows the activation efficiency spectra and corresponding hygroscopicity distributions for an SR-CCN experiment with the five-component mixture, with data points

removed to simulate the effect of supersaturation resolution on the basis set analysis. Panels A – D correspond to increasing resolution in s, with panel D showing the full activation efficiency spectrum, and the black dashed line is the calculated activation efficiency spectrum for an external mixture with the relative number concentrations listed above. In general, increasing resolution results in better characterization of the activation efficiency spectrum, as higher resolution promotes identification of activation of each component.

A key observation from the full activation efficiency spectrum (Fig. 2.3D) is that clear sigmoids are evident in the full activation curve, which corresponds to the activation of the individual particle types, and that the full activation curve has a slope that is approximately eight times broader than that of any pure compound or internal mixture when fit with a single sigmoid. This indicates that broadening of the activation efficiency spectrum occurs for an external mixture of particles that have a range of κ-values, generally consistent with ambient observations.[33, 45-47] This also demonstrates that with increasing chemical complexity it is increasingly difficult to fit a distinct number of sigmoids to determine the number of distinct particle types, as the activation efficiency spectrum becomes a broad continuum of activation for multiple populations. The ability to perform high-resolution SR-CCN scans will ultimately be determined by experimental parameters, such as the stability of the aerosol source, sampling time, etc.
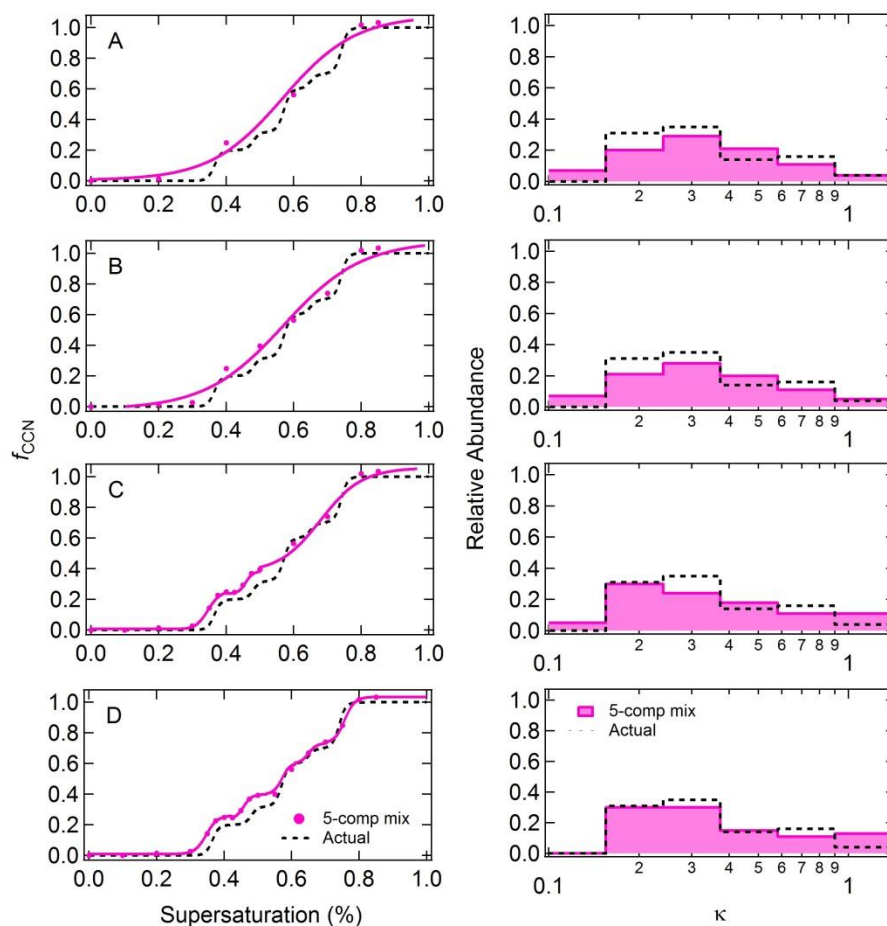
Figure 2.3: (left) CCN activation efficiency spectra and (right) hygroscopicity distributions for 50 nm particles of a five-component external mixture of sea salt, galactose, and internal mixtures of sea salt and galactose, with increasing resolution in supersaturation from panels A – D. The black dashed line is the calculated activation efficiency spectrum for an external mixture with the relative number concentrations listed above.

The five-component externally mixed model system was also used to assess the effect of the prescribed hygroscopicity bin width (user-defined input) on the κ basis set analysis. Fig. 2.4 shows the hygroscopicity distributions for the two- and five-component external model mixtures, with increasing κ resolution from panels B – E. The ideal hygroscopicity bin width is the one which populates the same number of bins as there are components in the model mixtures, which is known for these model systems. Importantly, this information is unknown for ambient systems,

so the utility of the κ basis set analysis is in the direct comparison of multiple activation efficiency spectra with the same κ resolution. Additional experiments need to be done to assess the appropriate amount of resolution for ambient data.
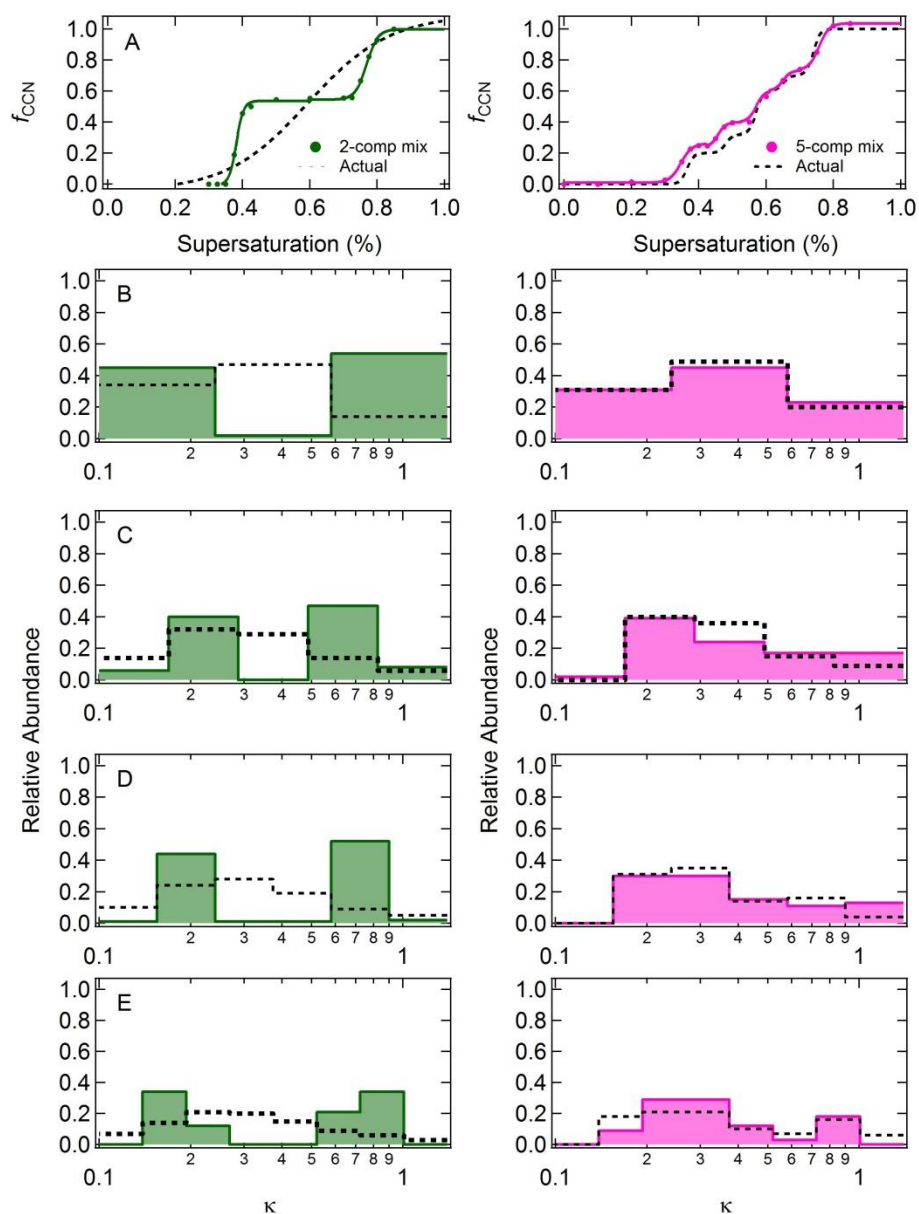
Figure 2.4: CCN activation efficiency spectra (A) and hygroscopicity distributions (B – E) for 50 nm particles of a two-component (left) and five-component (right) external mixture of sea salt, galactose, and internal mixtures of sea salt and galactose, with increasing resolution in κ with 3 (B), 5 (C), 6 (D), and 8 (E) bins between κ = 0.1 – 1.4.

2.4.4   Application Beyond Model Systems

The externally mixed model systems discussed above constrain the application and sensitivity of the κ basis set analysis. Next, we apply this analysis to SR-CCN spectra collected from real world systems.

2.4.4.1   Photooxidation Experiments

The κ basis set analysis was applied to naphthalene secondary organic aerosol (SOA) generated in the UC Irvine environmental chamber. The chamber and general experimental procedures are described in detail by Malecha and Nizkorodov[48]. Briefly, a 5 m^3 teflon chamber was used to generate SOA from naphthalene (200 ppb), ammonia (1000 ppb), and hydrogen peroxide (2000 ppb), in the absence of particles, with varying NO_x (low = 0 ppb, high = 200 ppb) and relative humidity (dry = 0% RH, wet > 85% RH). Hydrogen peroxide served as a source of OH radicals upon irradiation with UV-B lamps (λ = 310 nm), which were used to initiate photochemistry for all experiments.

Activation efficiency spectra and corresponding hygroscopicity distributions are shown in Fig. 2.5. Under both low and high NO_x, dry (low RH) conditions, the activation efficiency spectra show single activation curves with slope parameters (δ) of 0.0271 and 0.0403 respectively, corresponding to one representative composition for the population and suggesting internal mixing of reaction products. Note that the hygroscopicity distributions in Fig. 2.5 utilize a different basis set than those used in Fig. 2.1-2.4, which was chosen to include all components in the SOA chamber experiments. Under low and high NO_x, wet (high RH) conditions two distinct populations were observed, though the population observed at higher s under low NO_x conditions was only observed after addition of ammonia to the chamber. This effect was unique to this experiment, as addition of ammonia to all other experiments did not alter the activation efficiency spectrum (data not shown).
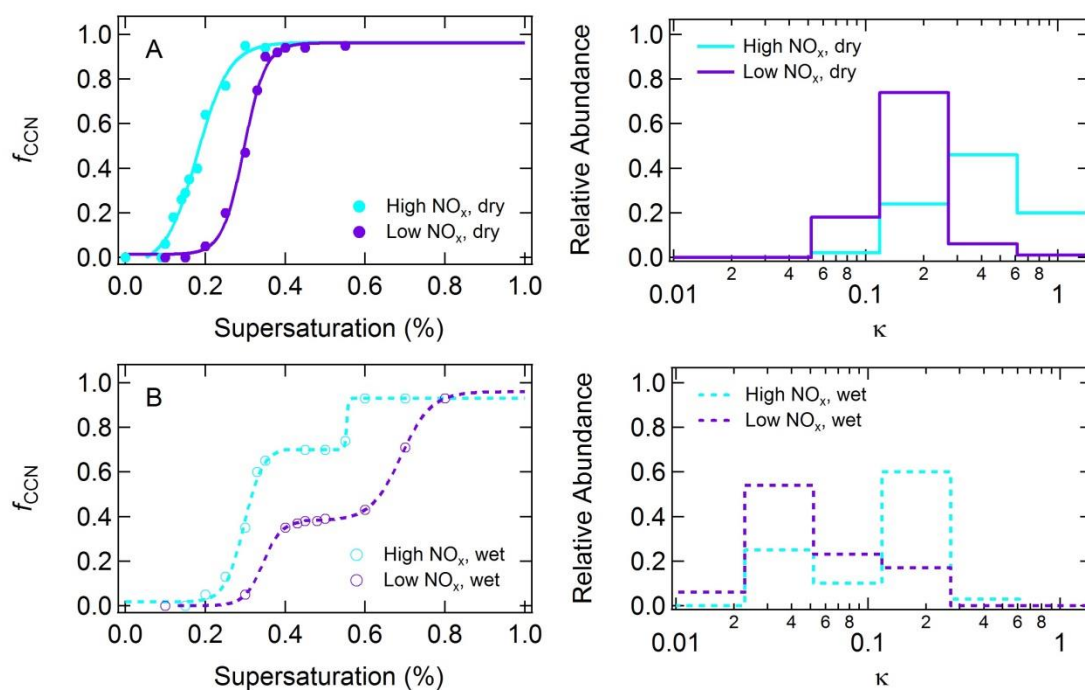
Figure 2.5: CCN activation efficiency spectra (left) and hygroscopicity distributions (right) for 100 nm naphthalene SOA particles under low (purple) and high (blue) NO_x and dry (top) and wet (bottom) conditions.

The κ-value corresponding to SOA particles generated under low NO_x, dry conditions was 0.12, in good agreement with previous reported measurements of naphthalene SOA by Saukko et al.[49] SOA particles that activate at higher s, such as the secondary populations identified under high and low NO_x, wet conditions, are therefore less hygroscopic than naphthalene. This could possibly be explained by a glassy transition state for naphthalene SOA identified by Saukko et al.[49] at > 80% RH, the effect of which on climate relevant properties remains unclear in the absence of additional measurements. Importantly, aerosol size distributions collected by a scanning mobility particle sizer (SMPS, data not shown) do not show evidence of any bimodality in particle size. Conversely, SOA particles that activate at lower s, such as the population identified under high NO_x, dry and wet conditions are more hygroscopic than

naphthalene and could indicate addition of nitrate to the particle, which would enhance the number of soluble moles in the particle. Note that pure ammonium nitrate particles are expected to have a $\kappa = 0.68$, and are not observed in this study.

The shift in the activation efficiency spectra from single (high and low NO_x, dry) to multiple sigmoids (high and low NO_x, wet) corresponds to the evolution of reaction products within the chamber. It is important to note that traditional SR-CCN analysis would only report a decrease in the average κ-value for the population whereas the κ basis set analysis identifies the occurrence of distinct particle types in real time and quantifies their differences in hygroscopicity. Interpretation of the chemical mechanisms behind the generation of an externally mixed particle population is beyond the scope of this technical report.

2.4.4.2   Ambient Marine SSA

The κ basis set analysis was also applied to SR-CCN measurements of nascent marine SSA generated from the surface ocean using the NOAA PMEL sea-sweep[50] during the WACS I cruise in the Atlantic Ocean.[51] The WACS sea-sweep measurements assessed here were made both within Georges Bank, a location where the surface chlorophyll-a concentration was relatively high which indicated fairly biologically active waters, and within the oligotrophic Sargasso Sea, a location where the surface chlorophyll-*a* concentration was relatively low. As no substantial differences were found between the measurements at these two locations, only the Georges Bank results are shown. Fig. 2.6 shows the activation efficiency spectra for 50 nm ambient SSA particles, and NaCl particles for reference, with slope parameters (δ) of 0.0273 and 0.0778 respectively.
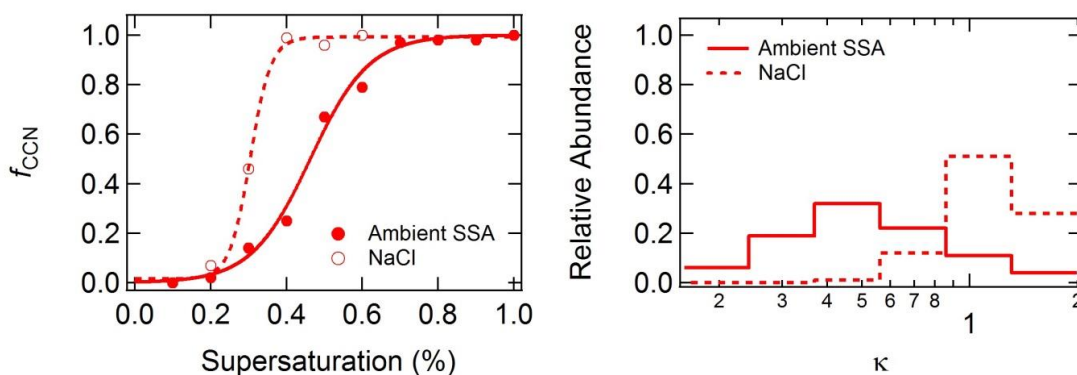
Figure 2.6: CCN activation efficiency spectrum (left) and hygroscopicity distribution (right) for 50 nm ambient SSA (solid) and NaCl (dashed) particles generated within Georges Bank.

A wide distribution of κ-values was observed for the ambient SSA, suggesting compositions ranging from purely sea salt to purely organic. For the basis set used in this study, the κ distribution peaks around $\kappa = 0.46$, compared to $\kappa = 0.51$ from the traditional SR-CCN analysis, suggesting that a substantial fraction of the nascent SSA particles had large organic fractions. By comparison, the hygroscopicity distribution for the NaCl reference particles peaks around $\kappa = 1.1$, compared to $\kappa = 1.19$ from traditional SR-CCN analysis. Importantly, the basis set used here was chosen such that the diversity of particle types for the ambient SSA was adequately captured, and the resulting bin width near the κ-value for the pure NaCl particles caused population of multiple hygroscopicity bins.

A major result from this analysis is that the κ basis set quantitatively constrains the relative abundance of various particle types, based on the prescribed hygroscopicity bin width, where traditional SR-CCN analysis would only report the decrease in κ for the population. This highlights the utility of SR-CCN measurements for extracting mixing state and composition information for small (50 nm) particles. The impact of accounting for these varied particle types *via* the κ basis set analysis, specifically in regards to marine SSA, has been described in further detail by Schill et al.[30]

2.5   Conclusions

A mathematical framework was developed to assess aerosol mixing state with high-resolution SR-CCN measurements in the form of a κ basis set analysis. Laboratory-generated model systems were used to constrain the characteristic slope of the activation efficiency spectrum, which is steep for pure or internally mixed compounds and broad for externally mixed and chemically complex systems. Application of the κ basis set analysis to real world systems provided quantitative characterization of distinct particle types (with respect to hygroscopicity) within a population, in comparison to traditional SR-CCN analysis, which can only assess a change in the population average value of κ. The utility of the basis set analysis is in the direct comparison of multiple SR-CCN data sets analyzed with the same prescribed hygroscopicity bin width, which plays a major role in determining the shape of the hygroscopicity distribution as shown by the sensitivity testing. The fully generalizable κ basis set analysis therefore highlights SR-CCN hygroscopicity measurements as a robust, high-throughput technique for generating real-time mixing state information on small (50 - 100 nm) aerosol particles.

2.6   Acknowledgements

2.7   Supporting Information

The supporting information includes the MATLAB code used for the κ basis set analysis.

```
%%%% Kappa Basis Set Analysis Code
%%%% Schill et al. in preparation (2017)

%%%% NOTE: To compare kappa distributions from multiple populations,
the
%%%% same basis set parameters must be defined for both samples!

%% Sample Data

% Compiled SR-CCN curve for 5-component mixture from Schill et al.
(2015) ACS Cent. Sci.
ss =
[0;0.100000000000000;0.200000000000000;0.300000000000000;0.350000000000
000;0.375000000000000;0.400000000000000;0.425000000000000;0.45000000000
0000;0.475000000000000;0.500000000000000;0.550000000000000;0.6000000000
00000;0.650000000000000;0.700000000000000;0.750000000000000;0.800000000
000000;0.850000000000000];
CAF =
[0;0;0.0135802520000000;0.0254592990000000;0.138657671000000;0.21864356
0000000;0.239906439000000;0.238599679000000;0.283938064000000;0.3564004
18000000;0.381415399000000;0.387229128000000;0.544061588000000;0.646817
189000000;0.715027740000000;0.821624365000000;0.984583712000000;1];

%% Plot Data

figure; plot(ss, CAF, 'bo')
axis([0, 1.1, -0.1, 1.1])
xlabel('Supersaturation (%)')
ylabel('f(CCN/CN)')
title('Activation Efficiency Spectrum f(CCN/CN)')

% Calculate Fit
sigmoid=@(beta,x) beta(1)+(beta(2)-beta(1))./(1+(x/beta(3)).^beta(4));
% Hill sigmoid fit
    [sig_fit{1,1}, resid{1,1}, J{1,1}] = nlinfit(ss, CAF, sigmoid, [1 1
1 1]);
beta{1,1} = sig_fit{1,1};
fit_x = [0:0.001:1.5]';
fit_y = (beta{1,1}(1)+(beta{1,1}(2)-
beta{1,1}(1))./(1+(fit_x/beta{1,1}(3)).^beta{1,1}(4)));
hold on; plot(fit_x, fit_y, 'k-')

%% Fit check

if sig_fit{1,1}(1,1)>0.975 & sig_fit{1,1}(1,1)<1.025

else
```

```matlab
        warndlg('Poor Sigmoid Fit - Consider External Mixing',
'!!Warning!!')
    Slope = diff(CAF);
    Ind = find(Slope<0.02);
    if length(Ind)<3

    else
    Cut = find(diff(Ind)==1);
    Ind(Cut,:)=[];
    Ind(end,:)=[];
    Ind(1,:)=[];
    Num_sig = length(Ind)+1;

    ACT_split{1,1}=[ss(1:Ind(1,1),1), CAF(1:Ind(1,1),1)];
    for i = 2:Num_sig-1
        ACT_split{i,1}=[ss(Ind(i-1,1):Ind(i,1),1), CAF(Ind(i-
1,1):Ind(i,1),1)];
    end
    ACT_split{Num_sig,1}=[ss(Ind(end,1)+1:end,1),
CAF(Ind(end,1)+1:end,1)];


    figure; plot(ss, CAF, 'bo')
    axis([0, 1, -0.1, 1.1])
    xlabel('Supersaturation (%)')
    ylabel('f(CCN/CN)')
    title('Activation Efficiency Spectrum f(CCN/CN)')
    for j = 1:length(ACT_split)
        sigmoid=@(beta,x) beta(1)+(beta(2)-
beta(1))./(1+(x/beta(3)).^beta(4)); % Hill sigmoid fit
        [sig_fit{1,1}, resid{1,1}, J{1,1}] =
nlinfit(ACT_split{j,1}(:,1),...
            ACT_split{j,1}(:,2), sigmoid, [1 1 1 1]);
        beta{1,1} = sig_fit{1,1};
        fit_x = [ACT_split{j,1}(1,1):0.001:ACT_split{j,1}(end,1)]';
        fit_y = (beta{1,1}(1)+(beta{1,1}(2)-
beta{1,1}(1))./(1+(fit_x/beta{1,1}(3)).^beta{1,1}(4)));
        fit_ACT_split{j,1} = [fit_x fit_y];
        hold on; plot(fit_x, fit_y, 'k-')
    end

    Combined_Fit = cell2mat(fit_ACT_split);
    hold on; plot(Combined_Fit(:,1), Combined_Fit(:,2), 'r-')
    end
end

%% Define supersaturation bins

% Dialogue Box
prompt = {'Minimum', 'Maximum', 'Number of Bins'};
inistr = {'0.275', '0.875', '6'};
dlg_title = 'Define supersaturation basis set bin width';
num_lines = 1;
Bin_Spacing = inputdlg(prompt, dlg_title, num_lines, inistr);
bin_min = str2num(Bin_Spacing{1,1});
```

```matlab
bin_max = str2num(Bin_Spacing{2,1});
bin_number = str2num(Bin_Spacing{3,1})+1;

% Convert SS values to log spacing
if bin_min ==0
    bin_min_log = -2; % Because log10(0) is undefined
else
    bin_min_log = log10(bin_min);
end
bin_max_log = log10(bin_max);

% SS Bin Spacing
ss_bins = logspace(bin_min_log, bin_max_log, bin_number)';
hold on; plot(ss_bins, ss_bins, 'r*')


%% Convert SS Bins to Kappa Bins

% Dialogue Box
prompt = {'Dry Diameter (nm)'};
inistr = {'50'};
dlg_title = 'Enter dry particle diameter';
num_lines = 1;
DIAM = inputdlg(prompt, dlg_title, num_lines, inistr);
diameter = str2num(DIAM{1,1});

% Calculate Kappa Bins
kappa_bins = [];
for i = 1:length(ss_bins)
    T_kappa = (4*(2.099E-
09^3))/(27*(((diameter*0.000000001)^3)*(log((ss_bins(i,1)/100)+1)^2)));
    kappa_bins = [kappa_bins; T_kappa];
end

%% Integrate SR-CCN curve

Check = exist('ACT_split');
if Check > 0
    fit_x = Combined_Fit(:,1);
    fit_y = Combined_Fit(:,2);
else

end

% Find Right-Edge Bin Corners
Indices = {};
for i = 1:length(ss_bins)-1
    Indices{1,i} = find(fit_x > ss_bins(i,1) & fit_x < ss_bins(i+1,1),
1, 'last');
end

% Find corresponding f(CCN/CN) counts at each bin corner
for j = 1:length(Indices)
    Numbers{j} = round(fit_y(Indices{1,j})*100);
    if Numbers{j}<0
```

```matlab
        Numbers{j}=0;
    elseif Numbers{j}>100
        Numbers{j}=100;
    else
    end
end

% Calculate Bin Height For Each Bin
BH{1,1} = Numbers{1};
for k = 2:length(Numbers)
    BH{k,1} = Numbers{k}-Numbers{k-1};
end
Bin_Heights = cell2mat(BH);

%% Populate Kappa Basis Set

% Organize Kappa Basis Set Values
kb_clip = kappa_bins(2:end);
kappa_bins_range = [kappa_bins(1:end-1) kb_clip];
kappa_bins_midpt = mean(kappa_bins_range,2);

% Prep Values for "Line Graph Histogram"
kappa_bins_stacked = [];
for m = 1:length(kappa_bins_range)
    T_kappa_bins_stacked = kappa_bins_range(m,:)';
    kappa_bins_stacked = [kappa_bins_stacked; T_kappa_bins_stacked];
end

bin_heights = [Bin_Heights Bin_Heights];
bin_heights_stacked = [];
for n = 1:length(bin_heights)
    T_bin_heights_stacked = bin_heights(n,:)';
    bin_heights_stacked = [bin_heights_stacked; T_bin_heights_stacked];
end

%% Plot Kappa Distribution

figure;semilogx(kappa_bins_stacked, bin_heights_stacked)
xlabel('Hygroscopicity Parameter ({\kappa})')
ylabel('Relative Abundance (%)')
title('Hygroscopicity Distribution ({\kappa})')
```

2.8   References

1.   IPCC, *Climate Change 2013: The Physical Science Basis. Contribution of Working Group I to the Fifth Assessment Report of the Intergovernmental Panel on Climate Change*, ed. T.F. Stocker, et al. 2013, Cambridge, United Kingdom and New York, NY, USA: Cambridge University Press. 1535.

2.   Hegg, D.A., D.S. Covert, H.H. Jonsson, and R.K. Woods, *A simple relationship between cloud drop number concentration and precursor aerosol concentration for the regions of Earth's large marine stratocumulus decks.* Atmospheric Chemistry and Physics, 2012. **12**(3): p. 1229-1238.

3.	Quinn, P.K., D.B. Collins, V.H. Grassian, K.A. Prather, and T.S. Bates, *Chemistry and Related Properties of Freshly Emitted Sea Spray Aerosol.* Chemical Reviews, 2015.

4.	O'Dowd, C.D. and G. De Leeuw, *Marine aerosol production: a review of the current knowledge.* Philosophical Transactions of the Royal Society a-Mathematical Physical and Engineering Sciences, 2007. **365**(1856): p. 1753-1774.

5.	O'Dowd, C.D., M.C. Facchini, F. Cavalli, D. Ceburnis, M. Mircea, S. Decesari, S. Fuzzi, Y.J. Yoon, and J.P. Putaud, *Biogenically driven organic contribution to marine aerosol.* Nature, 2004. **431**(7009): p. 676-680.

6.	Facchini, M.C., M. Rinaldi, S. Decesari, C. Carbone, E. Finessi, M. Mircea, S. Fuzzi, D. Ceburnis, R. Flanagan, E.D. Nilsson, G. de Leeuw, M. Martino, J. Woeltjen, and C.D. O'Dowd, *Primary submicron marine aerosol dominated by insoluble organic colloids and aggregates.* Geophysical Research Letters, 2008. **35**(17): p. 5.

7.	Keene, W.C., H. Maring, J.R. Maben, D.J. Kieber, A.A.P. Pszenny, E.E. Dahl, M.A. Izaguirre, A.J. Davis, M.S. Long, X.L. Zhou, L. Smoydzin, and R. Sander, *Chemical and physical characteristics of nascent aerosols produced by bursting bubbles at a model air-sea interface.* Journal of Geophysical Research-Atmospheres, 2007. **112**(D21): p. 16.

8.	Prather, K.A., T.H. Bertram, V.H. Grassian, G.B. Deane, M.D. Stokes, P.J. DeMott, L.I. Aluwihare, B.P. Palenik, F. Azam, J.H. Seinfeld, R.C. Moffet, M.J. Molina, C.D. Cappa, F.M. Geiger, G.C. Roberts, L.M. Russell, A.P. Ault, J. Baltrusaitis, D.B. Collins, C.E. Corrigan, L.A. Cuadra-Rodriguez, C.J. Ebben, S.D. Forestieri, T.L. Guasco, S.P. Hersey, M.J. Kim, W.F. Lambert, R.L. Modini, W. Mui, B.E. Pedler, M.J. Ruppel, O.S. Ryder, N.G. Schoepp, R.C. Sullivan, and D.F. Zhao, *Bringing the ocean into the laboratory to probe the chemical complexity of sea spray aerosol.* Proceedings of the National Academy of Sciences of the United States of America, 2013. **110**(19): p. 7550-7555.

9.	Ault, A.P., R.C. Moffet, J. Baltrusaitis, D.B. Collins, M.J. Ruppel, L.A. Cuadra-Rodriguez, D.F. Zhao, T.L. Guasco, C.J. Ebben, F.M. Geiger, T.H. Bertram, K.A. Prather, and V.H. Grassian, *Size-Dependent Changes in Sea Spray Aerosol Composition and Properties with Different Seawater Conditions.* Environmental Science & Technology, 2013. **47**(11): p. 5603-5612.

10.	Quinn, P.K., T.S. Bates, K.S. Schulz, D.J. Coffman, A.A. Frossard, L.M. Russell, W.C. Keene, and D.J. Kieber, *Contribution of sea surface carbon pool to organic matter enrichment in sea spray aerosol.* Nature Geosci, 2014. **7**(3): p. 228-232.

11.	Kaku, K.C., D.A. Hegg, D.S. Covert, J.L. Santarpia, H. Jonsson, G. Buzorius, and D.R. Collins, *Organics in the Northeastern Pacific and their impacts on aerosol hygroscopicity in the subsaturated and supersaturated regimes.* Atmos. Chem. Phys., 2006. **6**(12): p. 4101-4115.

12.	Ault, A.P., T.L. Guasco, J. Baltrusaitis, O.S. Ryder, J.V. Trueblood, D.B. Collins, M.J. Ruppel, L.A. Cuadra-Rodriguez, K.A. Prather, and V.H. Grassian, *Heterogeneous Reactivity of Nitric Acid with Nascent Sea Spray Aerosol: Large Differences Observed*

between and within Individual Particles. Journal of Physical Chemistry Letters, 2014. **5**(15): p. 2493-2500.

13.   Ault, A.P., T.L. Guasco, O.S. Ryder, J. Baltrusaitis, L.A. Cuadra-Rodriguez, D.B. Collins, M.J. Ruppel, T.H. Bertram, K.A. Prather, and V.H. Grassian, *Inside versus Outside: Ion Redistribution in Nitric Acid Reacted Sea Spray Aerosol Particles as Determined by Single Particle Analysis.* Journal of the American Chemical Society, 2013. **135**(39): p. 14528-14531.

14.   Ault, A.P., D.F. Zhao, C.J. Ebben, M.J. Tauber, F.M. Geiger, K.A. Prather, and V.H. Grassian, *Raman microspectroscopy and vibrational sum frequency generation spectroscopy as probes of the bulk and surface compositions of size-resolved sea spray aerosol particles.* Physical Chemistry Chemical Physics, 2013. **15**(17): p. 6206-6214.

15.   Guasco, T.L., L.A. Cuadra-Rodriguez, B.E. Pedler, A.P. Ault, D.B. Collins, D.F. Zhao, M.J. Kim, M.J. Ruppel, S.C. Wilson, R.S. Pomeroy, V.H. Grassian, F. Azam, T.H. Bertram, and K.A. Prather, *Transition Metal Associations with Primary Biological Particles in Sea Spray Aerosol Generated in a Wave Channel.* Environmental Science & Technology, 2014. **48**(2): p. 1324-1333.

16.   Petters, M.D. and S.M. Kreidenweis, *A single parameter representation of hygroscopic growth and cloud condensation nucleus activity.* Atmospheric Chemistry and Physics, 2007. **7**(8): p. 1961-1971.

17.   Gunthe, S.S., S.M. King, D. Rose, Q. Chen, P. Roldin, D.K. Farmer, J.L. Jimenez, P. Artaxo, M.O. Andreae, S.T. Martin, and U. Pöschl, *Cloud condensation nuclei in pristine tropical rainforest air of Amazonia: size-resolved measurements and modeling of atmospheric aerosol composition and CCN activity.* Atmos. Chem. Phys., 2009. **9**(19): p. 7551-7575.

18.   Rose, D., S.S. Gunthe, H. Su, R.M. Garland, H. Yang, M. Berghof, Y.F. Cheng, B. Wehner, P. Achtert, A. Nowak, A. Wiedensohler, N. Takegawa, Y. Kondo, M. Hu, Y. Zhang, M.O. Andreae, and U. Pöschl, *Cloud condensation nuclei in polluted air and biomass burning smoke near the mega-city Guangzhou, China – Part 2: Size-resolved aerosol chemical composition, diurnal cycles, and externally mixed weakly CCN-active soot particles.* Atmos. Chem. Phys., 2011. **11**(6): p. 2817-2836.

19.   Meskhidze, N., J. Xu, B. Gantt, Y. Zhang, A. Nenes, S.J. Ghan, X. Liu, R. Easter, and R. Zaveri, *Global distribution and climate forcing of marine organic aerosol: 1. Model improvements and evaluation.* Atmos. Chem. Phys., 2011. **11**(22): p. 11689-11705.

20.   Westervelt, D.M., R.H. Moore, A. Nenes, and P.J. Adams, *Effect of primary organic sea spray emissions on cloud condensation nuclei concentrations.* Atmos. Chem. Phys., 2012. **12**(1): p. 89-101.

21.   Cubison, M.J., B. Ervens, G. Feingold, K.S. Docherty, I.M. Ulbrich, L. Shields, K. Prather, S. Hering, and J.L. Jimenez, *The influence of chemical composition and mixing state of Los Angeles urban aerosol on CCN number and cloud properties.* Atmos. Chem. Phys., 2008. **8**(18): p. 5649-5667.

22.   Ervens, B., M. Cubison, E. Andrews, G. Feingold, J.A. Ogren, J.L. Jimenez, P. DeCarlo, and A. Nenes, *Prediction of cloud condensation nucleus number concentration using measurements of aerosol size distributions and composition and light scattering enhancement due to humidity.* Journal of Geophysical Research-Atmospheres, 2007. **112**(D10): p. 15.

23.   Asa-Awuku, A., R.H. Moore, A. Nenes, R. Bahreini, J.S. Holloway, C.A. Brock, A.M. Middlebrook, T.B. Ryerson, J.L. Jimenez, P.F. DeCarlo, A. Hecobian, R.J. Weber, R. Stickel, D.J. Tanner, and L.G. Huey, *Airborne cloud condensation nuclei measurements during the 2006 Texas Air Quality Study.* Journal of Geophysical Research-Atmospheres, 2011. **116**: p. 18.

24.   Levin, E.J.T., A.J. Prenni, B.B. Palm, D.A. Day, P. Campuzano-Jost, P.M. Winkler, S.M. Kreidenweis, P.J. DeMott, J.L. Jimenez, and J.N. Smith, *Size-resolved aerosol composition and its link to hygroscopicity at a forested site in Colorado.* Atmos. Chem. Phys., 2014. **14**(5): p. 2657-2667.

25.   Lance, S., A. Nenes, C. Mazzoleni, M.K. Dubey, H. Gates, V. Varutbangkul, T.A. Rissman, S.M. Murphy, A. Sorooshian, R.C. Flagan, J.H. Seinfeld, G. Feingold, and H.H. Jonsson, *Cloud condensation nuclei activity, closure, and droplet growth kinetics of Houston aerosol during the Gulf of Mexico Atmospheric Composition and Climate Study (GoMACCS).* Journal of Geophysical Research-Atmospheres, 2009. **114**: p. 21.

26.   Broekhuizen, K., R.Y.W. Chang, W.R. Leaitch, S.M. Li, and J.P.D. Abbatt, *Closure between measured and modeled cloud condensation nuclei (CCN) using size-resolved aerosol compositions in downtown Toronto.* Atmospheric Chemistry and Physics, 2006. **6**: p. 2513-2524.

27.   Medina, J., A. Nenes, R.E.P. Sotiropoulou, L.D. Cottrell, L.D. Ziemba, P.J. Beckman, and R.J. Griffin, *Cloud condensation nuclei closure during the International Consortium for Atmospheric Research on Transport and Transformation 2004 campaign: Effects of size-resolved composition.* Journal of Geophysical Research-Atmospheres, 2007. **112**(D10): p. 10.

28.   Padro, L.T., R.H. Moore, X. Zhang, N. Rastogi, R.J. Weber, and A. Nenes, *Mixing state and compositional effects on CCN activity and droplet growth kinetics of size-resolved CCN in an urban environment.* Atmospheric Chemistry and Physics, 2012. **12**(21): p. 10239-10255.

29.   Collins, D.B., A.P. Ault, R.C. Moffet, M.J. Ruppel, L.A. Cuadra-Rodriguez, T.L. Guasco, C.E. Corrigan, B.E. Pedler, F. Azam, L.I. Aluwihare, T.H. Bertram, G.C. Roberts, V.H. Grassian, and K.A. Prather, *Impact of marine biogeochemistry on the chemical mixing state and cloud forming ability of nascent sea spray aerosol.* Journal of Geophysical Research-Atmospheres, 2013. **118**(15): p. 8553-8565.

30.   Schill, S.R., D.B. Collins, C. Lee, H.S. Morris, G.A. Novak, K.A. Prather, P.K. Quinn, C.M. Sultana, A.V. Tivanski, K. Zimmermann, C.D. Cappa, and T.H. Bertram, *The*

Impact of Aerosol Particle Mixing State on the Hygroscopicity of Sea Spray Aerosol. Acs Central Science, 2015. **1**(3): p. 132-141.

31.   Swietlicki, E., H.C. Hansson, K. Hameri, B. Svenningsson, A. Massling, G. McFiggans, P.H. McMurry, T. Petaja, P. Tunved, M. Gysel, D. Topping, E. Weingartner, U. Baltensperger, J. Rissler, A. Wiedensohler, and M. Kulmala, *Hygroscopic properties of submicrometer atmospheric aerosol particles measured with H-TDMA instruments in various environments - a review.* Tellus Series B-Chemical and Physical Meteorology, 2008. **60**(3): p. 432-469.

32.   Wex, H., G. McFiggans, S. Henning, and F. Stratmann, *Influence of the external mixing state of atmospheric aerosol on derived CCN number concentrations.* Geophysical Research Letters, 2010. **37**.

33.   Cerully, K.M., T. Raatikainen, S. Lance, D. Tkacik, P. Tiitta, T. Petaja, M. Ehn, M. Kulmala, D.R. Worsnop, A. Laaksonen, J.N. Smith, and A. Nenes, *Aerosol hygroscopicity and CCN activation kinetics in a boreal forest environment during the 2007 EUCAARI campaign.* Atmospheric Chemistry and Physics, 2011. **11**(23): p. 12369-12386.

34.   Su, H., D. Rose, Y.F. Cheng, S.S. Gunthe, A. Massling, M. Stock, A. Wiedensohler, M.O. Andreae, and U. Poschl, *Hygroscopicity distribution concept for measurement data analysis and modeling of aerosol particle mixing state with regard to hygroscopic growth and CCN activation.* Atmospheric Chemistry and Physics, 2010. **10**(15): p. 7489-7503.

35.   Bzdek, B.R., M.R. Pennington, and M.V. Johnston, *Single particle chemical analysis of ambient ultrafine aerosol: A review.* Journal of Aerosol Science, 2012. **52**(0): p. 109-120.

36.   Frossard, A.A., L.M. Russell, S.M. Burrows, S.M. Elliott, T.S. Bates, and P.K. Quinn, *Sources and composition of submicron organic mass in marine aerosol particles.* Journal of Geophysical Research-Atmospheres, 2014. **119**(22): p. 12977-13003.

37.   Frossard, A.A., L.M. Russell, P. Massoli, T.S. Bates, and P.K. Quinn, *Side-by-Side Comparison of Four Techniques Explains the Apparent Differences in the Organic Composition of Generated and Ambient Marine Aerosol Particles.* Aerosol Science and Technology, 2014. **48**(3): p. V-X.

38.   Frossard, A.A., L.M. Russell, W.C. Keene, D.J. Kieber, P.K. Quinn, and T.S. Bates, *Regional Signatures in the Organic Composition of Marine Aerosol Particles.* Nucleation and Atmospheric Aerosols, 2013. **1527**: p. 543-546.

39.   Russell, L.M., L.N. Hawkins, A.A. Frossard, P.K. Quinn, and T.S. Bates, *Carbohydrate-like composition of submicron atmospheric particles and their production from ocean bubble bursting.* Proceedings of the National Academy of Sciences of the United States of America, 2010. **107**(15): p. 6652-6657.

40.   Slowik, J.G., D.J. Cziczo, and J.P.D. Abbatt, *Analysis of cloud condensation nuclei composition and growth kinetics using a pumped counterflow virtual impactor and*

aerosol mass spectrometer. Atmospheric Measurement Techniques, 2011. **4**(8): p. 1677-1688.

41.   Cahill, J.F., T.K. Darlington, C. Fitzgerald, N.G. Schoepp, J. Beld, M.D. Burkart, and K.A. Prather, *Online Analysis of Single Cyanobacteria and Algae Cells under Nitrogen-Limited Conditions Using Aerosol Time-of-Flight Mass Spectrometry.* Analytical Chemistry, 2015. **87**(16): p. 8039-8046.

42.   Collins, D.B., D.F. Zhao, M.J. Ruppel, O. Laskina, J.R. Grandquist, R.L. Modini, M.D. Stokes, L.M. Russell, T.H. Bertram, V.H. Grassian, G.B. Deane, and K.A. Prather, *Direct aerosol chemical composition measurements to evaluate the physicochemical differences between controlled sea spray aerosol generation schemes.* Atmospheric Measurement Techniques, 2014. **7**(11): p. 3667-3683.

43.   Moffet, R.C., R. O'Brien, A.P. Ault, D.B. Collins, M.J. Ruppel, D.Q. Pham, V.H. Grassian, A. Laskin, M.K. Gilles, and K.A. Prather, *Spectromicroscopic observation of sea spray composition and aging.* Abstracts of Papers of the American Chemical Society, 2014. **248**.

44.   Petters, M.D. and S.M. Kreidenweis, *A single parameter representation of hygroscopic growth and cloud condensation nucleus activity - Part 2: Including solubility.* Atmospheric Chemistry and Physics, 2008. **8**(20): p. 6273-6279.

45.   Quinn, P.K., D.B. Collins, V.H. Grassian, K.A. Prather, and T.S. Bates, *Chemistry and Related Properties of Freshly Emitted Sea Spray Aerosol.* Chemical Reviews, 2015. **115**(10): p. 4383-4399.

46.   Gunthe, S.S., D. Rose, H. Su, R.M. Garland, P. Achtert, A. Nowak, A. Wiedensohler, M. Kuwata, N. Takegawa, Y. Kondo, M. Hu, M. Shao, T. Zhu, M.O. Andreae, and U. Poschl, *Cloud condensation nuclei (CCN) from fresh and aged air pollution in the megacity region of Beijing.* Atmospheric Chemistry and Physics, 2011. **11**(21): p. 11023-11039.

47.   Rose, D., S.S. Gunthe, H. Su, R.M. Garland, H. Yang, M. Berghof, Y.F. Cheng, B. Wehner, P. Achtert, A. Nowak, A. Wiedensohler, N. Takegawa, Y. Kondo, M. Hu, Y. Zhang, M.O. Andreae, and U. Poschl, *Cloud condensation nuclei in polluted air and biomass burning smoke near the mega-city Guangzhou, China -Part 2: Size-resolved aerosol chemical composition, diurnal cycles, and externally mixed weakly CCN-active soot particles.* Atmospheric Chemistry and Physics, 2011. **11**(6): p. 2817-2836.

48.   Malecha, K.T. and S.A. Nizkorodov, *Photodegradation of Secondary Organic Aerosol Particles as a Source of Small, Oxygenated Volatile Organic Compounds.* Environmental Science & Technology, 2016. **50**(18): p. 9990-9997.

49.   Saukko, E., A.T. Lambe, P. Massoli, T. Koop, J.P. Wright, D.R. Croasdale, D.A. Pedernera, T.B. Onasch, A. Laaksonen, P. Davidovits, D.R. Worsnop, and A. Virtanen, *Humidity-dependent phase state of SOA particles from biogenic and anthropogenic precursors.* Atmospheric Chemistry and Physics, 2012. **12**(16): p. 7517-7529.

50.   Bates, T.S., P.K. Quinn, A.A. Frossard, L.M. Russell, J. Hakala, T. Petaja, M. Kulmala, D.S. Covert, C.D. Cappa, S.M. Li, K.L. Hayden, I. Nuaaman, R. McLaren, P. Massoli, M.R. Canagaratna, T.B. Onasch, D. Sueper, D.R. Worsnop, and W.C. Keene, *Measurements of ocean derived aerosol off the coast of California.* Journal of Geophysical Research-Atmospheres, 2012. **117**.

51.   Quinn, P.K., T.S. Bates, K.S. Schulz, D.J. Coffman, A.A. Frossard, L.M. Russell, W.C. Keene, and D.J. Kieber, *Contribution of sea surface carbon pool to organic matter enrichment in sea spray aerosol.* Nature Geoscience, 2014. **7**(3): p. 228-232.

Chapter 3   **The Impact of Aerosol Particle Mixing State on the Hygroscopicity of Sea-Spray Aerosol**

3.1   Abstract

Aerosol particles influence global climate by determining cloud drop number concentrations, brightness, and lifetime. Primary aerosol particles, such as those produced from breaking waves in the ocean, display large particle-particle variability in chemical composition, morphology, and physical phase state, all of which affect the ability of individual particles to accommodate water and grow into cloud droplets. Despite such diversity in molecular composition, there is a paucity of methods available to assess how particle-particle variability in chemistry translates to corresponding differences in aerosol hygroscopicity. Here, an approach has been developed that allows for characterization of the distribution of aerosol hygroscopicity within a chemically complex population of atmospheric particles. This methodology, when applied to the interpretation of nascent sea-spray aerosol (SSA), provides a quantitative framework for connecting results obtained using molecular mimics generated in the laboratory with chemically complex ambient aerosol. We show that nascent SSA, generated *in situ* in the Atlantic Ocean, displays a broad distribution of particle hygroscopicities, indicative of a correspondingly broad distribution of particle chemical composition. Molecular mimics of SSA organic material were used in the laboratory to assess the volume fractions and molecular functionality required to suppress SSA hygroscopicity to the extent indicated by field observations. We show that proper accounting for the distribution and diversity in particle hygroscopicity and composition are important to the assessment of particle impacts on clouds and global climate.
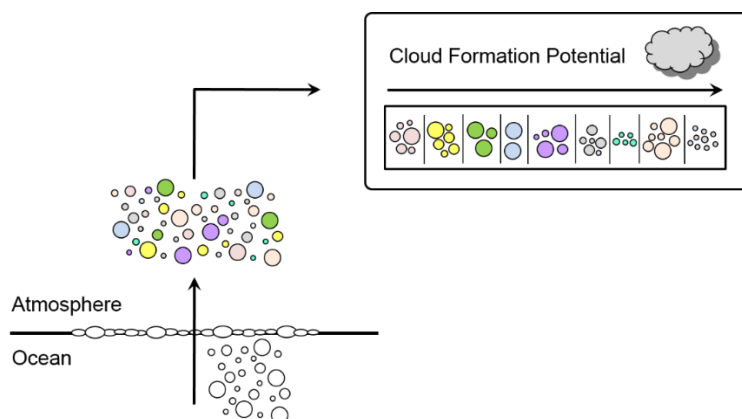
Figure 3.1 Schematic representation that sea-spray particles exhibit wide chemical diversity at the single particle level with consequent effects on cloud formation.

3.2 Introduction

Atmospheric aerosol particles impact global climate directly through interactions with incoming solar radiation, and indirectly by seeding the formation and controlling the properties of all cloud droplets, which alters Earth's radiation budget.[1] The ability of a particle to take up water from its surrounding environment and act as a cloud seed, or cloud condensation nucleus (CCN), is intimately linked to particle chemical composition, especially for particles with dry diameters less than 200 nm. [2] Measurements of the molecular composition of individual aerosol particles in this size regime are rare,[3] thus limiting our ability to connect heterogeneity in particle chemical composition with their ability to serve as CCN at a single particle level. Here, we present a new methodology for direct characterization of the distribution of aerosol hygroscopicity as driven by particle-particle compositional variability within a complex population of atmospheric particles. We demonstrate that this approach, when applied to nascent sea-spray aerosol (SSA), permits unique perspective on the influence that particle chemical diversity plays in determining the impacts of particles on climate. Further, we show that the generality of the approach permits quantitative comparison between laboratory generated molecular mimics with actual nascent SSA generated *in situ* in the Atlantic Ocean.

The hygroscopicity of an individual particle is a function of its chemical composition with, in general, inorganic salts leading to a more hygroscopic particle and organic materials leading to a less hygroscopic particle.[4] Hygroscopicity displays further variability within the organic and inorganic component classes, dependent upon factors such as solubility, molecular weight and surface tension. The hygroscopicity of particles can be characterized through measurements of their ability to activate into droplets or activation efficiency, i.e. the fraction of particles of a given size that grow into droplets when exposed to a given water supersaturation (s), or $f_{CCN}(s)$. More hygroscopic particles have larger the activation efficiencies. Such determinations are referred to as size-resolved CCN (SR-CCN) measurements. The activation efficiency for particles of fixed composition is also size dependent, with larger particles having a larger $f_{CCN}(s)$ at a given s. Therefore, particle hygroscopicity is routinely quantitatively characterized by converting direct measurements of a selected particle diameter (D_p) and the critical supersaturation (s_{crit} – where 50% of the particle population has activated) to a single parameter, κ;[5] smaller κ-values correspond to less hygroscopic particles and vice versa. The so-called κ-Köhler theory separates the intrinsic hygroscopicity (composition-dependence) from the particle size dependence, thereby allowing for assessment of the influence of composition more specifically. Typical values of κ range between $0 - 1.4$, with lower values generally associated with less (or non-) soluble organic compounds, and higher values generally associated with soluble inorganic compounds.[5, 6] For SSA particles, composition is dictated both by the chemistry and biology that occurs in the ocean to produce a wide variety of organic compounds, especially near the sea surface, and by the transfer of those compounds to SSA.[7, 8] Size-resolved particle composition measurements have demonstrated that the organic fraction increases as particle size decreases, when considered either by mass[9-11] or by number.[12, 13] The hygroscopicity of SSA in the sub-micron size regime has been previously found to vary with size,

especially for particles with diameters below 100 nm, which has been interpreted as indicating enrichment of organic material in smaller particles.[2, 14, 15]

On top of such general enrichment in SSA organic content with decreasing particle size, individual nascent SSA particles also display a wide diversity of individual particle types.[12, 13, 16-19] These different particle types have distinct compositions with respect to the relative abundance and chemical nature of the organic material. Such mixing-state effects will influence the actual overall activation behavior of a distribution of particles, as always exists in the ambient atmosphere and in some laboratory experiments. Despite this complexity, typical analyses of ambient particle CCN activation assume that all particles of a given size have identical composition (i.e. are internally mixed), and therefore report effective κ-values that may or may not fully describe the actual impacts of the distribution. As just a few examples, effective κ-values have been reported for pristine aerosols in the Amazonian rainforest,[20] aged aerosols in the highly polluted Chinese city of Guangzhou,[21] and nascent marine SSA from the WACS I cruise in the Atlantic Ocean.[14] Importantly, global models have suggested that aerosol mixing state can impact CCN concentrations by up to 20% in the case of marine SSA,[22, 23] indicating that improved constraints on aerosol mixing state and how this varies by source are still necessary for robust determination of CCN concentrations.

Direct measurements of CCN concentrations are often compared to volume mixing based predictions from Köhler theory, where incorporation of size-dependent chemical composition results in model-measurement agreement to within 10-20%,[24-30] but these still do not deal with the inherent particle-particle compositional variability at a given size. Padró et al.[31] found that accounting for external mixing improved CCN number concentration predictions (within 10-20% of measured), while the common internal mixing state assumption can have a significantly greater error associated with it (up to 100%), in agreement with prior studies focused on externally-mixed aerosols.[24, 25]

Of specific relevance to this work, Collins et al.[32] investigated the CCN activity of SSA generated from a large-scale mesocosm seawater experiment and found that the assumption that all particles were compositionally identical (internally mixed) was insufficient to explain the temporal changes in the SSA particle hygroscopicity. Instead, a model in which the SSA was assumed to contain a diversity of particles with distinct compositions (externally mixed) was needed.[32] The apparent need for robust methods that can account for mixing state in the interpretation of CCN measurements is supported by measurements of particle growth due to water uptake under subsaturated conditions, which often indicate the co-existence of particles with very different compositions and hygroscopicities.[33, 34] Despite the evident need for CCN-specific hygroscopicity analyses that routinely account for the actual diversity of particles, few CCN studies have considered implementing a distribution of hygroscopicity values, or how a distribution of hygroscopicity values may be detected using SR-CCN measurements.[35, 36]

In what follows, we develop a quantitative framework for assessing the distribution of aerosol hygroscopicity for populations of sub-100 nm aerosol particles. The methodology bridges molecular mimics of increasing complexity, from single-component particles to internally and externally-mixed heterogeneous populations, with nascent SSA particles generated from synthetic and microcosm phytoplankton bloom experiments and from the ambient surface ocean waters. Implications of this methodology for understanding chemical diversity and climate impacts of SSA particles specifically, and atmospheric aerosol particles in general, are discussed.

3.3   Influence of Mixing State on CCN Activity

In this section, a bottom-up approach is used to facilitate the development of a quantitative methodology to assess the influence of particle mixing state on CCN activity, starting with chemically simple (single-component) systems and systematically increasing the system complexity with respect to the particle-particle chemical diversity. The hygroscopicities of

internal and external particle mixtures of known composition have been characterized through measurement of CCN activation curves (Fig. 2.8.1). The compounds studied here were selected based on the consideration of the evolution of surface seawater chemical composition throughout the successive stages of an ocean phytoplankton bloom.[37-39] These SSA organic compound mimics included: a refractory hydrocarbon material (cholesterol), a sugar (galactose), a lipopolysaccharide (LPS, from *E. coli* 0111:B4), a protein (bovine serum albumin), and a fatty acid (DPPA, dipalmitoyl phosphatidic acid) (Table 3.1). The pure organic SSA mimics were considered either individually or as mixtures with synthetic sea salt, which is composed of inorganic ions in representative seawater concentrations. Model external mixtures were generated by multiple atomizers or nebulizers operating in parallel (*3.7 Methods*).

3.3.1   Single-Component SSA Mimics

κ-values were experimentally determined for the five pure organic SSA mimics and for synthetic sea salt from measurement of their activation curves (Table 3.1). These marine-focused measurements expand the database of compounds for which κ-values have been determined in the laboratory, which includes inorganic salts[5] and slightly soluble organics[40-42] that had generally been chosen based on their relevance to terrestrially-derived organics. It was not possible to determine κ-values for cholesterol specifically due to its poor solubility in water. Variability in the measured κ-values for the synthetic sea salt was observed between multiple lots as indicated by the range in values presented in Table 3.1. The κ-values measured for the organic compounds do not correlate directly with solubility (Table 3.1). The largest κ-value was observed for DPPA, which has the lowest solubility (excluding cholesterol), which we hypothesize is due in part to formation of vesicle structures by DPPA (critical micelle concentration = 0.46 nM) in an aqueous matrix. Despite its high solubility, the κ-value for galactose was lower than DPPA,

possibly due to the initially dry galactose particles existing in a highly viscous, glassy state that can impede water uptake.[43] Further, deviations between measured and predicted κ-values (based on solubility alone) may reflect differences in droplet surface tension due to surface partitioning.[44, 45] The smallest κ-values were measured for LPS and albumin, which were of intermediate relative solubility.

Table 3.1: Literature solubilities[46] and measured κ-values for single-component, pure, sea-spray aerosol model compounds.

Compound	Solubility (g/L)	κ		
Sea salt	360^{+}	$0.800 - 1.106^{++}$		
Cholesterol	5×10^{-3}	n/a		
Galactose	683	0.198	±	0.028
LPS	5	0.038	±	0.004
Albumin	40	0.031	±	0.002
DPPA	< 1	0.297	±	0.039

[+]The solubility of synthetic sea salt was assumed to be equivalent to sodium chloride.
[++]The κ-value for synthetic sea salt was found to vary from lot to lot. The reported κ-values indicate the range of obtained values.

3.3.2   Internally Mixed SSA Mimics

Experimental κ-values were determined for two-component internal mixtures of synthetic sea salt (κ = 1.22 for the specific lot used in this experiment) and galactose (κ = 0.198) of varying relative composition (Fig. 2.2). The κ value of an internal mixture ($\kappa_{mix,int}$) is commonly estimated from volume-mixing rules, where $\kappa_{mix,int} = \Sigma\varepsilon_i\kappa_i$ and ε_i is the volume fraction of each compound.[5] For a two-component mixture, the predicted $\kappa_{mix,int}$ varies linearly with ε_{org} and is dependent on the κ-value of the pure compounds. The observed and predicted κ-values for the sea salt:galactose mixtures agreed to within 20% (Fig. 2.2), consistent with previous laboratory observations for other mixtures.[5]

Field determinations of effective κ-values for nascent SSA[14] with dry diameters of 40 – 100 nm range between 0.4 – 0.9, which corresponds to ε_{org} between ca. 80% and 25% based on the sea salt:galactose mixture results (Fig. 2.2). Because the density of sea salt is similar to that of galactose, this corresponds to a mass fraction of approximately the same value. Variability in the actual density of ocean organics can complicate the volume to mass fraction conversion relationship. Previous studies suggest that total and/or water insoluble organic mass fractions for marine SSA are on the order of 80% for sub-100 nm particles,[10, 11] though only around 25% of this mass is water soluble organics such as galactose.[9] With regards to CCN, distinguishing between the contributions of water soluble versus water insoluble organics can additionally be important in obtaining closure.[47] These findings provide context for the validity of an 80% organic particle and how that may affect SSA hygroscopicity, though additional work needs to be done to better characterize the solubility effects of SSA organics, especially in light of the results for DPPA.
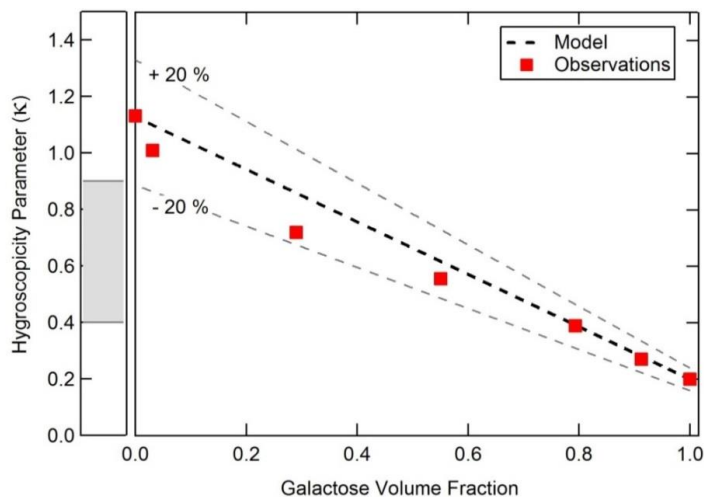
Figure 3.2: Predicted κ hygroscopicity parameter values for internally mixed, two-component particles of sea salt:galactose as a function of the organic volume fraction (black dashed line), compared with measured κ-values for several sea salt:galactose ratios (red squares). The gray bar on the left shows the range of effective κ-values observed for primary nascent SSA in the marine boundary layer.[14]

3.3.3 Externally Mixed SSA Mimics

The major existing framework for both measuring supersaturated aerosol hygroscopicity and interpreting the observations relies on the assumption that particles of a given size are internally mixed. However, field studies[48] and laboratory investigations[12, 13] have shown that the ensemble of nascent SSA particles is not internally mixed, but instead, individual particles exhibit a wide range of per-particle organic volume fractions and organic types. Further, the observed variability and absolute values of effective κ-values for nascent SSA particles that were produced during a large scale mesocosm experiment has been interpreted as indicating that explicit accounting of the particle mixing state in framework for interpreting CCN measurements is needed. One such framework was proposed by Su et al.,[36] who calculated cumulative distribution functions from CCN activation curves, which can be deconstructed into cumulative hygroscopicity distributions. Here, we expand on this framework and provide the explicit validation that has thus far been missing.

A necessary first step in assessing the extent to which CCN activation curves can be used to resolve aerosol mixing state is to characterize the behavior of known external mixtures using high-resolution SR-CCN measurements. It is commonly assumed that activation curves can be fit using a Boltzmann sigmoidal. The activation curve for a single particle type is associated with a characteristic sigmoid slope, or width in f_{CCN} versus s, that is set by the transfer function of the DMA (Fig. 2.8.2) and the distribution in s in the SR-CCN. Here, the average slope of the sigmoidal fits for all of the pure compounds studied was 0.0180 ± 0.0095 for κ-values between $0.031 - 1.106$, demonstrating uniform hygroscopicity amongst the particle population. Since the inherent methodologically-determined slope is very small, in theory the activation of the individual sub-populations of particle types within the overall distribution should be observable if the scanning resolution is sufficiently high. Here, this is examined explicitly by measuring activation curves for external mixtures of particles with known, but differing composition.

As a first test, activation curves were measured for pure sea salt particles, pure galactose particles, a 1:1 internal mixture of sea salt:galactose particles and a 1:1 external mixture (Fig. 2.3A). A small fraction (usually < 10%) of the aerosol population is doubly charged post size selection, and is observed as a plateau of activated particles at a lower s value with a sigmoid height much smaller than that of the majority singly charged population. This experimental artifact has been accounted for following the approach of Rose et al.,[49] whereby the doubly and singly charged populations are treated as distinct. The resulting normalized activation curves for this study, such as those in Fig 2.3A, are for the singly charged particles in the population. The activation curve for the external mixture is characterized by two clearly distinguishable sigmoids, which is distinct from the pure compounds and the 1:1 internal mixture, which are all characterized by a single sigmoid. This result highlights the capability of measurements at high s resolution to distinguish aerosol mixing state for sub-populations of particles that have different κ-values. In this example the fraction of particles that activated at the s_{crit} for galactose (0.740% s)

was 0.45, and the fraction of particles that activated at the s_{crit} for this sea salt lot (0.365% s) was 0.55, well within the uncertainty of the experimental number fractions. This demonstrates that the sigmoid analysis of high-resolution SR-CCN measurements can be used to quantitatively determine the relative concentrations of the externally mixed particle types and that the number of sigmoids corresponds to the number of particle types (with respect to hygroscopicity) while the magnitude of each sigmoid corresponds to the relative abundance of each type.
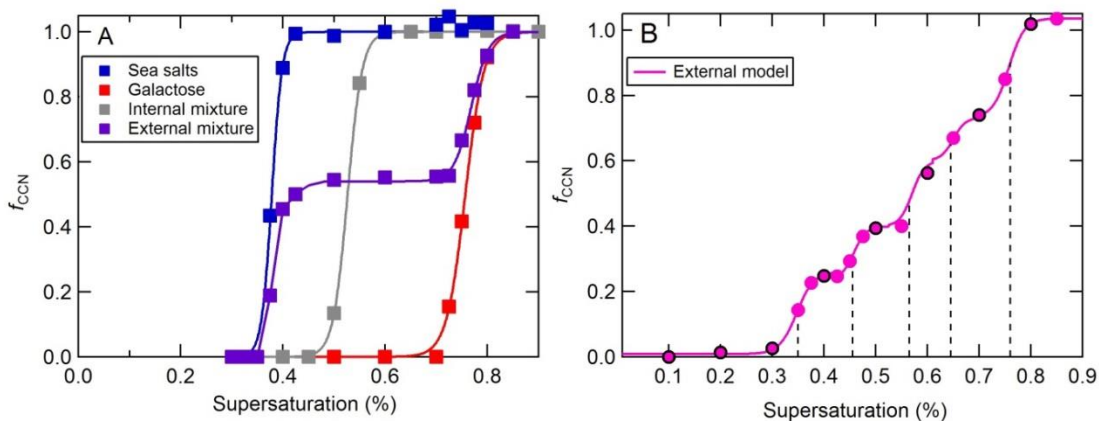
Figure 3.3: A) CCN activation curves for 50 nm size selected particles of sea salt (blue), galactose (red), and an internal and external mixture of 1:1 sea salt:galactose (gray and purple respectively). B) CCN activation curve for 50 nm size selected particles from an external mixture of five particle types: i) sea salt particles; ii) a 43:57 by mass sea salt:galactose mixture; iii) a 22:78 sea salt:galactose mixture; iv) a 9:91, sea salt:galactose mixture; and v) pure galactose particles. The points with black circles indicate the points that would have been measured in an SR-CCN experiment at typically-used resolution, while the pink points are the actual higher resolution data collected here. The vertical dashed lines show the theoretical s_{crit} for each particle type in the external mixture.

The two-component system above has been expanded upon by measuring the activation curve for an externally-mixed system with five distinct particle types, ranging from pure sea salt to pure organic. By systematically increasing the chemical complexity of the system, it is possible to assess the extent to which high s resolution SR-CCN measurements can provide quantitative information on the distribution of κ-values in a given particle population. The particle types considered were internal mixtures with sea salt:galactose mass ratios of: 100:0, 43:57, 22:78, 9:91

and 0:100, with corresponding $\kappa_{int,mix}$ values of 0.83, 0.48, 0.34, 0.26 and 0.2, respectively. The relative number concentrations of the different particle types were 0.2, 0.12, 0.28, 0.10 and 0.3. If all of the particle types were mixed together in these proportions, the overall $\kappa_{int,mix} = 0.40$ ($s_{crit,50nm} = 0.52\%$). A key observation is that clear steps are evident in the activation curve that correspond to the activation of the individual particle types (Fig. 2.3B). This demonstrates that it is possible to resolve the individual particle types within a chemically complex mixture in the activation curve when fine enough steps are taken in s. However, the overall activation curve has a slope that is approximately eight times broader than that of any pure compound or internal mixture when fit with a single sigmoid (Fig. 2.3B). This indicates that broadening of the activation curve occurs for an external mixture of particles that have a range of κ-values, generally consistent with the ambient observations.[7, 21, 35] It also demonstrates that, with increasing chemical complexity, it is increasingly difficult to fit a distinct number of sigmoids to determine the number of distinct particle types, as the activation curve becomes a broad continuum of activation for multiple populations. A second important observation is that the effective κ that is determined from the observed s_{crit} ($s_{crit,obs} = 0.58\%$) is smaller than that predicted from internal mixing of all the particle types in their known proportions. Specifically, the effective $\kappa_{obs} = 0.32$, whereas the predicted $\kappa_{int,mix} = 0.40$ (corresponding to $s_{crit,50nm} = 0.52\%$).

Using this well-constrained, yet complex (five-component) model system as a test bed, a model framework for fitting the multi-component activation curve has been developed in which the overall activation curve is quantitatively considered in terms of the contributions from the individual components. Specifically, the five-component external mixture activation curve was fit to five summed sigmoidal curves that were centered at the anticipated s_{crit} values that corresponded to the predicted κ-values of each particle type (Fig. 2.3B). The relative concentration of each particle type was then deduced from the height of each individual sigmoid,

and the derived fractions agreed to within 10% of the experimental values. This serves as proof of concept that, although complex systems result in visibly broad activation curves for a continuum of particle types, activation curves generated from SR-CCN data sets can be considered within a framework that treats the overall activation curve as the linear combination of the activation of individual particle types (i.e. that have distinct κ-values) in an external aerosol mixture.

These bottom-up observations, along with the multi-component activation framework, provide an experimental validation of the general idea that the slope of an activation curve when fit to a single sigmoid is related to the extent of chemical heterogeneity, with a wider sigmoid corresponding to greater chemical heterogeneity or more particle types.[31, 35, 47] For example, Cerully et al.[35] showed that the absolute value of the sigmoid slope was usually much larger for ambient aerosols than could be explained by the inherent width set by experimental factors, which they interpreted as an indication of the extent of external mixing. However, the use of a single sigmoid during fitting inherently assumes that there is a particular, continuous distribution in mixing state and therefore does not permit quantitative assessment of aerosol populations that display extreme heterogeneity, such as those shown in Fig. 2.3, and that preclude fitting with a single sigmoid. The multi-component activation framework has the ability to allow for more comprehensive examination of the particle mixing state compared to single-sigmoid methods, and also facilitates explicit determination of actual hygroscopicity distributions, as is developed further below.

3.4   Hygroscopicity Diversity of Sea-Spray Aerosol Particles

The bottom-up assessment and analysis methodology of the influence of particle mixing state on CCN activation curves developed above is extended and applied to the interpretation of activation curves for nascent SSA particles, which have been shown to exist as a complex, external mixture of varying particle types.[12, 13] In one case, naturally more complex internal and

external mixtures of SSA specifically were generated in the laboratory from synthetic and microcosm phytoplankton blooms in a manner analogous to wave breaking in the ocean using a Marine Aerosol Reference Tank (MART) (Fig. 2.8.3).[50] In a second case, nascent SSA particles were generated directly from the ocean surface using the NOAA PMEL sea-sweep[51] during the WACS I cruise in the Atlantic Ocean.[14] The observed activation curves for these systems have been interpreted using the concept of treating activation curves as a summation over individual sigmoids, as developed in Section 2.4. However, one challenge in developing a broadly applicable framework for external mixing is that it is best applied to SR-CCN data sets collected with high resolution in s, in which case explicit fitting of distinct sigmoids is possible (Fig. 2.3B), but many data sets already exist that were collected with moderate to low s resolution. Further, the use of high s resolution requires longer overall scan times, which may not be amenable to all experiments.

We have therefore generalized the explicit multiple-sigmoid framework as a κ "basis-set" model in which the fraction of activated particles in a sample population can be deconstructed into prescribed hygroscopicity bins. This relaxes the need for the distinct steps in the activation curve, which are evident in the model five-component system, to be clearly observable for robust data fitting. In the general model, a range of κ-values is selected and divided logarithmically into bins, corresponding to s_{crit} bins of equal magnitude. For this study a κ range between 0 and 1.4 was used with six equivalent bins in s. The impact of κ bin resolution on our results is shown in Fig. 2.8.4. These κ bins are converted to equivalent s_{crit} bins for the selected particle diameter. The observed normalized activation curves are integrated between sequential s_{crit} basis-set values (left-edge centered) to calculate the relative abundance of particles in each bin, resulting in a number-weighted κ distribution. The basis-set methodology extends beyond the general shape analysis of Su et al.[36] by generating an actual distribution of κ-values that characterizes the

sample population. The basis-set methodology provides an explicit measure of mixing state diversity, in contrast to the traditional ensemble average κ value calculated using the s_{crit} of the entire activation curve, which assumes the population is internally mixed. The general features of the κ basis-set model permit extension of this analysis to any SR-CCN measurement, whether high or typical resolution, to determine κ distributions for samples ranging from simple model to complex ambient systems.

The basis-set model has been applied to SR-CCN measurements on the following marine-relevant systems: the laboratory generated (i) two- and (ii) five-component external mixtures discussed above; nascent SSA from (iii) synthetic and (iv) microcosm phytoplankton bloom experiments conducted in a MART[50]; and (v) nascent SSA generated from the surface ocean using the sea-sweep during the WACS I cruise in the Atlantic Ocean.[14] The synthetic bloom was produced from synthetic seawater after sequential addition of the five marine organic mimics in Table 1 (Fig. 2.8.5). The transfer of organic species from the bulk water to aerosol phase during the synthetic bloom experiment was confirmed by measuring distributions (ranging from 0.1 – 0.3 organic volume fraction) of organic volume fractions by atomic force microscopy (AFM) for aerosol particles with diameters between 300-500 nm (Fig. 2.8.6). The measurements for the microcosm bloom were performed at the beginning and end of the phytoplankton bloom life cycle for a bloom grown from ocean water collected off the Scripps Pier in La Jolla, CA; only the measurements made at the end are shown here, as no substantial difference was found between the measurements made at the beginning and end, indicating that biological productivity did not impact measured hygroscopicity distributions. The WACS sea-sweep measurements assessed here were made both within Georges Bank,[14] a location where the surface chlorophyll-*a* concentration was relatively high, indicating fairly biologically active waters and within the oligotrophic Sargasso Sea, a location where the surface chlorophyll-*a* concentration was

relatively low. As no substantial differences were found between the measurements at these two

locations, only the Georges Bank results are shown here.
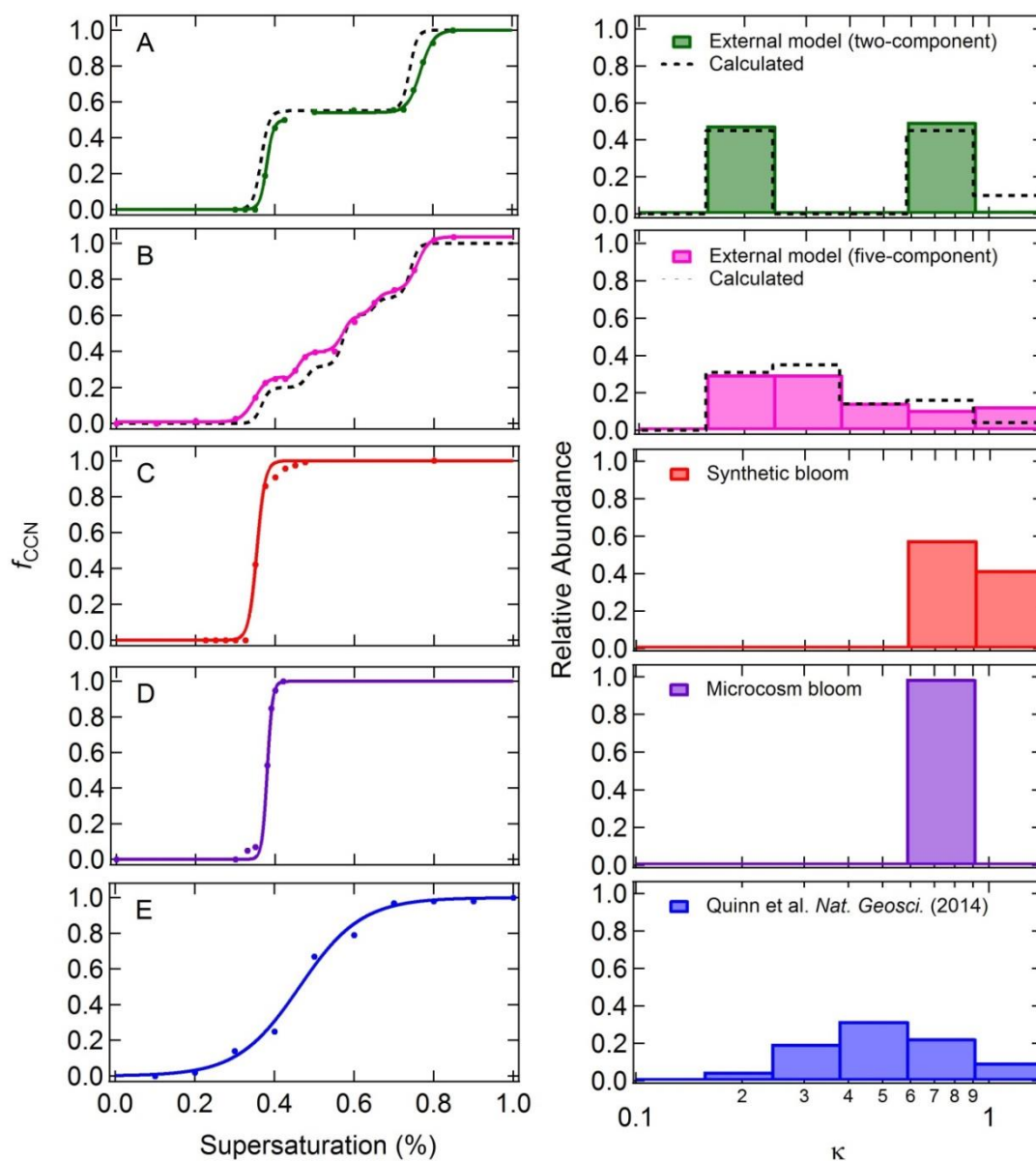
Figure 3.4: (left) SR-CCN activation curves and (right) κ distributions as determined from analysis of high-resolution *s* scans of model (A) two-component and (B) five-component externally mixed populations, laboratory based (C) synthetic and (D) microcosm phytoplankton bloom experiments conducted in a MART, and (E) from underway measurements of nascent SSA generated by the sea-sweep during the WACS cruise in the Atlantic Ocean.

The resulting κ distributions are distinct for each system, highlighting the sensitivity of the κ basis set method to the distribution of particle mixing state (Fig. 2.4). When applied to the two-component and five-component systems, the expected κ distribution is generally recovered, although some edge effects are evident (Fig. 2.4A-B) where multiple κ bins are populated for the same model component as a result of the finite κ bin width and activation curve integration. It is also important to note that due to the variation in κ for different lots of sea salt, the "salt" κ bin appears at different values between model systems. The activation curves for both the synthetic and microcosm phytoplankton bloom experiments are relatively sharp, and the κ distributions are correspondingly relatively narrow (Fig. 2.4C-D). This indicates a small degree of mixing state diversity for these dry 50 nm SSA and a particle population that was largely internally mixed with respect to hygroscopicity. The most probable κ value was determined to be 0.6-0.7, which translates to an ε_{org} = 0.45-0.57, assuming that the organic component had a pure κ value of 0.2. This range is somewhat larger than the ε_{org} determined by AFM (median ~ 0.2), although is likely explained by the AFM having characterized particles that were >50 nm, specifically 300-500 nm.

A much wider distribution of κ-values was observed for nascent SSA generated by the sea-sweep during the WACS I cruise (Fig. 2.4E) compared to the synthetic and microcosm bloom experiments. This suggests that a wide variety of particle types were emitted during that experiment. The range of derived κ-values indicates that the nascent SSA had compositions ranging from purely sea salt to purely organic, providing a quantitative explanation for the observed breadth of the SR-CCN activation curves (Fig 2.4E). However, the suggested abundance of SSA with purely sea salt composition is potentially overestimated by the presence of doubly charged particles, which have been accounted for in the laboratory studies. The κ distribution peaks around κ = 0.26, suggesting that a substantial fraction of the nascent SSA particles had large organic fractions, with ε_{org} > 80%. Overall, application of the κ basis-set

methodology to these various case studies demonstrates the potential for high-resolution SR-CCN measurements to be used in the determination of the distribution of κ-values, which is related to the particle mixing state diversity and goes beyond the typically-reported effective κ, which may not actually represent the true system average, nor characterize the actual behavior of the distribution within the atmosphere.

3.5   CCN in Marine Environments and Beyond

The broader implications towards cloud droplet properties of considering atmospheric particulates as having unique distributions of particles with different chemical composition (and therefore different hygroscopicities), as opposed to an internal mixture, are illustrated as a thought experiment in Fig. 2.5. The particle-particle chemical diversity within a given air mass, can be highly variable and is determined by the fundamental diversity in sources (such as those illustrated in Fig. 2.4), chemical transformations of atmospheric particles, and mixing of different air masses.[52] This chemical diversity is represented here by using a variety of κ distributions of varying shape (Fig. 2.5C). Using these distributions, the ratio between the number of particles that would activate at a given supersaturation for an external mixture versus an equivalent internal mixture (i.e. an internal mixture where the κ is calculated using volume mixing rules) has been calculated as $R_{CCN,E/I}(s) = [CCN]_{external}/[CCN]_{internal}$. The resulting $R_{CCN,E/I}$ values characterize the extent to which treating the particle population as an internal mixture leads to an under ($R_{CCN,E/I} < 1$) or over ($R_{CCN,E/I} > 1$) prediction in the actual fraction of CCN activated particles. A representative log-normal particle size distribution has been used (median $D_p = 80$ nm and $\sigma_g = 1.7$) and, although particle composition can be size dependent, each particle type (i.e. different κ) was assumed to have the same overall size distribution shape (Fig. 2.8.7).

The importance of considering the particle mixing state explicitly depends on both the nature of the κ distribution and on the supersaturation (Fig. 2.5A). The $R_{CCN,E,I}$ exhibit a distinct minimum with s for all κ distributions, around $s = 0.25\%$ for the size distribution used here, and are greater than unity at all but the smallest s ($<0.1\%$). This indicates that an external mixing assumption will generally underestimate the extent of cloud droplet activation. The $R_{CCN,E/I}$ at larger s asymptotically approach unity because as s increases, an increasingly large fraction of the total particle number can activate (Fig. 2.5B). The calculated minimum $R_{CCN,E/I}$ range from close to 1 for relatively narrow κ distributions (e.g. Mixture 5) to < 0.9 for broad κ mixtures comprised of particles with very different κ-values. The calculated minimum $R_{CCN,E/I}$ generally increases as the diversity of and difference between particle types increases with respect to their κ-values. The smallest $R_{CCN,E/I}$ values occur for mixtures where the less hygroscopic particle type is in higher abundance than the more hygroscopic particle type. The results shown in Fig. 2.5 are particular to the assumed size distribution, and the s at which the minimum in $R_{CCN,E/I}$ occurs is nominally linked to the overlap between the median D_p that characterizes the distribution and the s_{crit} vs. size relationship for the internally mixed particles (Fig. 2.8.8). Consequently, the position of the $R_{CCN,E/I}$ minimum increases if the median D_p were assumed smaller, and vice versa, and is more sensitive to shifts towards smaller sizes. However, shifts in the assumed D_p do not impact the minimum value of $R_{CCN,E/I}$ (Fig. 2.8.9). The overall s dependence of $R_{CCN,E/I}$ indicates that proper accounting for mixing state will generally have a larger impact on cloud droplet properties in cloud systems where the maximum s remains below approximately 0.5%, such as those typically associated with stratocumulus clouds where typical values for s are around 0.2%.
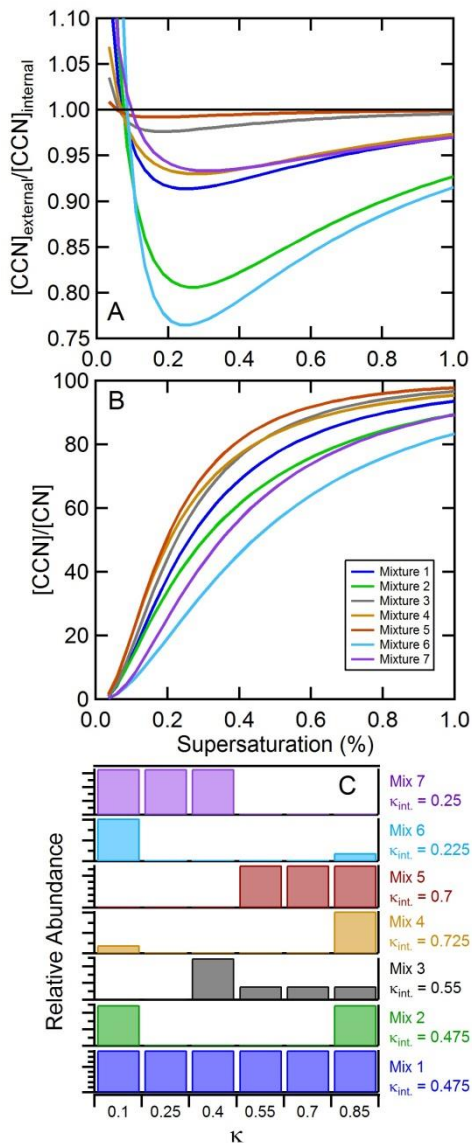
Figure 3.5: (A) The ratio between the number of particles activated (i.e. [CCN]) for an external mixture versus an internal mixture of particles and (B) the percent of particles activated for the external mixing case as a function of *s* for the κ distributions shown in (C). The associated κ-value for each distribution, assuming internal mixing, is shown next to the distribution.

3.6   Conclusions

A framework for the interpretation of CCN activation curves that accounts for diversity in individual particle hygroscopicity, which is driven by compositional diversity, has been introduced. The capabilities of this multi-component framework were demonstrated using molecular mimics in which the activation of internally and externally mixed particle distributions

of varying complexity was measured. The molecular mimics considered here were of particular relevance to marine environments in which SSA particles with a wide range of individual particle compositions are known to be generated. It was shown that by considering a CCN activation curve as a sum of activation curves for individual particle types (i.e. particles with distinct composition and hygroscopicity), the relative populations of these particle types can be retrieved. This represents an important advance over typical methods, which consider only the effective behavior and underplay the complicating influence of particle mixing state. The new framework was applied to the interpretation of laboratory and field observations of nascent SSA particles, which are complex mixtures of particle types with varying composition, to retrieve population-weighted distributions of κ hygroscopicity parameters. The importance of considering mixing state effects when interpreting the activation of such complex mixtures is apparent in the retrieved κ distributions, especially in the case of the field observations for which very broad distributions are obtained, indicating that a wide diversity of particle types existed. Proper accounting for particle mixing state was shown to be important to the assessment of the proper influence of particle composition, and more importantly compositional diversity, on clouds and global climate.

3.7   Methods

Values of κ were measured for 50 nm dry diameter particles composed of single compounds or their internal and external aerosol mixtures using a SR-CCN method (Fig. 3.6). The analysis can also be extended to particles with dry diameters other than 50 nm (Fig. 3.15). Briefly, for each system, the ratio between the total particle number concentration (CN) and the cloud active particle concentration (CCN) was measured as a function of supersaturation (s), from s between $0.1 - 1.0\%$, with $f_{CCN}(s) = [CCN]/[CN]$. The s_{crit} values for each given chemical system were determined either by visual inspection or fitting of a sigmoid to the observed activation curves (f_{CCN} versus s), from which effective κ-values were determined[5] (larger s_{crit} correspond to

smaller κ). The SR-CCN measurements were made using high s resolution, up to four points per 0.1% s (see SI). This is a much higher resolution than is commonly used[14] and was found to provide more accurate constraints on the shape of the activation curve. The shapes of the activation curves and the associated s_{crit} and κ-values for the pure compounds and internal mixtures used in this study were highly dependent on the s resolution used, especially when there were few f_{CCN} measurements near the s_{crit}. The collection of high s resolution scans enables determination of well-constrained κ-values and very sharp SR-CCN activation curves. Activation curves were measured for internal and external mixtures of varying chemical complexity that were generated using a few different methods (see SI for more details). Simple internal mixtures (in which all particles have the same composition) of pure compounds and model multi-component systems were generated by atomization or nebulization.

3.8   Supporting Information

3.8.1   Supersaturated Hygroscopicity Measurement

3.8.1.1   Size-Resolved Cloud Condensation Nuclei System (SR-CCN)

The size resolved cloud condensation nuclei system (SR-CCN) consisted of three stages: 1) aerosol particle generation, ii) size selection, and iii) measurement of cloud active fraction. The aerosol sources are described in detail in section 2.8.1, and the size selection is detailed below in section 2.8.3.2. After size selection, the monodisperse aerosol population was split between a condensation particle counter (CPC, TSI model 3787) which provides a measurement of total aerosol count, and a CCN counter (CCNc, DMT model CCN-100), which provides a measurement of cloud active aerosols as a function of supersaturation. These two measurements were ratioed to generate a cloud active fraction (f_{CCN} = [CCN]/[CN]) for a number of supersaturation settings to generate the resulting activation curves (f_{CCN} versus s).

$$F(CCN/CN) = 3/5 = 0.6$$
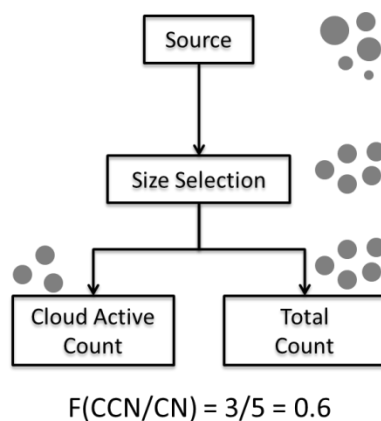
Figure 3.6: Experimental schematic for the SR-CCN system. For the hypothetical scenario illustrated, five particles are measured by the condensation particle counter, while the supersaturation settings of the CCN counter result in a measurement of three particles. These measurements are ratioed to provide a cloud active fraction; in this case 3/5 or 0.6.

3.8.2   Aerosol Size Selection

3.8.2.1   Differential Mobility Analyzer (DMA) Transfer Function

Monodisperse particles were selected from the polydisperse particle distribution according to their mobility diameters using a differential mobility analyzer (DMA, TSI model 3071). The monodisperse particle stream is sent to the CPC and CCNc for measurement of the activation curves as discussed in Section 2.3.1. All SR-CCN measurements included in this study were performed with a DMA sheath:sample flow rate ratio of 10:1.

The degree of polydispersity associated with the size-selected aerosol population was characterized by measuring the size distribution of the monodisperse particle stream. The monodisperse particles were sampled into a second DMA (TSI model 3081), behind which was a condensation particle counter (CPC, TSI model 3010). The second DMA+CPC were used together as a scanning mobility particle sizer to measure the distribution of the monodisperse aerosol population (Fig. 3.7). The distribution centered at 51.4 nm exhibited a full width half maximum of approximately 5 nm.
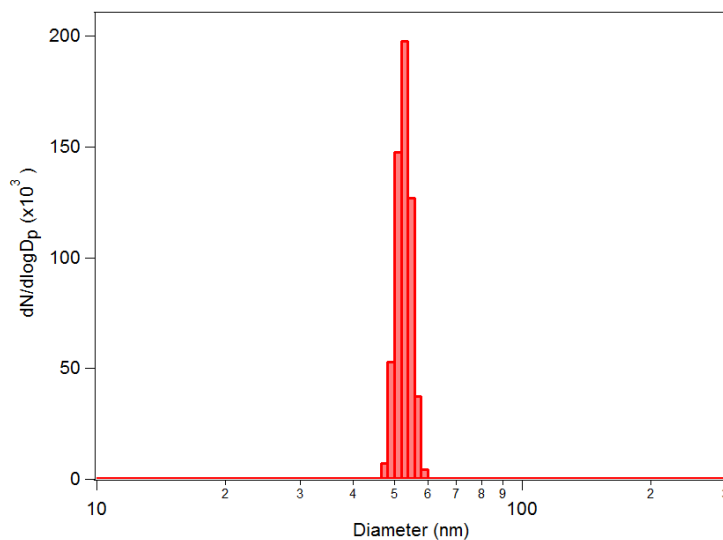
Figure 3.7: Scanning mobility particle sizer (SMPS) distribution of 50 nm size selected aerosols.

3.8.3   Aerosol Generation

3.8.3.1   Pure Compounds and Model Mixtures

Aerosol samples were generated in a laboratory setting for pure compounds and internal and external model mixtures using a constant output atomizer (TSI model 3076), custom-fabricated miniature atomizers, and fritted glass bubblers. Nitrogen was used as an inert carrier gas to generate and transport aerosol particles from aqueous stock solutions through silica gel diffusion dryers and into the SR-CCN inlet. Each solution was less than 1 L in volume, and the dissolved concentration of each solution was selected so that particle number concentration after size selection was above 10 #/cc. The constant output atomizer was used for all experiments performed using pure compounds or for single internal mixtures. For the two- and five-component external mixture experiments, the constant-output atomizer was used in conjunction with the custom atomizers and fritted glass bubblers. The particle-laden air streams from each particle generation device were combined before drying and size selection. The relative abundance of particles produced from each generation device was determined by isolating each

generation device and matching the combined flow of the four other units with nitrogen before size selecting and measuring the number concentration generated by each device.

3.8.3.2   Marine Aerosol Reference Tank (MART)

For the synthetic and microcosm bloom experiments, aerosols were generated using a Marine Aerosol Reference Tank (MART) system.[50] Briefly, the MART consists of a plexiglass tank that can be filled with ~120 L of artificial or natural seawater. A centrifugal pump periodically circulates water from the bottom of the tank to a top-mounted spillway. This generates a plunging sheet of water that impinges on the seawater surface, generating a distribution of sea-spray aerosol (SSA). The generation process produces particle size distributions that are very similar to those produced from the breaking of actual waves in a wave flume, and is therefore thought to be analogous to wave breaking in the ocean.[50] Nitrogen was used as the carrier gas for the synthetic bloom MART experiments, as well as for dilution given the high concentrations (up to 20,000 #/cc) of aerosol particles generated with this technique. Ultra-high purity zero air was used for the microcosm bloom experiment. A representative size distribution of sea salt aerosols generated using the MART system is shown in Figure 3.8, and was collected with an ultra-high sensitivity aerosol spectrometer (DMT UHSAS).
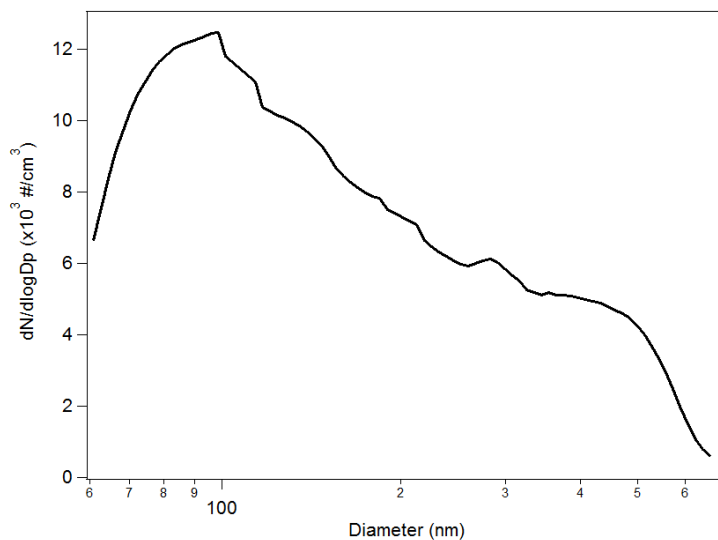
Figure 3.8: Representative aerosol size distribution for SSA generated for synthetic seawater using the MART system.

3.8.3.3 NOAA PMEL Sea-sweep

Nascent SSA particles were generated directly from the ocean surface using the NOAA PMEL sea-sweep[51] during the WACS I cruise in the Atlantic Ocean.[14] The sea-sweep was deployed alongside the research vessel, and generates bubbles from stainless steel frits at a depth of 0.75 m below the ocean surface. As the bubbles rise to and burst through the ocean surface SSA particles are generated. The SSA particles generated by the Sea Sweep are swept into a hood that is connected to a vacuum hose and are transported to a suite of aerosol instrumentation on board the research vessel. Additional details on aerosol generation with the Sea Sweep have been previously discussed.[14, 51]

3.8.4 Hygroscopicity Distribution Model

3.8.4.1 Effect of Bin Resolution on Retrieved κ Distribution

The κ basis set model was constructed to reflect diversity in aerosol composition and mixing state by calculating a distribution of hygroscopicity values for a sample population, in

contrast to a single effective value. To achieve this, SR-CCN activation curves were integrated over defined supersaturation bins, corresponding to defined κ bins for the particle size of interest, and the relative abundance of particles in each bin composed the hygroscopicity distribution. For this study, a κ range between 0 and 1.4 was divided into nine linearly spaced bins equivalent in magnitude (Fig. 3.4). Because this definition was prescribed, the effect of bin size resolution was explored. Figure 3.9 contains the same hygroscopicity distribution analysis for the prescribed range in κ, linearly divided into 14, 12, and 7 equivalent bins. In general, a larger number of bins over-resolved the characteristics of the hygroscopicity distribution, while fewer bins resulted in broader grouping of particle types with respect to hygroscopicity.
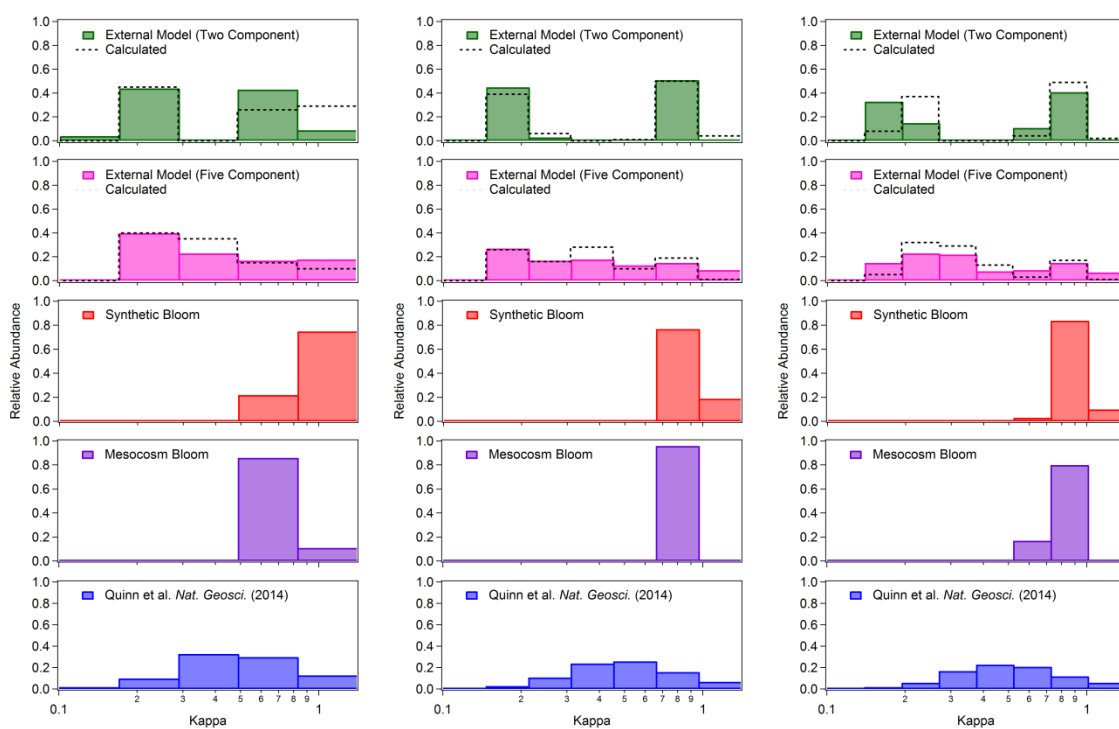
Figure 3.9: Effect of bin size resolution in κ basis set analysis for a κ range of 0 − 1.4, logarithmically divided into 5, 7, and 8 bins of equivalent magnitude in *s*.

3.8.5   Chemical Materials

3.8.5.1   Synthetic Bloom Experiment

The synthetic bloom experiment was designed to capture some of the chemical complexity present in ocean phytoplankton blooms in a system that was highly characterized. The chemical mimics used were selected based on the consideration of the evolution of surface seawater chemical composition throughout the successive stages of an ocean phytoplankton bloom.[37-39] Specifically, the system considered was a biological model whereby the growth of phytoplankton motivated growth of bacteria, which fed on the phytoplankton and in turn motivated the presence of viruses. At various stages of this evolutionary model, a class of chemical compounds was assigned, including: a refractory hydrocarbon material (cholesterol, Sigma Aldrich #C8667), a sugar (galactose, Sigma Aldrich #G0750), a lipopolysaccharide (LPS, from *E. coli* 0111:B4, Sigma Aldrich #L4130), a protein (bovine serum albumin, Sigma Aldrich #A2153), and a fatty acid (DPPA, dipalmitoyl phosphatidic acid, Avanti Polar Lipids #830855P). A synthetic sea salt mixture (Brightwell Aquatics, Neomarine precision salts for reef aquaria) composed of inorganic ions in representative seawater concentrations, was added to Milli-Q water (18.2 MΩ) to generate the mock ocean matrix. Each compound was added to the synthetic bloom in the succession described in Figure 3.10, in concentrations equivalent to 70μM carbon. After each addition, the MART plunging was used to mix the system for approximately 30 minutes, after which aerosols in the headspace of the MART were evacuated with nitrogen gas (ca. 3 hours). SR-CCN sampling commenced in triplicate measurements over a six-hour duty cycle (18 hours total), and aerosol particles were collected for AFM analysis *via* a micro orifice uniform deposition impactor (MOUDI, MSP model 110-NR).
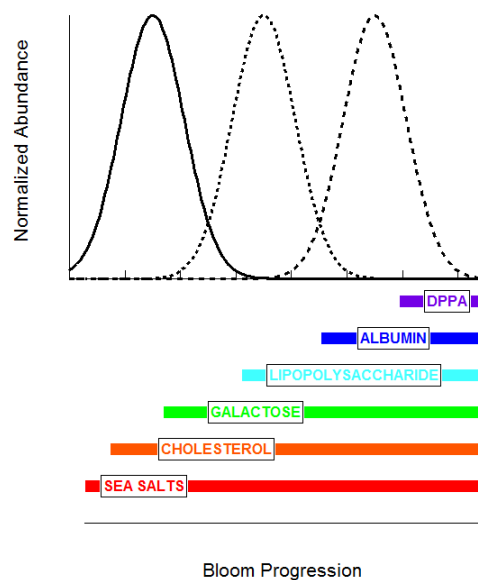
Figure 3.10: Theoretical schematic of biological growth model for phytoplankton, bacteria, and viruses, with corresponding additions of chemical mimics.

3.8.5.2   Microcosm Bloom Experiment

Seawater was collected from the Scripps Pier (La Jolla, CA, 250 m offshore; 32°51′56.8″N: 117° 15′38.48″W) and filtered through a 50 μm mesh to remove debris and zooplankton prior to the microcosm bloom. Nutrients including f/2 algae growth medium (Proline, Aquatic Eco-Systems, Apopka, FL) and solutions of sodium metasilicate were added to the collected seawater, which was constantly illuminated to stimulate phytoplankton growth. During non-sampling periods of the initial growth period of the bloom, particle free air was introduced *via* bubbling to encourage phytoplankton growth and mixing. The microcosm was incubated inside using 5700 K full spectrum lights 24 hours-a-day for the entirety of the experiment. Further details on the bloom concentrations and the method for incubating a microcosm in the MART have been described previously.[53]

3.8.6   Organic Volume Fraction

3.8.6.1   Atomic Force Microscopy (AFM)

Particles from the synthetic bloom MART experiments were collected onto silicon substrates at UC San Diego. Following collection, the samples were stored under ambient temperature and RH conditions for approximately one month, and shipped to the University of Iowa for analysis with AFM. AFM images were collected with an Asylum research Molecular Force Probe 3D AFM (Santa Barbara, CA). Images were collected in AC mode using silicon probes (MikroMasch, Model CSC37) with a nominal spring constant of 0.35 N/m and a typical tip radius of curvature of 10 nm. Imaging was performed at 20-21% RH (room RH). Height, amplitude, and phase images were used to create particle masks over the whole particle or the core of the particle. The volume of the masked area was directly determined with an Asylum research particle analyzer procedure file. Organic volume fraction was defined as the whole particle volume minus the volume of the core, divided by the total particle volume. Approximately 50 individual particles were analyzed for each sample.
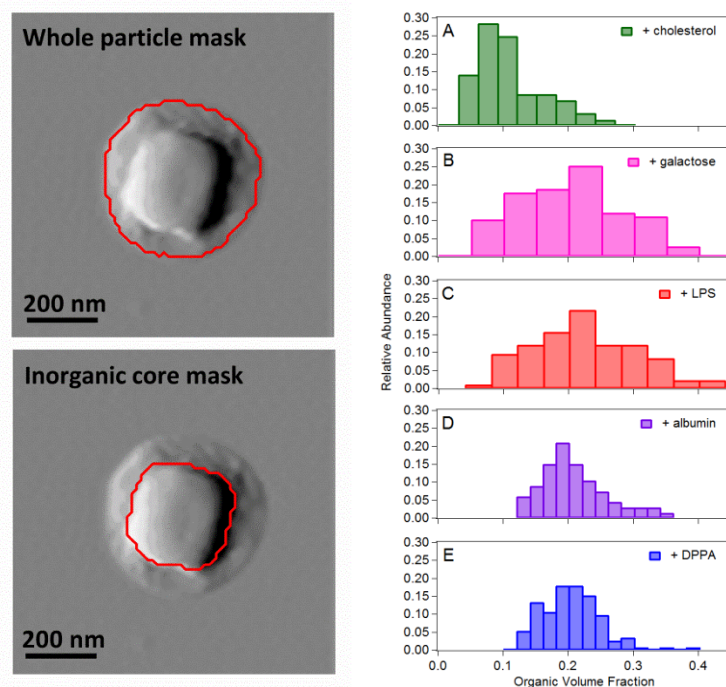
Figure 3.11: (left) AFM amplitude images demonstrating the definition of the whole particle (top) and inorganic core (bottom) masks for calculation of organic volume fraction. (right) Organic volume fraction, measured by AFM, of SSA particles generated from a MART system for each organic addition during the synthetic bloom experiment. The SR-CCN measurements examined in this study were made after addition of all components, corresponding to panel (E).

3.8.7   Climate Impacts

3.8.7.1   "Thought Experiment" Parameters

The CCN "thought experiment" results (Section 2.5) require as input an assumed particle size distribution and the fraction of each particle type that comprises that size distribution. The shape and relative composition of the assumed aerosol size distributions are shown in Figure 3.12. The size distributions for particles of each type are assumed to have the same shape, but different total particle concentrations and relative fractions based on the assumed κ distribution. The relationship between critical supersaturation (s_{crit}) and particle diameter for equivalent internal mixtures that correspond to the external mixtures shown in Fig. 3.12 is shown in Fig. 3.13. This illustrates why the difference between the internal and external mixing assumptions decrease as the assumed critical supersaturation increases. Figure 3.14 illustrates the sensitivity of

the results to the assumed size distribution. For all of these figures, the different colors within each distribution correspond to the various chemical components, i.e. different κ-values, considered. The different mixtures correspond to those shown in Fig. 3.5.
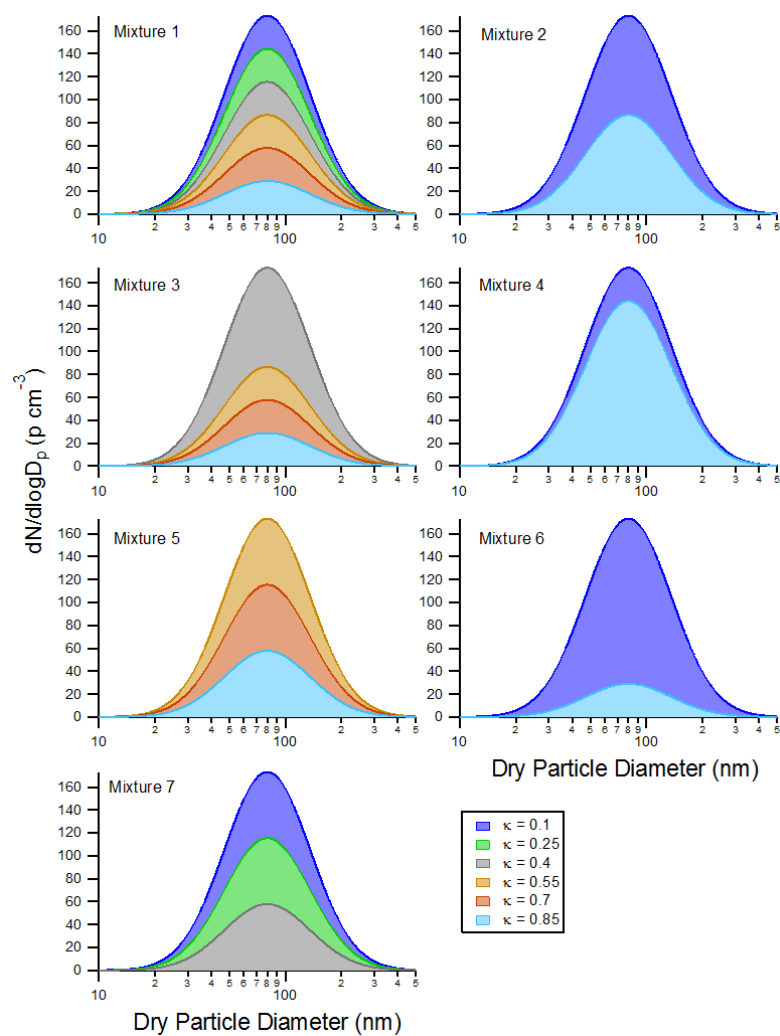
Figure 3.12: An illustration of the size distributions for each of the different κ mixtures associated with Fig. 3.5.
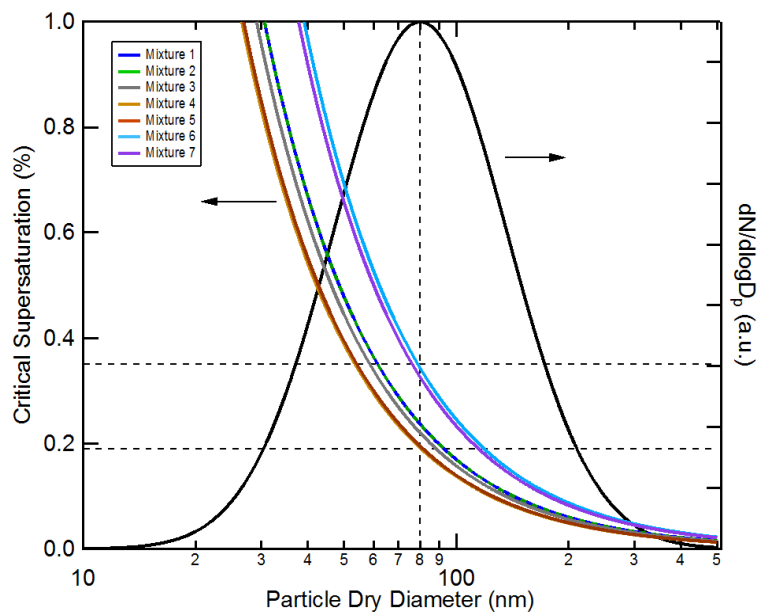
Figure 3.13: (left axis) The critical supersaturation (in percent) versus particle dry diameter relationship of the various mixtures considered in Fig. 3.5, assuming internally mixed particles (colored lines). (right axis) The size distribution used for the calculations in Fig. 3.5 (solid black line). The horizontal dashed lines show the minimum and maximum critical supersaturation values that correspond to the median particle diameter for the distribution, shown as the vertical dashed line.
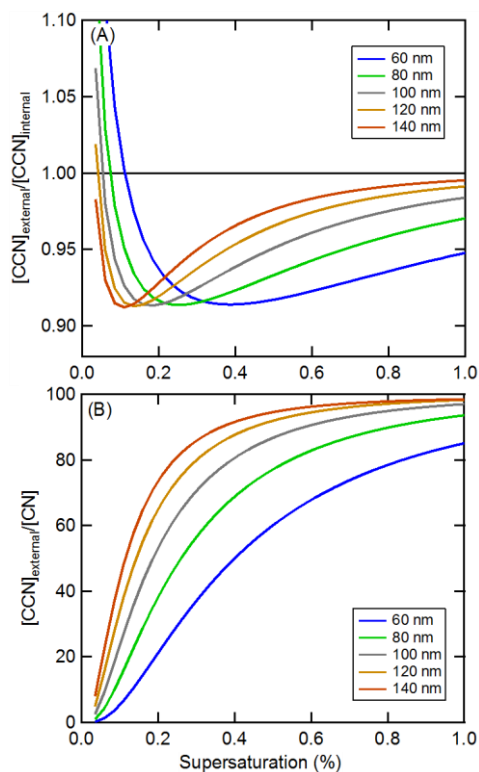
Figure 3.14: An illustration of the dependence of the (A) ratio between the external mixture versus internal mixture assumption and (B) the total CCN active particle percentage on the assumed particle size distribution, as characterized by the median diameter of the distribution (given in the legends). The curves shown here correspond to κ Mixture 1 (i.e. an equimolar mixture) shown in Fig. 3.5. All distributions are assumed to have a width of $\sigma_g = 1.7$.

3.8.8   Size-Dependence of κ Basis Set Analysis

To assess the potential dependence of particle size on the κ basis set analysis, κ distributions were measured for 50 nm and 35 nm ammonium sulfate aerosols. The analysis for both sizes generated the same single κ bin, which was expected for pure compounds given that the κ parameter inherently removes size dependence by definition. It is important to note, however, that a slight dependence of activation curve width with aerosol particle size was observed. Specifically at smaller sizes, the activation curve was broadened. This was attributed to the DMA transfer function associated with aerosol size selection, since increasing polydispersity in aerosol size could result in a slightly broadened activation curve. Regardless, the proposed

κ basis set analysis reliably extracted the same κ distribution for pure ammonium sulfate aerosols at multiple sizes.
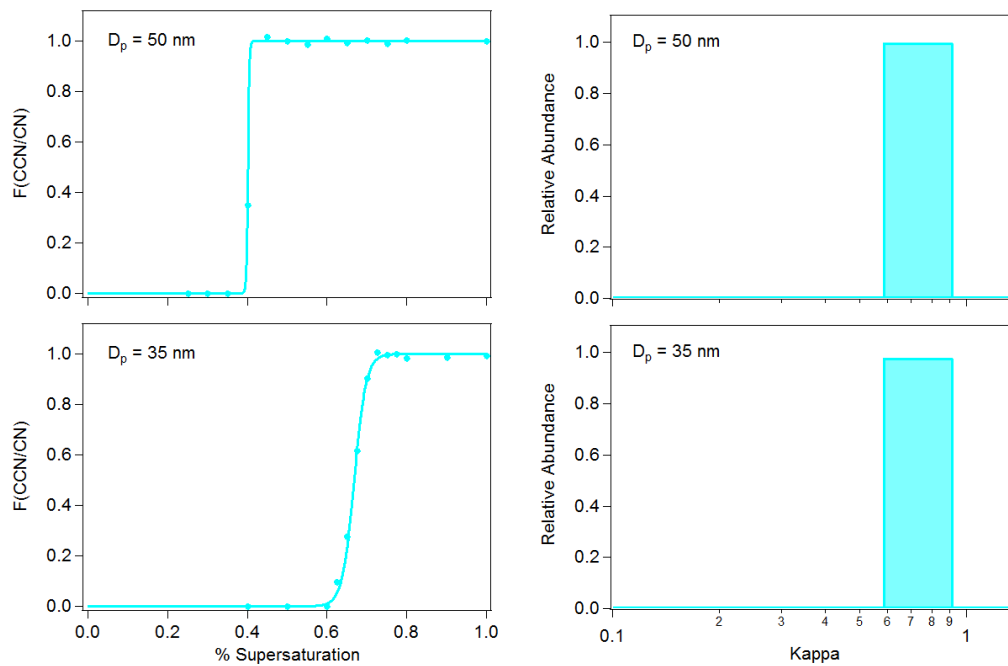
Figure 3.15: (left) SR-CCN activation curves and (right) κ distributions as determined from analysis of high-resolution *s* scans of (top) 50 nm (bottom) 35 nm ammonium sulfate aerosols.

3.9   Acknowledgments

3.10   References

1.   IPCC, *Climate Change 2013: The Physical Science Basis. Contribution of Working Group I to the Fifth Assessment Report of the Intergovernmental Panel on Climate Change*, ed. T.F. Stocker, et al. 2013, Cambridge, United Kingdom and New York, NY, USA: Cambridge University Press. 1535.

2.   Hegg, D.A., D.S. Covert, H.H. Jonsson, and R.K. Woods, *A simple relationship between cloud drop number concentration and precursor aerosol concentration for the regions of Earth's large marine stratocumulus decks.* Atmospheric Chemistry and Physics, 2012. **12**(3): p. 1229-1238.

3.   Bzdek, B.R., M.R. Pennington, and M.V. Johnston, *Single particle chemical analysis of ambient ultrafine aerosol: A review.* Journal of Aerosol Science, 2012. **52**(0): p. 109-120.

4.   Farmer, D.K., C.D. Cappa, and S.M. Kreidenweis, *Atmospheric Processes and Their Controlling Influence on Cloud Condensation Nuclei Activity.* Chemical Reviews, 2015.

5.   Petters, M.D. and S.M. Kreidenweis, *A single parameter representation of hygroscopic growth and cloud condensation nucleus activity.* Atmos. Chem. Phys., 2007. **7**(8): p. 1961-1971.

6.   Kreidenweis, S.M. and A. Asa-Awuku, *Aerosol Hygroscopicity: Particle Water Content and Its Role in Atmospheric Processes*, in *Treatise on Geochemistry*, H.D. Holland and K.K. Turekian, Editors. 2014, Elsevier: Oxford. p. 331-361.

7.   Quinn, P.K., D.B. Collins, V.H. Grassian, K.A. Prather, and T.S. Bates, *Chemistry and Related Properties of Freshly Emitted Sea Spray Aerosol.* Chemical Reviews, 2015.

8.   O'Dowd, C.D. and G. De Leeuw, *Marine aerosol production: a review of the current knowledge.* Philosophical Transactions of the Royal Society a-Mathematical Physical and Engineering Sciences, 2007. **365**(1856): p. 1753-1774.

9.   O'Dowd, C.D., M.C. Facchini, F. Cavalli, D. Ceburnis, M. Mircea, S. Decesari, S. Fuzzi, Y.J. Yoon, and J.P. Putaud, *Biogenically driven organic contribution to marine aerosol.* Nature, 2004. **431**(7009): p. 676-680.

10.   Facchini, M.C., M. Rinaldi, S. Decesari, C. Carbone, E. Finessi, M. Mircea, S. Fuzzi, D. Ceburnis, R. Flanagan, E.D. Nilsson, G. de Leeuw, M. Martino, J. Woeltjen, and C.D. O'Dowd, *Primary submicron marine aerosol dominated by insoluble organic colloids and aggregates.* Geophysical Research Letters, 2008. **35**(17): p. 5.

11.   Keene, W.C., H. Maring, J.R. Maben, D.J. Kieber, A.A.P. Pszenny, E.E. Dahl, M.A. Izaguirre, A.J. Davis, M.S. Long, X.L. Zhou, L. Smoydzin, and R. Sander, *Chemical and physical characteristics of nascent aerosols produced by bursting bubbles at a model air-sea interface.* Journal of Geophysical Research-Atmospheres, 2007. **112**(D21): p. 16.

12.   Prather, K.A., T.H. Bertram, V.H. Grassian, G.B. Deane, M.D. Stokes, P.J. DeMott, L.I. Aluwihare, B.P. Palenik, F. Azam, J.H. Seinfeld, R.C. Moffet, M.J. Molina, C.D. Cappa, F.M. Geiger, G.C. Roberts, L.M. Russell, A.P. Ault, J. Baltrusaitis, D.B. Collins, C.E. Corrigan, L.A. Cuadra-Rodriguez, C.J. Ebben, S.D. Forestieri, T.L. Guasco, S.P. Hersey, M.J. Kim, W.F. Lambert, R.L. Modini, W. Mui, B.E. Pedler, M.J. Ruppel, O.S. Ryder, N.G. Schoepp, R.C. Sullivan, and D.F. Zhao, *Bringing the ocean into the laboratory to probe the chemical complexity of sea spray aerosol.* Proceedings of the National Academy of Sciences of the United States of America, 2013. **110**(19): p. 7550-7555.

13.   Ault, A.P., R.C. Moffet, J. Baltrusaitis, D.B. Collins, M.J. Ruppel, L.A. Cuadra-Rodriguez, D.F. Zhao, T.L. Guasco, C.J. Ebben, F.M. Geiger, T.H. Bertram, K.A. Prather, and V.H. Grassian, *Size-Dependent Changes in Sea Spray Aerosol Composition and Properties with Different Seawater Conditions.* Environmental Science & Technology, 2013. **47**(11): p. 5603-5612.

14.   Quinn, P.K., T.S. Bates, K.S. Schulz, D.J. Coffman, A.A. Frossard, L.M. Russell, W.C. Keene, and D.J. Kieber, *Contribution of sea surface carbon pool to organic matter enrichment in sea spray aerosol.* Nature Geosci, 2014. **7**(3): p. 228-232.

15.   Kaku, K.C., D.A. Hegg, D.S. Covert, J.L. Santarpia, H. Jonsson, G. Buzorius, and D.R. Collins, *Organics in the Northeastern Pacific and their impacts on aerosol hygroscopicity in the subsaturated and supersaturated regimes.* Atmos. Chem. Phys., 2006. **6**(12): p. 4101-4115.

16.   Ault, A.P., T.L. Guasco, J. Baltrusaitis, O.S. Ryder, J.V. Trueblood, D.B. Collins, M.J. Ruppel, L.A. Cuadra-Rodriguez, K.A. Prather, and V.H. Grassian, *Heterogeneous Reactivity of Nitric Acid with Nascent Sea Spray Aerosol: Large Differences Observed between and within Individual Particles.* Journal of Physical Chemistry Letters, 2014. **5**(15): p. 2493-2500.

17.   Ault, A.P., T.L. Guasco, O.S. Ryder, J. Baltrusaitis, L.A. Cuadra-Rodriguez, D.B. Collins, M.J. Ruppel, T.H. Bertram, K.A. Prather, and V.H. Grassian, *Inside versus Outside: Ion Redistribution in Nitric Acid Reacted Sea Spray Aerosol Particles as Determined by Single Particle Analysis.* Journal of the American Chemical Society, 2013. **135**(39): p. 14528-14531.

18.   Ault, A.P., D.F. Zhao, C.J. Ebben, M.J. Tauber, F.M. Geiger, K.A. Prather, and V.H. Grassian, *Raman microspectroscopy and vibrational sum frequency generation spectroscopy as probes of the bulk and surface compositions of size-resolved sea spray aerosol particles.* Physical Chemistry Chemical Physics, 2013. **15**(17): p. 6206-6214.

19.   Guasco, T.L., L.A. Cuadra-Rodriguez, B.E. Pedler, A.P. Ault, D.B. Collins, D.F. Zhao, M.J. Kim, M.J. Ruppel, S.C. Wilson, R.S. Pomeroy, V.H. Grassian, F. Azam, T.H. Bertram, and K.A. Prather, *Transition Metal Associations with Primary Biological Particles in Sea Spray Aerosol Generated in a Wave Channel.* Environmental Science & Technology, 2014. **48**(2): p. 1324-1333.

20.   Gunthe, S.S., S.M. King, D. Rose, Q. Chen, P. Roldin, D.K. Farmer, J.L. Jimenez, P. Artaxo, M.O. Andreae, S.T. Martin, and U. Pöschl, *Cloud condensation nuclei in pristine tropical rainforest air of Amazonia: size-resolved measurements and modeling of atmospheric aerosol composition and CCN activity.* Atmos. Chem. Phys., 2009. **9**(19): p. 7551-7575.

21.   Rose, D., S.S. Gunthe, H. Su, R.M. Garland, H. Yang, M. Berghof, Y.F. Cheng, B. Wehner, P. Achtert, A. Nowak, A. Wiedensohler, N. Takegawa, Y. Kondo, M. Hu, Y. Zhang, M.O. Andreae, and U. Pöschl, *Cloud condensation nuclei in polluted air and biomass burning smoke near the mega-city Guangzhou, China – Part 2: Size-resolved aerosol chemical composition, diurnal cycles, and externally mixed weakly CCN-active soot particles.* Atmos. Chem. Phys., 2011. **11**(6): p. 2817-2836.

22.   Meskhidze, N., J. Xu, B. Gantt, Y. Zhang, A. Nenes, S.J. Ghan, X. Liu, R. Easter, and R. Zaveri, *Global distribution and climate forcing of marine organic aerosol: 1. Model improvements and evaluation.* Atmos. Chem. Phys., 2011. **11**(22): p. 11689-11705.

23.   Westervelt, D.M., R.H. Moore, A. Nenes, and P.J. Adams, *Effect of primary organic sea spray emissions on cloud condensation nuclei concentrations.* Atmos. Chem. Phys., 2012. **12**(1): p. 89-101.

24.   Cubison, M.J., B. Ervens, G. Feingold, K.S. Docherty, I.M. Ulbrich, L. Shields, K. Prather, S. Hering, and J.L. Jimenez, *The influence of chemical composition and mixing state of Los Angeles urban aerosol on CCN number and cloud properties.* Atmos. Chem. Phys., 2008. **8**(18): p. 5649-5667.

25.   Ervens, B., M. Cubison, E. Andrews, G. Feingold, J.A. Ogren, J.L. Jimenez, P. DeCarlo, and A. Nenes, *Prediction of cloud condensation nucleus number concentration using measurements of aerosol size distributions and composition and light scattering enhancement due to humidity.* Journal of Geophysical Research-Atmospheres, 2007. **112**(D10): p. 15.

26.   Asa-Awuku, A., R.H. Moore, A. Nenes, R. Bahreini, J.S. Holloway, C.A. Brock, A.M. Middlebrook, T.B. Ryerson, J.L. Jimenez, P.F. DeCarlo, A. Hecobian, R.J. Weber, R. Stickel, D.J. Tanner, and L.G. Huey, *Airborne cloud condensation nuclei measurements during the 2006 Texas Air Quality Study.* Journal of Geophysical Research-Atmospheres, 2011. **116**: p. 18.

27.   Levin, E.J.T., A.J. Prenni, B.B. Palm, D.A. Day, P. Campuzano-Jost, P.M. Winkler, S.M. Kreidenweis, P.J. DeMott, J.L. Jimenez, and J.N. Smith, *Size-resolved aerosol composition and its link to hygroscopicity at a forested site in Colorado.* Atmos. Chem. Phys., 2014. **14**(5): p. 2657-2667.

28.   Lance, S., A. Nenes, C. Mazzoleni, M.K. Dubey, H. Gates, V. Varutbangkul, T.A. Rissman, S.M. Murphy, A. Sorooshian, R.C. Flagan, J.H. Seinfeld, G. Feingold, and H.H. Jonsson, *Cloud condensation nuclei activity, closure, and droplet growth kinetics of Houston aerosol during the Gulf of Mexico Atmospheric Composition and Climate Study (GoMACCS).* Journal of Geophysical Research-Atmospheres, 2009. **114**: p. 21.

29.   Broekhuizen, K., R.Y.W. Chang, W.R. Leaitch, S.M. Li, and J.P.D. Abbatt, *Closure between measured and modeled cloud condensation nuclei (CCN) using size-resolved aerosol compositions in downtown Toronto.* Atmospheric Chemistry and Physics, 2006. **6**: p. 2513-2524.

30.   Medina, J., A. Nenes, R.E.P. Sotiropoulou, L.D. Cottrell, L.D. Ziemba, P.J. Beckman, and R.J. Griffin, *Cloud condensation nuclei closure during the International Consortium for Atmospheric Research on Transport and Transformation 2004 campaign: Effects of size-resolved composition.* Journal of Geophysical Research-Atmospheres, 2007. **112**(D10): p. 10.

31.   Padro, L.T., R.H. Moore, X. Zhang, N. Rastogi, R.J. Weber, and A. Nenes, *Mixing state and compositional effects on CCN activity and droplet growth kinetics of size-resolved CCN in an urban environment.* Atmospheric Chemistry and Physics, 2012. **12**(21): p. 10239-10255.

32.   Collins, D.B., A.P. Ault, R.C. Moffet, M.J. Ruppel, L.A. Cuadra-Rodriguez, T.L. Guasco, C.E. Corrigan, B.E. Pedler, F. Azam, L.I. Aluwihare, T.H. Bertram, G.C. Roberts, V.H. Grassian, and K.A. Prather, *Impact of marine biogeochemistry on the chemical mixing state and cloud forming ability of nascent sea spray aerosol.* Journal of Geophysical Research-Atmospheres, 2013. **118**(15): p. 8553-8565.

33.   Swietlicki, E., H.C. Hansson, K. Hameri, B. Svenningsson, A. Massling, G. McFiggans, P.H. McMurry, T. Petaja, P. Tunved, M. Gysel, D. Topping, E. Weingartner, U. Baltensperger, J. Rissler, A. Wiedensohler, and M. Kulmala, *Hygroscopic properties of submicrometer atmospheric aerosol particles measured with H-TDMA instruments in various environments - a review.* Tellus Series B-Chemical and Physical Meteorology, 2008. **60**(3): p. 432-469.

34.   Wex, H., G. McFiggans, S. Henning, and F. Stratmann, *Influence of the external mixing state of atmospheric aerosol on derived CCN number concentrations.* Geophysical Research Letters, 2010. **37**.

35.   Cerully, K.M., T. Raatikainen, S. Lance, D. Tkacik, P. Tiitta, T. Petaja, M. Ehn, M. Kulmala, D.R. Worsnop, A. Laaksonen, J.N. Smith, and A. Nenes, *Aerosol hygroscopicity and CCN activation kinetics in a boreal forest environment during the*

2007 EUCAARI campaign. Atmospheric Chemistry and Physics, 2011. **11**(23): p. 12369-12386.

36. Su, H., D. Rose, Y.F. Cheng, S.S. Gunthe, A. Massling, M. Stock, A. Wiedensohler, M.O. Andreae, and U. Poschl, *Hygroscopicity distribution concept for measurement data analysis and modeling of aerosol particle mixing state with regard to hygroscopic growth and CCN activation.* Atmospheric Chemistry and Physics, 2010. **10**(15): p. 7489-7503.

37. Burrows, S.M., O. Ogunro, A.A. Frossard, L.M. Russell, P.J. Rasch, and S.M. Elliott, *A physically based framework for modeling the organic fractionation of sea spray aerosol from bubble film Langmuir equilibria.* Atmospheric Chemistry and Physics, 2014. **14**(24): p. 13601-13629.

38. Long, M.S., W.C. Keene, D.J. Kieber, D.J. Erickson, and H. Maring, *A sea-state based source function for size- and composition-resolved marine aerosol production.* Atmospheric Chemistry and Physics, 2011. **11**(3): p. 1203-1216.

39. Hansell, D.A., *Recalcitrant Dissolved Organic Carbon Fractions.* Annual Review of Marine Science, 2013. **5**(1): p. 421-445.

40. Corrigan, C.E. and T. Novakov, *Cloud condensation nucleus activity of organic compounds: a laboratory study.* Atmospheric Environment, 1999. **33**(17): p. 2661-2668.

41. Hartz, K.E.H., J.E. Tischuk, M.N. Chan, C.K. Chan, N.M. Donahue, and S.N. Pandis, *Cloud condensation nuclei activation of limited solubility organic aerosol.* Atmospheric Environment, 2006. **40**(4): p. 605-617.

42. Hori, M., S. Ohta, N. Murao, and S. Yamagata, *Activation capability of water soluble organic substances as CCN.* Journal of Aerosol Science, 2003. **34**(4): p. 419-448.

43. Lu, J.W., A.M.J. Rickards, J.S. Walker, K.J. Knox, R.E.H. Miles, J.P. Reid, and R. Signorell, *Timescales of water transport in viscous aerosol: measurements on sub-micron particles and dependence on conditioning history.* Physical Chemistry Chemical Physics, 2014. **16**(21): p. 9819-9830.

44. Ruehl, C.R., P.Y. Chuang, A. Nenes, C.D. Cappa, K.R. Kolesar, and A.H. Goldstein, *Strong evidence of surface tension reduction in microscopic aqueous droplets.* Geophysical Research Letters, 2012. **39**: p. 5.

45. Ruehl, C.R. and K.R. Wilson, *Surface Organic Mono layers Control the Hygroscopic Growth of Submicrometer Particles at High Relative Humidity.* Journal of Physical Chemistry A, 2014. **118**(22): p. 3952-3966.

46. Haynes, W.M. and D.R. Lide, *CRC handbook of chemistry and physics : a ready-reference book of chemical and physical data*. 95th ed. 2014, Boca Raton, FL: CRC Press.

47. Bougiatioti, A., A. Nenes, C. Fountoukis, N. Kalivitis, S.N. Pandis, and N. Mihalopoulos, *Size-resolved CCN distributions and activation kinetics of aged continental and marine aerosol.* Atmospheric Chemistry and Physics, 2011. **11**(16): p. 8791-8808.

48. Leck, C. and E.K. Bigg, *Source and evolution of the marine aerosol - A new perspective.* Geophysical Research Letters, 2005. **32**(19): p. 4.

49. Rose, D., S.S. Gunthe, E. Mikhailov, G.P. Frank, U. Dusek, M.O. Andreae, and U. Poschl, *Calibration and measurement uncertainties of a continuous-flow cloud condensation nuclei counter (DMT-CCNC): CCN activation of ammonium sulfate and sodium chloride aerosol particles in theory and experiment.* Atmospheric Chemistry and Physics, 2008. **8**(5): p. 1153-1179.

50. Stokes, M.D., G.B. Deane, K. Prather, T.H. Bertram, M.J. Ruppel, O.S. Ryder, J.M. Brady, and D. Zhao, *A Marine Aerosol Reference Tank system as a breaking wave analogue for the production of foam and sea-spray aerosols.* Atmospheric Measurement Techniques, 2013. **6**(4): p. 1085-1094.

51. Bates, T.S., P.K. Quinn, A.A. Frossard, L.M. Russell, J. Hakala, T. Petäjä, M. Kulmala, D.S. Covert, C.D. Cappa, S.M. Li, K.L. Hayden, I. Nuaaman, R. McLaren, P. Massoli, M.R. Canagaratna, T.B. Onasch, D. Sueper, D.R. Worsnop, and W.C. Keene, *Measurements of ocean derived aerosol off the coast of California.* J. Geophys. Res., 2012. **117**: p. D00V15.

52. Fierce, L., N. Riemer, and T.C. Bond, *When is cloud condensation nuclei activity sensitive to particle characteristics at emission?* Journal of Geophysical Research: Atmospheres, 2013. **118**(24): p. 13,476-13,488.

53. Lee, C., C.M. Sultana, D.B. Collins, M.V. Santander, J.L. Axson, F. Malfatti, G.C. Cornwell, J. Grandquist, G.B. Deane, M.D. Stokes, F. Azam, V.H. Grassian, and K.A. Prather, *Reproducing the chemical complexity of tropospheric aerosols in a laboratory setting.* Journal of Physical Chemistry A. **Submitted**.

Chapter 4   The Impact of Divalent Cations on the Enrichment of Soluble Saccharides

   in Primary Sea-Spray Aerosol

4.1   Abstract

Field measurements, supported by laboratory investigations, have shown previously that sub-micrometer sea-spray aerosol (SSA) is significantly enriched in organic material, of which a significant amount has been attributed to soluble saccharides. Existing mechanistic models of SSA production struggle to replicate the observed enhancement of soluble organic material in SSA. Here, we assess the potential for divalent cation mediated co-adsorption of charged surfactants and saccharides in the enrichment of soluble saccharides in SSA. Using high throughput measurements of particle supersaturated hygroscopicity, we calculate organic volume fractions for an array of SSA generated from a Marine Aerosol Reference Tank (MART). Significant SSA organic volume fractions ($X_{org} > 0.3$) were observed for 50 nm particles for systems with cooperative ionic interactions (e.g., palmitate, Mg^{2+}, and glucuronic acid) at seawater organic concentrations (TOC < 1.15 mM C). The results presented here support the proposed mechanism of ion-mediated co-adsorption of soluble organics to insoluble surfactants at the ocean surface. The extent to which this mechanism contributes to the observed enhancement in saccharides in nascent SSA depends strongly on the speciation and charge of saccharides in the SSML.

4.2   Introduction

Oceans cover more than 70% of the Earth's surface and serve as a major source of natural aerosol particles resulting from wave breaking processes. SSA are important drivers for global climate and regional atmospheric chemistry as they directly scatter incoming solar radiation,[1] serve as cloud condensation[2, 3] and ice nuclei[4-6] (CCN and IN), and provide interfaces for catalyzing chemical reactions.[7, 8] These properties are critically dependent on SSA chemical

89

composition, size, morphology, and phase. Previous laboratory and field investigations have shown that the chemical composition of SSA is a complex function of ocean chemistry,[9-12] biological activity of the surface ocean,[10, 13-17] and physically-mediated transfer processes that govern how various compounds are distributed at the air-sea interface and how they are transported from the ocean surface into the aerosol phase,[10, 18-20] though the impact of these on SSA climate properties is less clear.

In contrast to the high salt concentration of the surface ocean (475 mM Cl⁻),[19, 21-24] the total organic carbon concentration is routinely less than 100 μM C,[12, 25-30] rising to several hundred μM C during intense phytoplankton blooms.[11, 19, 25, 31-33]. Only about 15% of marine DOC has been identified at the molecular level, but saccharides make up the largest identified fraction at 10-15%.[34, 35] It has been demonstrated that SSA is highly enriched in organic material,[15, 21, 36] on the order of 85% by mass [Cochran et al. (2017) *in preparation*], and the enriched organic species (e.g., saccharides) are often highly soluble.[19, 34, 37, 38] For example, ambient filter samples collected over the Northeast Pacific Ocean suggest glucose and other saccharides comprise 7-20% of organic aerosol mass,[39] and FTIR spectroscopy of ambient aerosol filter samples collected in the North Atlantic and Arctic Oceans have identified a substantial saccharide-like, ocean-derived organic signature responsible for 68% and 37% of the submicron aerosol organic mass, respectively, which corresponded to 7 – 37% of the total aerosol organic mass.[34]. Similar results have also been observed in the Southeast Pacific Ocean, and at coastal sites in northern Alaska (Barrow) and Northeastern North America (Appledore Island and Chebogue Point).[34] In a recent mesocosm study where aerosols were generated from a ~13,000-L wave channel in which a phytoplankton bloom was induced,[14] organic carbon mass was determined to be 7.5% of fine (PM2.5) and 1.2% of coarse (PM10-PM2.5) aerosols, with several saccharides (primarily polysaccharides) composing 11% and 27% of the aerosol organic mass, respectively.[19] These values are in good agreement with the ambient measurements of Russell et

al.[34] However, current mechanistic models of SSA production cannot replicate the observed enhancement in highly soluble organic material, which would not typically be expected to be enriched in the bubble cap from which SSA are generated.

Previous laboratory and field studies of size-resolved particle chemical composition[10, 13, 40] have demonstrated that the organic fraction of SSA increases with decreasing particle diameter, when considered either by mass[15, 21, 36] or by number,[41, 42] affecting the climate properties of aerosols particularly for particles less than 200 nm in diameter.[43] The preferential enrichment of organic material at small diameters has been attributed to the role of the bubble size distribution in the bulk[44-46] and the bubble bursting production mechanism at the surface on the resulting SSA properties,[41, 47-49] where smaller film droplets produce aerosols enriched in organics and larger jet droplets produce aerosols that contain inorganics. This physically-mediated enrichment process provides insight on how surfactant molecules (e.g., lipids) and insoluble macromolecules such as exudate aggregates or lipopolysaccharides (LPS) could be concentrated in the sea-surface microlayer (SSML), making them available for ejection into the aerosol phase. The ejection of an intact marine aggregate is one scenario by which an almost entirely organic particle could be produced from the aqueous saline solution. To this end, a number of studies have explored the relative abundance of marine gel particles,[36, 50-52] including their concentration as a function of ocean depth.[53] These particles have also generated recent interest for their potential ability to impact climate since they themselves exist at sizes relevant for seeding cloud formation.[50, 54] This scenario relies on the statistical probability of having an aggregates in an ejected sea-spray droplet, which is likely a rare event at small droplet diameters given existing knowledge of aggregate concentrations in the surface ocean ($< 10^4$ cm^{-3})[53] and the fact that concentrations of these non-sinking microscopic gel particles remain highly stratified.[55, 56]

A wide range of saccharide compounds have been identified in the ocean including dissolved free monosaccharides, polysaccharides, and sugar alcohols and monosaccharide anhydrates,[57-59] with varying composition dependent on marine biological activity.[60-64] These saccharides comprise upwards of 21% of dissolved organic carbon (DOC), with polysaccharides as the dominant form (71% of total saccharides) near the ocean surface, and monosaccharides present in the deep ocean.[65, 66] Most analytical techniques used to detect saccharides do not account for charged compounds such as uronic acids so these are often cited as lower limits, but the relative abundance of charged saccharides is generally regarded as much lower than that of the free monosaccharides.[67-69]

There is increasing evidence that polysaccharides are surface-active[69, 70] and may play an important role in bubble bursting at the ocean surface[71] and resulting SSA composition.[34, 37, 38] However, the transfer processes between the air-sea interface are complex and poorly understood. One study by Frossard et al.[38] measured the characteristic functional group composition with Fourier Transform Infrared Spectroscopy of atmospheric marine aerosol particles in five ocean regions, and found that aerosols generated from biologically productive ocean water had a hydroxyl group absorption peak location characteristic of monosaccharides and disaccharides, whereas the seawater organic mass hydroxyl group peak location was closer to that of polysaccharides. This suggests that larger saccharides may preferentially stay in the seawater during aerosol production, contributing to an outsized impact of monosaccharides and disaccharides on the composition of SSA relative to their concentrations in the bulk and surface water.

It is commonly assumed that the distribution of organic compounds within the SSML is driven by solubility and surface activity, where insoluble organics are concentrated at the air-sea interface whereas soluble organic species, such as biologically-derived saccharides, are more evenly distributed through the SSML. One idea for explaining the observed enrichment of soluble

organics in SSA is that they are covalently bonded to lipid head groups, such as in lipopolysaccharides (LPS). Chemical processing and/or enzymatic breakdown of a compound such as LPS in SSA would result in an observed enrichment of soluble saccharides in SSA, as illustrated in Fig. 4.1A. For this mechanism to explain observed enhancements of saccharides in SSA, it would be expected that high concentrations of phosphate groups would also be observed, which has indeed been observed for bubble-bursting processes in surface waters[71] and in SSA.[72]
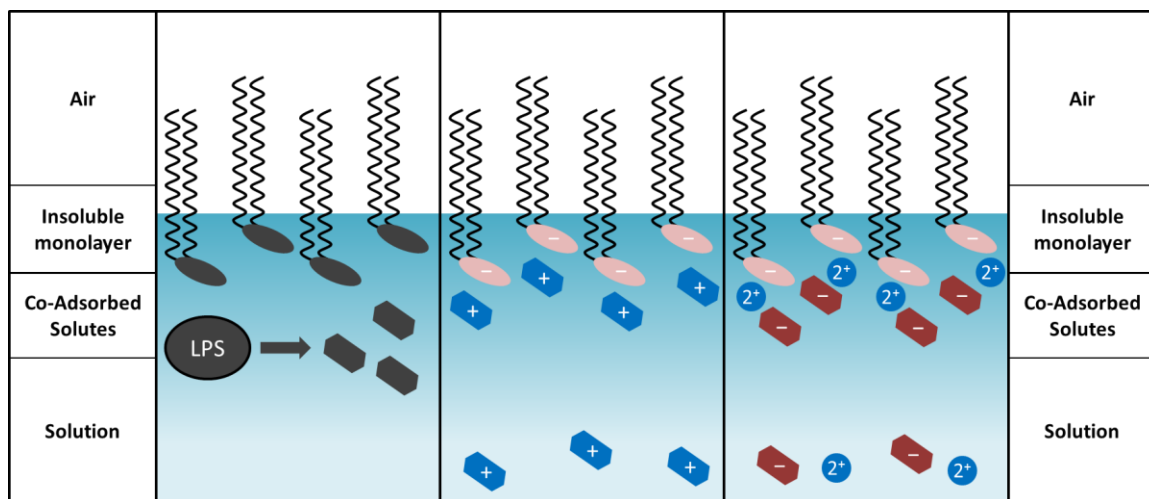
Figure 4.1: Conceptual overview of soluble organic distribution in the sea-surface microlayer (SSML) for the A) macromolecule-derived mechanism, B) ion-mediated co-adsorption mechanism put forth by Burrows et al.[73] and C) divalent cation mediated co-adsorption, proposed in this work.

A second possible explanation for the observed enrichment of soluble organics in SSA is that they are not uniformly distributed throughout the water column, but rather are enriched at the ocean surface. This was the underlying idea presented by Burrows et al.[74] by the SSA process model known as Organic Compounds from Ecosystems to Aerosols: Natural Films and Interfaces via Langmuir Molecular Surfactants, or OCEANFILMS, which used a Langmuir adsorption equilibrium model to describe the interactions of compounds in the bulk ocean with the surfaces of bubbles entrained into the water column by wave breaking events. By defining several broad

classes of compounds, OCEANFILMS described how molecules adsorbed to the bubble surfaces were subsequently transferred into the aerosol phase according to their competitive affinities for surface coverage. This approach was shown to be well suited for describing seasonal and geographic variability in aerosol organic mass, but the estimated organic mass fractions remained less than 0.4 over a wide range of chlorophyll concentrations,[74] which was much smaller than observations of ambient aerosols suggest (upwards of 0.8). To account for this, OCEANFILMS-2[73] considered the possibility of ionic interactions between the insoluble and soluble organics, and a second layer of cooperatively adsorbed soluble saccharides was added to the original layer of insoluble organics in the model SSML (Fig. 4.1B). This model achieved better closure between estimated SSA organic mass fractions (0.2 – 1, depending on model parameters)[73] and observed values from ambient aerosol measurements. In support of this fundamental proof of concept, a series of sum-frequency generation (SFG) experiments with dipalmitoylphosphatidylcholine (DPPC, pKa = 3.8[75, 76]) and glucosamine (pKa = 7.58[77]) model systems showed that glucosamine altered the surface structure of the DPPC monolayer, and that the Langmuir isotherm adequately described the magnitude of this effect. These results confirmed that the proposed mechanism relying on ionic interactions to bind compounds with varying solubility at the ocean surface was feasible, but it is important to note that because the pK_a of the saccharide ultimately determines the extent of ionization, these experiments were conducted at a pH much lower (pH = 5.5) than that of the ocean (pH = 8.1) to ensure complete ionization of glucosamine. This mechanism is most relevant to saccharide compounds that readily ionize at ocean pH, which significantly decreases the scope of compounds that will participate. Under these considerations the extent to which these results can be used to describe ocean-relevant processes will likely be driven by the magnitude of enhancement observed, and not by the quantity of compounds that will be enriched in SSA according to this mechanism.

In this study we extend the concept of ionically-mediated co-operative adsorption of soluble saccharides to a largely insoluble SSML at the surface of a synthetic ocean matrix, with model compounds appropriate to ocean-relevant pH. Palmitic acid (pKa = 8.6-8.8[78]) and glucuronic acid (pKa = 2.93[79]) were chosen as proxies for the insoluble surfactant and soluble saccharide, respectively. In this study, because both compounds formed anions in solution, we considered the role of biologically-derived divalent metal cations as an ionic bridge necessary for the proposed mechanism.

Experimental validation of soluble organic enrichment for SSA at sizes relevant to climate processes such as cloud formation (20 – 200 nm) is difficult because most techniques rely on offline trace analysis of collected bulk aerosol samples to provide quantitative results. For reference, accumulation times to collect sufficient mass of 100 nm particles to complete these analyses are on the order of 8-12 hours from an aerosol generation system[80, 81] with a total particle output of approximately 20,000 cm^{-1}. It is well known that aerosol water uptake (hygroscopicity) is intimately linked to its chemical composition, especially for particles with dry diameters less than 200 nm,[43] with the presence of inorganic salts leading to a more hygroscopic particle and organic compounds generally leading to a less hygroscopic particle.[82] Hygroscopicity displays further variability within the organic and inorganic component classes dependent upon factors such as solubility, molecular weight and surface tension. As such, high precision measurements of size resolved supersaturated hygroscopicity provide unique insight into the chemical composition of aerosol particles generated from a select number of chemical species. In this study, we use direct measurement of aerosol supersaturated hygroscopicity as a high-throughput, online analysis technique for detecting changes in particle composition; specifically the enrichment of soluble organics in SSA generated from a synthetic ocean matrix.

4.3   Materials and Methods

4.3.1   Aerosol Generation

Prior to the synthetic sea-spray experiments, hygroscopicity factors (κ) for the pure compounds used in this study were determined by aerosolizing compounds using a constant output atomizer (TSI model 3076). Nitrogen was used as an inert carrier gas to generate and transport aerosol particles from aqueous stock solutions, through silica gel diffusion dryers, and to a cloud condensation nuclei counter instrument (DMT model CCN-100) paired with size selection and operated in scanning supersaturation mode, as described in detail below. Each solution was less than 1 L in volume, and the dissolved concentration of each solution was selected so that monodisperse particle number concentrations were approximately $200 - 1000 \text{ cm}^{-1}$.

The synthetic sea-spray experiments were conducted using a Marine Aerosol Reference Tank (MART) system, which has been described previously.[80, 81] Briefly, the MART consists of a plexiglass tank filled with ~120 L of artificial seawater. A centrifugal pump periodically circulates water from the bottom of the tank to a top-mounted spillway, creating a plunging sheet of water that impinges on the seawater surface and generates a distribution of SSA size and composition. The generation process produces particle size distributions that are similar to those produced from the breaking of actual waves in a wave flume, and is therefore thought to be analogous to wave breaking in the ocean.[80] Nitrogen was again used as a carrier gas as well as for dilution given the high concentrations (up to $20,000 \text{ cm}^{-1}$) of aerosol particles generated with this technique.

4.3.2   Overview of Experiments

Each SSA experiment consisted of three sequential additions to a synthetic ocean matrix:

i) artificial seawater, ii) soluble organic proxy (e.g. saccharide), and iii) insoluble surfactant proxy

(e.g., surfactant). Compound identity and concentrations are listed in Table 1.

Table 4.1: Predicted, water-side concentrations of individual compounds in the Marine Aerosol Reference Tank (MART). Each experiment (control (C), experiment 1 (E1), experiment 2 (E2), experiment 3 (E3)) was initiated with a synthetic seasalt mixture, followed by sequential additions of soluble (+ saccharide) and insoluble (+ surfactant) organics.

	Artificial Seawater				+ Saccharide		+ Surfactant
	Na^+	Mg^{2+}	Ca^{2+}	Cl^-	+ Glucose	+ Glucuronic Acid	+ Palmitic Acid
C	470 mM	145 mM	0	600 mM	95 μM (575 μM C)	0	35 μM (575 μM C)
E1	470 mM	145 mM	0	600 mM	0	95 μM (575 μM C)	35 μM (575 μM C)
E2	470 mM	0	10 mM	490 mM	0	95 μM (575 μM C)	35 μM (575 μM C)
E3	470 mM	0	0	470 mM	0	95 μM (575 μM C)	35 μM (575 μM C)

Artificial seawater was generated from milli-q water (EMD Millipore, Z00QSV001) and

reagent grade salts including sodium chloride (Sigma-Aldrich, S9888), magnesium chloride

hexahydrate (Sigma-Aldrich, M9272), and calcium chloride dihydrate (Sigma-Aldrich, 223506).

A soluble organic proxy was then added to the salt matric, either glucose ($C_6H_{12}O_6$; Sigma-

Aldrich D9434) or glucuronic acid ($C_6H_{10}O_7/C_6H_9O_7^-$; Sigma-Aldrich G5269), selected for their

similar saccharide backbones but dissimilar ionic properties. Lastly, palmitic acid (Sigma-Aldrich, P0500) was added to each experimental matrix as a proxy for an insoluble surfactant. Actual concentrations of proxies added to the MART were within approximately 2% and 4% by mass for the salts and organics respectively. After each addition, aerosols were generated from the matrix in the MART, where continuous measurements of particle hygroscopic properties were made and particles were collected for offline chemical analysis.

4.3.3   Direct Measurement of Aerosol Hygroscopicity

The particle activation efficiency (i.e. the fraction of particles of a given size that grow into droplets when exposed to a given water supersaturation (s), or $f_{CCN}(s)$) was measured for all SSA particles generated from the MART and model aerosol generated by the constant output atomizer. Measurement of $f_{CCN}(s)$ were made using a size resolved cloud condensation nuclei (SR-CCN) system, consisting of three stages: i) aerosol particle generation, ii) size selection, and iii) measurement of cloud active fraction. The aerosol sources have been described in detail above. Monodisperse particles were selected from the polydisperse distribution according to their mobility diameters using a differential mobility analyzer (DMA, TSI model 3071) with a sheath:sample flow rate ratio of 10:1. The resulting aerosol stream was subsequently split between a condensation particle counter (CPC, TSI model 3787) measuring total aerosol count, and a CCN counter (CCNc, DMT model CCN-100), counting cloud active aerosols as a function of supersaturation. These two measurements were ratioed to generate a cloud active fraction (f_{CCN} = [CCN]/[CN]) for a number of supersaturation settings, referred to as a CCN activation efficiency spectra (f_{CCN} versus s). From these spectra, measurements of a selected particle diameter (D_p) and the critical supersaturation (s_{crit} – where 50% of the particle population has activated) are converted to a single parameter, κ.[83] Smaller κ-values correspond to less hygroscopic particles and vice versa. κ-Köhler theory separates the intrinsic hygroscopicity

(composition-dependence) from the particle size dependence, thereby allowing for assessment of the influence of composition more specifically. Typical values of κ range between $0 - 1.4$, with lower values generally associated with less (or non-) soluble organic compounds, and higher values generally associated with soluble inorganic compounds.[83, 84]

In general, changes in κ over the course of each experiment can be attributed to changes in the chemical composition of aerosols generated from each matrix. For internally-mixed aerosol populations where all particles have one representative composition, the observed κ-value is a linear combination of the pure κ-values and relative volume fractions of the individual components.[83] Observed κ-values from the sequential addition experiments were used with measured values of the pure components in the mock ocean matrix to estimate the volume fractions of organics in the aerosols. Under these conditions, this approach highlights the ability of the SR-CCN as a high-throughput technique to probe organic enhancement on aerosols at sub-100 nm diameters.

4.3.4   Ion Exchange Chromatography Analysis

Aerosols were generated from the sequential addition experiments using the MART system and particles < 0.25 μm in diameter, the minimum size cut selected for best overlap with the 50 nm particles analyzed with the SR-CCN, were deposited onto a quartz fiber after-filter for offline analysis using a Sioutas Personal Cascade Impactor (PCIS, SKC model 225-370). Particle-free, inert, low humidity (RH $< 15\%$) room air from a zero air generator (ZAG, Sabio model 1001) was used for dilution during PCIS sample collection. Samples were stored frozen and later extracted into ultra-pure water (Thermo, BARNSTED EasyPure-II; 18.2 MΩ resistivity) from whole 37 mm quartz fiber filters for analysis via ion exchange chromatography. An aqueous extraction proved sufficient for all samples, which were filtered prior to analysis (Quartz PALL Filter (90mmqff) with Whatman TM puredisc 25 mmspp filters).

Aqueous extractions were analyzed by ion exchange chromatography (Dionex-ICS5000). For saccharide analysis, a Dionex CarboPac PA20 column was used. For glucose, the mobile phase consisted initially of 200 sodium hydroxide (NaOH) with a gradient up to 450 mM NaOH from 7 to 10 minutes. For glucuronic acid, a mobile phase of 190 mM NaOH and 190 mM sodium acetate was used. In both cases, the flow rate was 0.48 mL min^{-1}. An electrochemical detector (Thermo) was used for detection. Saccharides were identified against self-prepared calibration solutions of glucose (Sigma) and glucuronic acid (Alpha Aesar) and quantified with seven-point calibration curves. For anion analysis, a Dionex IonPac AS22 anion column was used. The mobile phase consisted of 4.5 mM sodium carbonate (Na_2CO_3) and 1.4 mM sodium bicarbonate ($NaHCO_3$) at a flow rate of 1.2 mL min^{-1}. For cation analysis, a Dionex IonPac CS12A cation column was used. The mobile phase consisted of 20 mM methanesulfonic acid and flowed at 0.5 mL min^{-1}. A conductivity detector (Thermo) was used for detection and was preceded by a self-regenerating suppressor (AERS 500 for anions and CERS 500 for cations). Anions and cations were identified against authentic standards (Dionex) and quantified with seven-point calibration curves. All the reported ambient concentrations (nmol/sccm) correspond to ambient temperature and pressure and have been field blank subtracted. Air volumes were calculated from the average of initial and final flow rates and total sampling time of the PCIS.

4.4   Results and Discussion

4.4.1   Hygroscopicity of Pure SSA Mimics

The hygroscopicity parameter is sensitive to changes in aerosol composition, making it a good metric for probing organic enhancement due to ionic interactions at the surface of the mock ocean matrix. For quantitative analysis with the κ mixing rule, a necessary first step was measuring the κ-values of the pure model compounds used in the sequential addition experiments. Table 2 presents values for reference (literature) and intrinsic[85] (solubility

weighted) κ-values where available, as well as measured values for the pure mimics used in this study presented as a three-trial average ± σ, though the contribution of the accuracy to the uncertainty of the measurement may be much higher. The intrinsic κ-values can be thought of as upper limits for κ, because they only account for the solubility of the solute, and are tabulated according to the method of Sullivan et al. [85] (Equation 4.1) where i is the number of ions formed when one molecule of solute dissolves, and ρ and M are the density and molar mass of the solute (s) and water (w), respectively.

$$\kappa_{intrinsic} = \frac{i \times \rho_s \times M_w}{\rho_w \times M_s} \qquad \text{E4.1}$$

Measured κ-values account for more than just the solubility of the seed particle, such as kinetic effects of water accommodation, which could explain the differences observed in the measured κ-values in this study, particularly for compounds that undergo hydrate formation. However, because κ is ultimately dependent on the amount of soluble material in the seed particle, the number of soluble moles for a 50 nm particle of each mimic, which was the diameter of particle analyzed in this work, is tabulated according to Equation 4.2, and presented in Table 4.2. There is good general agreement between measured κ-values from this study and the $n_{soluble}$ for each particle.

$$n_{soluble} = \frac{\left[\left(\frac{4}{3}\right)\pi\left(\frac{d_p}{2}\right)^3\right] \times \rho}{M} \qquad \text{E4.2}$$

Table 4.2: Measured hygroscopicity values (κ) for pure compounds used in this study. The calculated number of soluble moles ($n_{soluble}$) in the 50 nm particle is also included for reference.

Compound	κ (literature)	κ (intrinsic)[*]	κ (this study)	$n_{soluble}$ ($d_p = 50$ nm)
NaCl	1.2[†] 1.28[‡]	1.34	0.892 – 0.925	2.43×10^{-18}
MgCl₂	0.47[§]	1.32		1.60×10^{-18}
MgCl₂ · 6H₂O		0.42	0.3453 ± 0.001	5.01×10^{-19}
CaCl₂	0.64[§] 0.48*	1.05	0.391 ± 0.006	1.27×10^{-18}
CaCl₂ · 2H₂O		0.68		7.61×10^{-19}
Glucose	n/a	0.15	0.272 ± 0.005	5.59×10^{-19}
Glucuronic Acid	n/a	0.14	0.244 ± 0.006	5.19×10^{-19}

[*]Calculated using the method of Sullivan et al. (2009)[85]
[†]Quinn et al. (2014)[10]
[‡]Petters and Kriedenweis (2007)[83]
[§]Drozd et al. (2014)[86]

There are limited studies of κ-value measurements for SSA mimics.[81] Despite what is known about kinetic limitations of water uptake of saccharides,[87, 88] to our knowledge the κ-values reported here are the only reported measurements of κ for glucose and glucuronic acid. It has been shown elsewhere[86] that the intrinsic κ-values do not necessarily trend with observed values, particularly for species that undergo hydrate formation, and we observe that in this work specifically for divalent salts known to undergo hydrate formation. For these reasons the number of soluble moles in a 50 nm particle of each compound is tabulated to illustrate dependence of hygroscopicity on available soluble material. Though this analysis may not accurately describe saccharide compounds in general, which have been shown to exhibit significant kinetic limitation

in their water uptake processes,[89] the model compounds selected in this study will be used to estimate the organic component in SSA using SR-CCN measurements and the linear κ mixing rule.

4.4.2   Organic Enhancement via Hygroscopicity Analysis

In all sequential addition experiments, the starting ocean matrices consisted only of salt(s) and measured κ-values were > 0.75, with the value depending on the salt identity and exact mass (precision). Each experiment consisted of the sequential addition of a soluble organic (e.g. glucose) followed by the addition of an insoluble organic (e.g. palmitic acid). To test the hypothesis that soluble organic enrichment in SSA could be a result of ionic interactions between soluble organics and insoluble surfactants, a control experiment was designed by pairing glucose (pKa = 12.28,[90] neutral in solution) with palmitic acid (pKa = 8.6-8.8,[78] anionic in solution). At ocean pH, no ionic interactions would be expected as glucose is charge neutral. The CCN activation spectra (Fig. 4.2A) do not demonstrate any statistically significant change upon the addition of glucose to the salt matrix, corresponding to no significant change in the measured κ-value. This implies that the relative abundance of glucose in the aerosol particles was negligible compared to the salt, in agreement with the relative bulk concentrations of approximately 600 mM salt and 95 μM glucose (Table 4.1), which correspond to a mixing rule-derived estimated change in κ on the order of uncertainty of the κ measurement. Furthermore, addition of palmitic acid also resulted in no change to the measured κ-value, indicating that the presence of palmitic acid, at the concentrations present in this experiment, did not on its own affect aerosol hygroscopicity.

Experiment 1 (E1, Fig. 4.2B) was designed to probe potential ionic interactions between glucuronic acid (pKa = 2.93,[79] anionic in solution) and palmitic acid in the presence of divalent metal cations. In this case there was a slight shift of the CCN activation curve to higher

supersaturations upon addition of glucuronic acid corresponding to a slight decrease in the measured κ-value. Upon addition of palmitic acid, this effect was far more dramatic. The resulting suppression in hygroscopicity implies pronounced enhancement of organic material in the aerosol particles upon addition of the palmitic acid. Based on the results of the control experiment, we interpret this as evidence for ionic interactions between the saccharide and the surfactant at the surface of the synthetic ocean matrix that act to concentrate the soluble organic and make it more available for ejection to the aerosol phase.
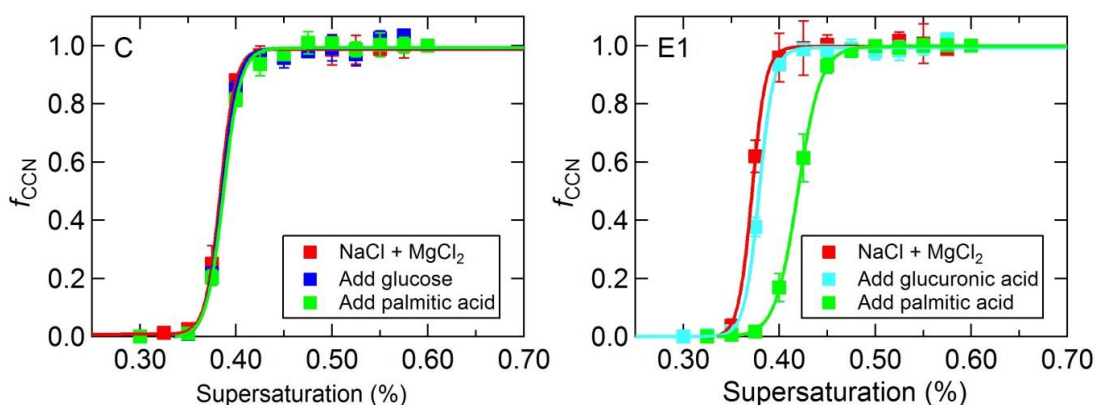
Figure 4.2: Representative CCN activation spectra for the control experiment ("C", left) and experiment 1 ("E1", right) MART experiments consisting of a starting salt matrix (red), addition of 95 μM glucose (dark blue, left) or glucuronic acid (light blue, right), and subsequent addition of 35 μM palmtic acid (green).

4.4.3   Estimating Organic Enrichment

To calculate the enrichment in organic material in the SSA from measurements of SSA hygroscopicity (κ), we assume that κ follows a linear mixing rule (Equation 4.3) where X is the volume fraction of each aerosol component.

$$\kappa_{obs} = \kappa_{salt}X_{salt} + \kappa_{org}X_{org} \qquad\qquad \text{E4.3}$$

The initial hygroscopicity value (κ_{salt}) for particles generated in the MART experiments depends on the relative amounts of individual salts in the sea-spray particle (e.g., Na^+, Mg^{2+},

Ca^{2+}). In the control experiment, no significant change in the measured κ-value was observed following addition of glucose or palmitic acid to the MART. This suggests very limited enrichment of organic material ($X_{org} \approx 0$; $X_{salt} \approx 1$) in the aerosol as the hygroscopicity of the particle remains dominated by the high concentrations of salt in the system. For the paired case of glucuronic acid and palmitic acid (E1) a 4% decrease in κ was observed following the addition of glucuronic acid and a further 21% decrease in κ was observed upon addition of the surfactant. This decrease in hygroscopicity suggests enhancement of organics in the aerosol and supports the mechanism of a co-operatively adsorbed saccharide layer to the insoluble surfactant layer at the surface of the mock ocean matrix. Utilizing the κ mixing rule (*via* Equation 1),[83] which assumes internal mixing, the 21% decrease in κ corresponds to an organic volume fraction of 0.30 for the 50 nm particles analyzed. It is important to note that this (and all subsequent) calculation assumes only glucuronic acid is enriched in the particles, which is supported by the negligible change in hygroscopicity for the control experiment, which also had palmitic acid. However, given that the proposed mechanism for enrichment of soluble organics *via* co-operative adsorption to insoluble surfactants at the surface involves a "glucuronic acid – divalent metal cation – palmitic acid" motif, it is presumed that the organic volume fraction of the resulting aerosols actually has a 1:1 molar equivalence of glucuronic acid and palmitic acid. Under these assumptions, the distribution of the 0.30 organic volume fraction of the 50 nm SSA particles is 70% palmitic acid and 30% glucuronic acid.

To determine the effect of the divalent metal cation on the selective transfer of soluble saccharides, we replaced magnesium with calcium, which is known to have a greater binding affinity for palmitic acid.[91] As shown in Table 4.3, the calculated volume fraction of glucuronic acid (calculated relative to the starting κ for each salt matrix) was 0.40 for Experiment 2 (E2), which is comparable to that of the Mg^{2+} experiments, despite the fact that the concentration of

Ca^{2+} was an order of magnitude smaller than the concentration of Mg^{2+} using in Experiment 1. This result suggests that the identity of the divalent metal cation plays a critical role in the suggested mechanism involving a co-operatively adsorbed layer at the surface of the mock ocean matrix.

A final experiment (E3) was designed to arrest the organic enhancement mechanism by removing the divalent cations from the salt mix. However, a 13% decrease in κ (indicative of organic enhancement) was observed in E3. This is attributed to the trace divalent metal cations present in the water supply and as impurities in the monovalent salts. It is possible that an additional chelation could more effectively shut down the organic enhancement, though the addition of a chelating agent would complicate the interpretation of the hygroscopicity results significantly.

Table 4.3: Observed κ-values (three-trial average ± σ) and corresponding aerosol organic volume fractions ($X_{org, \kappa}$) for each addition of the MART experiments. Percent changes in κ, relative to the salt matrix, are shown in brackets.

	Artificial Seawater	**+ Saccharide**		**+ Surfactant**	
	(κ)	(κ)	$X_{org, \kappa}$	(κ)	$X_{org, \kappa}$
C	0.749 ± 0.010	0.744 ± 0.002 [- 1%]	0.01	0.734 ± 0.001 [- 2%]	0.03
E1	0.797 ± 0.005	0.767 ± 0.004 [- 4%]	0.05	0.630 ± 0.009 [- 21%]	0.30
E2	0.921 ± 0.013	0.907 ± 0.014 [- 2%]	0.02	0.646 ± 0.006 [- 30%]	0.40
E3	0.892 ± 0.005	0.889 ± 0.026 [- 0%]	5×10^{-3}	0.773 ± 0.013 [- 13%]	0.18

4.4.4 Quantitative Closure Between Methods

Aerosols were collected *via* an impactor for offline analysis to quantitatively assess organic enrichment in the particles, as discussed in Section 3.4. IEC measurements of saccharide:salt molar ratios in SSA with dry diameters (d_p) < 250 nm for all of the sequential MART experiments ranged from $0.3 - 7 \times 10^{-4}$, which is comparable to the bulk water ratio (Table 1, 7×10^{-4}). To directly compare with hygroscopicity measurements, the aerosol organic volume fraction ($X_{organic}$) is obtained from IEC measurements according to Equation 4.4, where $n_{saccharide}$ and n_{salt} is the collection volume-normalized moles of saccharide and salt respectively, M is the molar mass, and ρ is the density.

$$X_{org, \; IEC} = \frac{\left[{(n_{saccharide} \times M_{saccharide})}/{\rho_{saccharide}} \right]}{\left[{(n_{saccharide} \times M_{saccharide})}/{\rho_{saccharide}} \right] + \left[{(n_{salt} \times M_{salt})}/{\rho_{salt}} \right]}$$

E4.4

Table 4.4 shows tabulated $X_{org, \, IEC}$ values for each addition in each MART experiment. Volume fractions of glucose in the control experiment are approximately one order of magnitude greater than those measured for experiments with glucuronic acid, which is thought to be a result of an error in background correction specific to that experiment. Little variation with no apparent trend is observed in the glucose volume fraction after each addition in the control experiment, which is in good agreement with the proposed mechanism for organic enrichment that necessitates ionic interactions in solution, which glucose does not exhibit. In E1 and E2, an increase in glucuronic volume fraction was observed, particularly after the addition of the surfactant. These correspond to a 5x and 3.5x increase in total saccharide mass for E1 and E2, respectively, compared to increases in aerosol mass (60 nm $< d_p <$ 250 nm) of 1.4x and 1.6x, which demonstrates saccharide enrichment in both experiments. E3 was also associated with saccharide enrichment despite the absence of added divalent cations, though the effect was weaker with an increase in total saccharide mass of 1.8x compared to an increase in aerosol mass (60 nm $< d_p <$ 250 nm) of 1.6x.

Table 4.4: Measured organic volume fractions ($X_{org, IEC}$) as determined by IEC for particles with diameters less than 250 nm for each addition of the MART experiments.

	Artificial Seawater $X_{org, IEC}$	**+ Saccharide** $X_{org, IEC}$	**+Surfactant** $X_{org, IEC}$
C	2.7×10^{-3}	3.1×10^{-3}	2.4×10^{-3}
E1	ND	1.3×10^{-4}	4.6×10^{-4}
E2	ND	1.9×10^{-4}	5.3×10^{-4}
E3	ND	5.9×10^{-4}	8.0×10^{-4}

Comparison of aerosol organic volume fractions calculated from hygroscopicity ($X_{org, \kappa}$) and IEC measurements ($X_{org, IEC}$) is shown in Figure 4.3 for the seawater, glucuronic acid, and palmitic acid experiment. The trend in X_{org} between the two experiments is in strong agreement, where X_{org} increases substantially upon addition of the surfactant. However, as shown in Fig. 4.3, the two determinations differ by almost a 1000. Surprisingly, the average organic volume fraction from IEC measurements ($X_{org, IEC, avg} = 6.0 \times 10^{-4}$) are not only much smaller than any of the $X_{org, \kappa}$ values, they are in strong agreement with the tabulated value for the bulk water in the MART ($X_{org, bulk} = 6.9 \times 10^{-4}$) according to saccharide and salt concentrations shown in Table 4.1.
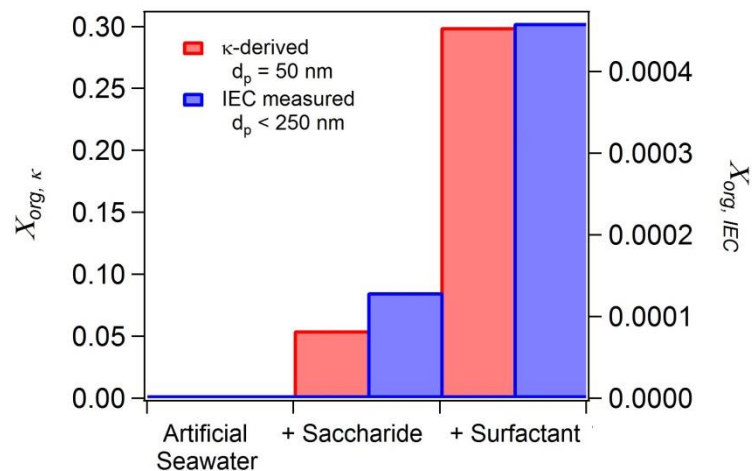
Figure 4.3: Aerosol organic volume fraction estimates for the seawater, glucuronic acid, palmitic acid sequential addition MART experiment (E1), calculated from hygroscopicity measurements ($X_{org, \kappa}$; red) and IEC measurements ($X_{org, IEC}$; blue).

Calculations of $X_{org, \kappa}$ for 50 nm (d_p) particles range from 0.03 – 0.40 for the sequential addition MART experiments in this study. For comparison, calculations of organic volume fractions from hygroscopicity measurements made on SSA generated from seawater in the Atlantic Ocean[10] indicate substantial enrichment in organic material, and a strong size dependence to $X_{org, \kappa}$.
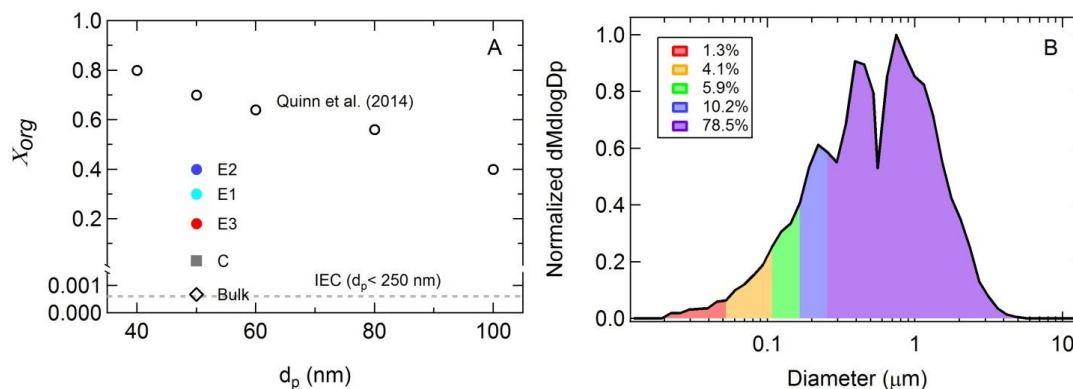
Figure 4.4: (A) Aerosol organic volume fraction X_{org} measurements as a function of dry particle diameter for each of the experiments described here (colored circles), alongside calculations of X_{org} derived from hygroscopicity measurements made on SSA generated from seawater in the Atlantic Ocean by Quinn et al.[10]. (B) Aerosol mass distribution for representative, laboratory-generated SSA from Prather et al.[41].

The most notable difference between $X_{org, IEC}$ values in this study and $X_{org, \kappa}$ is the particle size regime over which the measurements are made. It is possible that $X_{org, IEC}$ is strongly influenced by particles of much larger diameters, that are expected to be significantly less enriched in organic material, as noted by Quinn et al., compared with the 50 nm particles analyzed for determinations of $X_{org, \kappa}$. To illustrate this point, the size-fractionated aerosol mass distribution from representative marine SSA generated by Prather et al.[41] is shown in Fig. 4.4B. As shown, the mass distribution is dominated (more than 95%) by particles > 250 nm in diameter. Given that the particle size of interest (50 nm) in this study accounts for less than 24% of the SSA mass that is less than 250 nm, this could explain some fraction of the disagreement in magnitude. The approach presented here demonstrates the utility of the SR-CCN analysis to effectively extract composition information for particles that double or triple in their organic volume fractions over size ranges that account for less than 5% of total aerosol mass, in the case of marine SSA.

4.5 Conclusions

Marine SSA were generated in a laboratory setting from a synthetic ocean matrix containing soluble (saccharide) and insoluble (surfactant) organic compounds to assess the role of divalent cation mediated co-adsorption of charged surfactants and saccharides in the enrichment of soluble saccharides in SSA. Measurements of aerosol hygroscopicity and saccharide concentration were made to assess the presence of organics in sub 250 nm particles. Statistically significant enrichment was observed in 50 nm particles for systems with cooperative ionic interactions (e.g., palmitate, Mg^{2+}, and glucuronic acid). The results presented here support the proposed mechanism of ion-mediated co-adsorption of soluble organics to insoluble surfactants at the ocean surface. This proposed mechanism is further supported by the critical role of the divalent metal cation which, in this study, greatly impacted the observed level of enrichment. The extent to which this mechanism contributes to the observed enhancement in saccharides in nascent SSA depends strongly on the speciation and charge of saccharides in the SSML.

4.6 Acknowledgements

4.7 References

1. Boucher, O., D. Randall, P. Artaxo, C. Bretherton, G. Feingold, P. Forster, V.M. Kerminen, Y. Kondo, H. Liao, U. Lohmann, P. Rasch, S.K. Satheesh, S. Sherwood, B. Stevens and X.Y. Zhang, *Clouds and Aerosols*, in *Climate Change 2013: The Physical Science Basis. Contribution of Working Group ! to the Fifth Assessment Report of the Intergovernmental Panel on Climate Change.* 2013: Cambridge, United Kingdom and New York, NY, USA.

2. Aitken, J., *XII.—On Dust, Fogs, and Clouds.* Earth and Environmental Science Transactions of the Royal Society of Edinburgh, 1881. **30**(01): p. 337-368.

3. Andreae, M.O. and D. Rosenfeld, *Aerosol-cloud-precipitation interactions. Part 1. The nature and sources of cloud-active aerosols.* Earth-Science Reviews, 2008. **89**(1-2): p. 13-41.

4. DeMott, P.J., T.C.J. Hill, C.S. McCluskey, K.A. Prather, D.B. Collins, R.C. Sullivan, M.J. Ruppel, R.H. Mason, V.E. Irish, T. Lee, C.Y. Hwang, T.S. Rhee, J.R. Snider, G.R. McMeeking, S. Dhaniyala, E.R. Lewis, J.J.B. Wentzell, J. Abbatt, C. Lee, C.M. Sultana, A.P. Ault, J.L. Axson, M.D. Martinez, I. Venero, G. Santos-Figueroa, M.D. Stokes, G.B. Deane, O.L. Mayol-Bracero, V.H. Grassian, T.H. Bertram, A.K. Bertram, B.F. Moffett, and G.D. Franc, *Sea spray aerosol as a unique source of ice nucleating particles.* Proceedings of the National Academy of Sciences of the United States of America, 2016. **113**(21): p. 5797-5803.

5. Schnell, R.C., *Ice Nuclei Produced by Laboratory Cultured Marine Phytoplankton.* Geophysical Research Letters, 1975. **2**(11): p. 500-502.

6. Wilson, T.W., L.A. Ladino, P.A. Alpert, M.N. Breckels, I.M. Brooks, J. Browse, S.M. Burrows, K.S. Carslaw, J.A. Huffman, C. Judd, W.P. Kilthau, R.H. Mason, G. McFiggans, L.A. Miller, J.J. Najera, E. Polishchuk, S. Rae, C.L. Schiller, M. Si, J.V. Temprado, T.F. Whale, J.P.S. Wong, O. Wurl, J.D. Yakobi-Hancock, J.P.D. Abbatt, J.Y. Aller, A.K. Bertram, D.A. Knopf, and B.J. Murray, *A marine biogenic source of atmospheric ice-nucleating particles.* Nature, 2015. **525**(7568): p. 234-+.

7. Ryder, O.S., N.R. Campbell, H. Morris, S. Forestieri, M.J. Ruppel, C. Cappa, A. Tivanski, K. Prather, and T.H. Bertram, *Role of Organic Coatings in Regulating N2O5 Reactive Uptake to Sea Spray Aerosol.* Journal of Physical Chemistry A, 2015. **119**(48): p. 11683-11692.

8. Ault, A.P., T.L. Guasco, J. Baltrusaitis, O.S. Ryder, J.V. Trueblood, D.B. Collins, M.J. Ruppel, L.A. Cuadra-Rodriguez, K.A. Prather, and V.H. Grassian, *Heterogeneous Reactivity of Nitric Acid with Nascent Sea Spray Aerosol: Large Differences Observed between and within Individual Particles.* Journal of Physical Chemistry Letters, 2014. **5**(15): p. 2493-2500.

9.   Forestieri, S.D., G.C. Cornwell, T.M. Helgestad, K.A. Moore, C. Lee, G.A. Novak, C.M. Sultana, X.F. Wang, T.H. Bertram, K.A. Prather, and C.D. Cappa, *Linking variations in sea spray aerosol particle hygroscopicity to composition during two microcosm experiments.* Atmospheric Chemistry and Physics, 2016. **16**(14): p. 9003-9018.

10.   Quinn, P.K., T.S. Bates, K.S. Schulz, D.J. Coffman, A.A. Frossard, L.M. Russell, W.C. Keene, and D.J. Kieber, *Contribution of sea surface carbon pool to organic matter enrichment in sea spray aerosol.* Nature Geoscience, 2014. **7**(3): p. 228-232.

11.   Collins, D.B., T.H. Bertram, C.M. Sultana, C. Lee, J.L. Axson, and K.A. Prather, *Phytoplankton blooms weakly influence the cloud forming ability of sea spray aerosol.* Geophysical Research Letters, 2016. **43**(18): p. 9975-9983.

12.   Aluwihare, L.I., D.J. Repeta, and R.F. Chen, *A major biopolymeric component to dissolved organic carbon in surface sea water.* Nature, 1997. **387**(6629): p. 166-169.

13.   Hoffman, E.J. and R.A. Duce, *Factors Influencing Organic-Carbon Content of Marine Aerosols - Laboratory Study.* Journal of Geophysical Research-Oceans and Atmospheres, 1976. **81**(21): p. 3667-3670.

14.   Wang, X.F., C.M. Sultana, J. Trueblood, T.C.J. Hill, F. Malfatti, C. Lee, O. Laskina, K.A. Moore, C.M. Beall, C.S. McCluskey, G.C. Cornwell, Y.Y. Zhou, J.L. Cox, M.A. Pendergraft, M.V. Santander, T.H. Bertram, C.D. Cappa, F. Azam, P.J. DeMott, V.H. Grassian, and K.A. Prather, *Microbial Control of Sea Spray Aerosol Composition: A Tale of Two Blooms.* Acs Central Science, 2015. **1**(3): p. 124-131.

15.   O'Dowd, C.D., M.C. Facchini, F. Cavalli, D. Ceburnis, M. Mircea, S. Decesari, S. Fuzzi, Y.J. Yoon, and J.P. Putaud, *Biogenically driven organic contribution to marine aerosol.* Nature, 2004. **431**(7009): p. 676-680.

16.   Langmann, B., C. Scannell, and C. O'Dowd, *New Directions: Organic matter contribution to marine aerosols and cloud condensation nuclei.* Atmospheric Environment, 2008. **42**(33): p. 7821-7822.

17.   Mochida, M., Y. Kitamori, K. Kawamura, Y. Nojiri, and K. Suzuki, *Fatty acids in the marine atmosphere: Factors governing their concentrations and evaluation of organic films on sea-salt particles.* Journal of Geophysical Research-Atmospheres, 2002. **107**(D17).

18.   Cochran, R.E., T. Jayarathne, E.A. Stone, and V.H. Grassian, *Selectivity Across the Interface: A Test of Surface Activity in the Composition of Organic-Enriched Aerosols from Bubble Bursting.* Journal of Physical Chemistry Letters, 2016. **7**(9): p. 1692-1696.

19.   Jayarathne, T., C.M. Sultana, C. Lee, F. Malfatti, J.L. Cox, M.A. Pendergraft, K.A. Moore, F. Azam, A.V. Tivanski, C.D. Cappa, T.H. Bertram, V.H. Grassian, K.A. Prather, and E.A. Stone, *Enrichment of Saccharides and Divalent Cations in Sea Spray Aerosol During Two Phytoplankton Blooms.* Environmental Science & Technology, 2016. **50**(21): p. 11511-11520.

20.   O'Dowd, C.D. and G. De Leeuw, *Marine aerosol production: a review of the current knowledge.* Philosophical Transactions of the Royal Society a-Mathematical Physical and Engineering Sciences, 2007. **365**(1856): p. 1753-1774.

21.   Keene, W.C., H. Maring, J.R. Maben, D.J. Kieber, A.A.P. Pszenny, E.E. Dahl, M.A. Izaguirre, A.J. Davis, M.S. Long, X.L. Zhou, L. Smoydzin, and R. Sander, *Chemical and physical characteristics of nascent aerosols produced by bursting bubbles at a model air-sea interface.* Journal of Geophysical Research-Atmospheres, 2007. **112**(D21).

22.   Barker, D.R. and H. Zeitlin, *Metal-Ion Concentrations in Sea-Surface Microlayer and Size-Separated Atmospheric Aerosol Samples in Hawaii.* Journal of Geophysical Research, 1972. **77**(27): p. 5076-&.

23.   Holland, H.D., *The Chemistry of Atmosphere and Oceans*. 1978: John Wiley & Sons Inc.

24.   Sarmiento, J.L., Gruber, N., *Ocean Biogeochemical Dynamics*. 2006: Princeton University Press.

25.   Lee, C., C.M. Sultana, D.B. Collins, M.V. Santander, J.L. Axson, F. Malfatti, G.C. Cornwell, J.R. Grandquist, G.B. Deane, M.D. Stokes, F. Azam, V.H. Grassian, and K.A. Prather, *Advancing Model Systems for Fundamental Laboratory Studies of Sea Spray Aerosol Using the Microbial Loop.* Journal of Physical Chemistry A, 2015. **119**(33): p. 8860-8870.

26.   McCarthy, M.D., J.I. Hedges, and R. Benner, *Major bacterial contribution to marine dissolved organic nitrogen.* Science, 1998. **281**(5374): p. 231-234.

27.   DeLong, E.F., C.M. Preston, T. Mincer, V. Rich, S.J. Hallam, N.U. Frigaard, A. Martinez, M.B. Sullivan, R. Edwards, B.R. Brito, S.W. Chisholm, and D.M. Karl, *Community genomics among stratified microbial assemblages in the ocean's interior.* Science, 2006. **311**(5760): p. 496-503.

28.   Aristegui, J., C.M. Duarte, S. Agusti, M. Doval, X.A. Alvarez-Salgado, and D.A. Hansell, *Dissolved organic carbon support of respiration in the dark ocean.* Science, 2002. **298**(5600): p. 1967-1967.

29.   Peltzer, E.T. and N.A. Hayward, *Spatial and temporal variability of total organic carbon along 140 degrees W in the equatorial Pacific Ocean in 1992.* Deep-Sea Research Part Ii-Topical Studies in Oceanography, 1996. **43**(4-6): p. 1155-1180.

30.   Copinmontegut, G. and B. Avril, *Vertical-Distribution and Temporal Variation of Dissolved Organic-Carbon in the North-Western Mediterranean-Sea.* Deep-Sea Research Part I-Oceanographic Research Papers, 1993. **40**(10): p. 1963-1972.

31.   Kirchman, D.L., Y. Suzuki, C. Garside, and H.W. Ducklow, *High Turnover Rates of Dissolved Organic-Carbon during a Spring Phytoplankton Bloom.* Nature, 1991. **352**(6336): p. 612-614.

32.   Norrman, B., U.L. Zweifel, C.S. Hopkinson, and B. Fry, *Production and Utilization of Dissolved Organic-Carbon during an Experimental Diatom Bloom.* Limnology and Oceanography, 1995. **40**(5): p. 898-907.

33.   Gobler, C.J. and S.A. Sanudo-Wilhelmy, *Cycling of colloidal organic carbon and nitrogen during an estuarine phytoplankton bloom.* Limnology and Oceanography, 2003. **48**(6): p. 2314-2320.

34.   Russell, L.M., L.N. Hawkins, A.A. Frossard, P.K. Quinn, and T.S. Bates, *Carbohydrate-like composition of submicron atmospheric particles and their production from ocean bubble bursting.* Proceedings of the National Academy of Sciences of the United States of America, 2010. **107**(15): p. 6652-6657.

35.   Benner, R., *Biogeochemistry of marine dissolved organic matter*. 2002, San Diego, CA: Academic Press.

36.   Facchini, M.C., M. Rinaldi, S. Decesari, C. Carbone, E. Finessi, M. Mircea, S. Fuzzi, D. Ceburnis, R. Flanagan, E.D. Nilsson, G. de Leeuw, M. Martino, J. Woeltjen, and C.D. O'Dowd, *Primary submicron marine aerosol dominated by insoluble organic colloids and aggregates.* Geophysical Research Letters, 2008. **35**(17).

37.   Hawkins, L.N. and L. Russell, *Polysaccharides, Proteins, and Phytoplankton Fragments: Four Chemically Distinct Types of Marine Primary Organic Aerosol Classified by Single Particle Spectromicroscopy.* Advances in Meteorology, 2010.

38.   Frossard, A.A., L.M. Russell, S.M. Burrows, S.M. Elliott, T.S. Bates, and P.K. Quinn, *Sources and composition of submicron organic mass in marine aerosol particles.* Journal of Geophysical Research-Atmospheres, 2014. **119**(22): p. 12977-13003.

39.   Crahan, K.K., D.A. Hegg, D.S. Covert, H. Jonsson, J.S. Reid, D. Khelif, and B.J. Brooks, *Speciation of organic aerosols in the tropical mid-pacific and their relationship to light scattering.* Journal of the Atmospheric Sciences, 2004. **61**(21): p. 2544-2558.

40.   Quinn, P.K., D.B. Collins, V.H. Grassian, K.A. Prather, and T.S. Bates, *Chemistry and Related Properties of Freshly Emitted Sea Spray Aerosol.* Chemical Reviews, 2015. **115**(10): p. 4383-4399.

41.   Prather, K.A., T.H. Bertram, V.H. Grassian, G.B. Deane, M.D. Stokes, P.J. DeMott, L.I. Aluwihare, B.P. Palenik, F. Azam, J.H. Seinfeld, R.C. Moffet, M.J. Molina, C.D. Cappa, F.M. Geiger, G.C. Roberts, L.M. Russell, A.P. Ault, J. Baltrusaitis, D.B. Collins, C.E. Corrigan, L.A. Cuadra-Rodriguez, C.J. Ebben, S.D. Forestieri, T.L. Guasco, S.P. Hersey, M.J. Kim, W.F. Lambert, R.L. Modini, W. Mui, B.E. Pedler, M.J. Ruppel, O.S. Ryder, N.G. Schoepp, R.C. Sullivan, and D.F. Zhao, *Bringing the ocean into the laboratory to probe the chemical complexity of sea spray aerosol.* Proceedings of the National Academy of Sciences of the United States of America, 2013. **110**(19): p. 7550-7555.

42.   Ault, A.P., R.C. Moffet, J. Baltrusaitis, D.B. Collins, M.J. Ruppel, L.A. Cuadra-Rodriguez, D.F. Zhao, T.L. Guasco, C.J. Ebben, F.M. Geiger, T.H. Bertram, K.A. Prather, and V.H. Grassian, *Size-Dependent Changes in Sea Spray Aerosol Composition*

and Properties with Different Seawater Conditions. Environmental Science & Technology, 2013. **47**(11): p. 5603-5612.

43.   Hegg, D.A., D.S. Covert, H.H. Jonsson, and R.K. Woods, *A simple relationship between cloud drop number concentration and precursor aerosol concentration for the regions of Earth's large marine stratocumulus decks.* Atmospheric Chemistry and Physics, 2012. **12**(3): p. 1229-1238.

44.   Spiel, D.E., *On the births of film drops from bubbles bursting on seawater surfaces.* Journal of Geophysical Research-Oceans, 1998. **103**(C11): p. 24907-24918.

45.   Resch, F. and G. Afeti, *Film Drop Distributions from Bubbles Bursting in Seawater.* Journal of Geophysical Research-Oceans, 1991. **96**(C6): p. 10681-10688.

46.   Wu, J., *Jet drops produced by bubbles bursting at the surface of seawater.* Journal of Physical Oceanography, 2002. **32**(11): p. 3286-3290.

47.   Fuentes, E., H. Coe, D. Green, G. de Leeuw, and G. McFiggans, *Laboratory-generated primary marine aerosol via bubble-bursting and atomization.* Atmospheric Measurement Techniques, 2010. **3**(1): p. 141-162.

48.   Collins, D.B., D.F. Zhao, M.J. Ruppel, O. Laskina, J.R. Grandquist, R.L. Modini, M.D. Stokes, L.M. Russell, T.H. Bertram, V.H. Grassian, G.B. Deane, and K.A. Prather, *Direct aerosol chemical composition measurements to evaluate the physicochemical differences between controlled sea spray aerosol generation schemes.* Atmospheric Measurement Techniques, 2014. **7**(11): p. 3667-3683.

49.   Sellegri, K., C.D. O'Dowd, Y.J. Yoon, S.G. Jennings, and G. de Leeuw, *Surfactants and submicron sea spray generation.* Journal of Geophysical Research-Atmospheres, 2006. **111**(D22).

50.   Verdugo, P., *Marine Microgels.* Annual Review of Marine Science, Vol 4, 2012. **4**: p. 375-400.

51.   Chin, W.C., M.V. Orellana, and P. Verdugo, *Spontaneous assembly of marine dissolved organic matter into polymer gels.* Nature, 1998. **391**(6667): p. 568-572.

52.   Ding, Y.X., W.C. Chin, A. Rodriguez, C.C. Hung, P.H. Santschi, and P. Verdugo, *Amphiphilic exopolymers from Sagittula stellata induce DOM self-assembly and formation of marine microgels.* Marine Chemistry, 2008. **112**(1-2): p. 11-19.

53.   Wells, M.L. and E.D. Goldberg, *Occurrence of Small Colloids in Sea-Water.* Nature, 1991. **353**(6342): p. 342-344.

54.   Orellana, M.V., P.A. Matrai, C. Leck, C.D. Rauschenberg, A.M. Lee, and E. Coz, *Marine microgels as a source of cloud condensation nuclei in the high Arctic.* Proceedings of the National Academy of Sciences of the United States of America, 2011. **108**(33): p. 13612-13617.

55. Baltar, F., J. Aristegui, E. Sintes, J.M. Gasol, T. Reinthaler, and G.J. Herndl, *Significance of non-sinking particulate organic carbon and dark CO2 fixation to heterotrophic carbon demand in the mesopelagic northeast Atlantic.* Geophysical Research Letters, 2010. **37**.

56. Burd, A.B., D.A. Hansell, D.K. Steinberg, T.R. Anderson, J. Aristegui, F. Baltar, S.R. Beaupre, K.O. Buesseler, F. DeHairs, G.A. Jackson, D.C. Kadko, R. Koppelmann, R.S. Lampitt, T. Nagata, T. Reinthaler, C. Robinson, B.H. Robison, C. Tamburini, and T. Tanaka, *Assessing the apparent imbalance between geochemical and biochemical indicators of meso- and bathypelagic biological activity: What the @$#! is wrong with present calculations of carbon budgets?* Deep-Sea Research Part Ii-Topical Studies in Oceanography, 2010. **57**(16): p. 1557-1571.

57. van Pinxteren, M., C. Muller, Y. Iinuma, C. Stolle, and H. Herrmann, *Chemical Characterization of Dissolved Organic Compounds from Coastal Sea Surface Micro layers (Baltic Sea, Germany).* Environmental Science & Technology, 2012. **46**(19): p. 10455-10462.

58. Compiano, A.M., J.C. Romano, I. Delagiraudiere, and P. Laborde, *Monosaccharide Composition of Suspended Organic Particulate Matter in Relation to Its Origin.* Oceanologica Acta, 1993. **16**(2): p. 135-144.

59. Compiano, A.M., J.C. Romano, F. Garabetian, P. Laborde, and I. Delagiraudiere, *Monosaccharide Composition of Particulate Hydrolyzable Sugar Fraction in Surface Microlayers from Brackish and Marine Waters.* Marine Chemistry, 1993. **42**(3-4): p. 237-251.

60. Haug, A. and S. Myklestad, *Polysaccharides of Marine Diatoms with Special Reference to Chaetoceros Species.* Marine Biology, 1976. **34**(3): p. 217-222.

61. Verdugo, P., A.L. Alldredge, F. Azam, D.L. Kirchman, U. Passow, and P.H. Santschi, *The oceanic gel phase: a bridge in the DOM-POM continuum.* Marine Chemistry, 2004. **92**(1-4): p. 67-85.

62. Ittekkot, V., *Variations of Dissolved Organic-Matter during a Plankton Bloom - Qualitative Aspects, Based on Sugar and Amino-Acid Analyses.* Marine Chemistry, 1982. **11**(2): p. 143-158.

63. Ittekkot, V., E.T. Degens, and U. Brockmann, *Monosaccharide Composition of Acid-Hydrolyzable Carbohydrates in Particulate Matter during a Plankton Bloom.* Limnology and Oceanography, 1982. **27**(4): p. 770-776.

64. Liebezeit, G., M. Bolter, I.F. Brown, and R. Dawson, *Dissolved Free Amino-Acids and Carbohydrates at Pycnocline Boundaries in the Sargasso Sea and Related Microbial Activity.* Oceanologica Acta, 1980. **3**(3): p. 357-362.

65. Pakulski, J.D. and R. Benner, *An Improved Method for the Hydrolysis and Mbth Analysis of Dissolved and Particulate Carbohydrates in Seawater.* Marine Chemistry, 1992. **40**(3-4): p. 143-160.

66. Benner, R., J.D. Pakulski, M. Mccarthy, J.I. Hedges, and P.G. Hatcher, *Bulk Chemical Characteristics of Dissolved Organic-Matter in the Ocean.* Science, 1992. **255**(5051): p. 1561-1564.

67. Mopper, K., *Sugars and Uronic-Acids in Sediment and Water from Black Sea and North-Sea with Emphasis on Analytical Techniques.* Marine Chemistry, 1977. **5**(4-6): p. 585-603.

68. Sakugawa, H. and N. Handa, *Isolation and Chemical Characterization of Dissolved and Particulate Polysaccharides in Mikawa Bay.* Geochimica Et Cosmochimica Acta, 1985. **49**(5): p. 1185-1193.

69. Mopper, K., J.A. Zhou, K.S. Ramana, U. Passow, H.G. Dam, and D.T. Drapeau, *The Role of Surface-Active Carbohydrates in the Flocculation of a Diatom Bloom in a Mesocosm.* Deep-Sea Research Part Ii-Topical Studies in Oceanography, 1995. **42**(1): p. 47-73.

70. Gao, Q., C. Leck, C. Rauschenberg, and P.A. Matrai, *On the chemical dynamics of extracellular polysaccharides in the high Arctic surface microlayer.* Ocean Science, 2012. **8**(4): p. 401-418.

71. Zhou, J., K. Mopper, and U. Passow, *The role of surface-active carbohydrates in the formation of transparent exopolymer particles by bubble adsorption of seawater.* Limnology and Oceanography, 1998. **43**(8): p. 1860-1871.

72. Cochran, R.E., O. Laskina, T. Jayarathne, A. Laskin, J. Laskin, P. Lin, C. Sultana, C. Lee, K.A. Moore, C.D. Cappa, T.H. Bertram, K.A. Prather, V.H. Grassian, and E.A. Stone, *Analysis of Organic Anionic Surfactants in Fine and Coarse Fractions of Freshly Emitted Sea Spray Aerosol.* Environmental Science & Technology, 2016. **50**(5): p. 2477-2486.

73. Burrows, S.M., E. Gobrogge, L. Fu, K. Link, S.M. Elliott, H.F. Wang, and R. Walker, *OCEANFILMS-2: Representing coadsorption of saccharides in marine films and potential impacts on modeled marine aerosol chemistry.* Geophysical Research Letters, 2016. **43**(15): p. 8306-8313.

74. Burrows, S.M., O. Ogunro, A.A. Frossard, L.M. Russell, P.J. Rasch, and S.M. Elliott, *A physically based framework for modeling the organic fractionation of sea spray aerosol from bubble film Langmuir equilibria.* Atmospheric Chemistry and Physics, 2014. **14**(24): p. 13601-13629.

75. Nakahara, H., S. Lee, Y. Shoyama, and O. Shibata, *The role of palmitic acid in pulmonary surfactant systems by Langmuir monolayer study: Lipid-peptide interactions.* Soft Matter, 2011. **7**(24): p. 11351-11359.

76. Papahadjopoulos, D., *Surface Properties of Acidic Phospholipids - Interaction of Monolayers and Hydrated Liquid Crystals with Uni-and Bi-Valent Metal Ions.* Biochimica Et Biophysica Acta, 1968. **163**(2): p. 240-+.

77.   Bichsel, Y. and U. von Gunten, *Formation of iodo-trihalomethanes during disinfection and oxidation of iodide containing waters.* Environmental Science & Technology, 2000. **34**(13): p. 2784-2791.

78.   Kanicky, J.R., A.F. Poniatowski, N.R. Mehta, and D.O. Shah, *Cooperativity among molecules at interfaces in relation to various technological processes: Effect of chain length on the pK(a) of fatty acid salt solutions.* Langmuir, 2000. **16**(1): p. 172-177.

79.   Wang, H.M., D. Loganathan, and R.J. Linhardt, *Determination of the Pka of Glucuronic-Acid and the Carboxy Groups of Heparin by C-13-Nuclear-Magnetic-Resonance Spectroscopy.* Biochemical Journal, 1991. **278**: p. 689-695.

80.   Stokes, M.D., G.B. Deane, K. Prather, T.H. Bertram, M.J. Ruppel, O.S. Ryder, J.M. Brady, and D. Zhao, *A Marine Aerosol Reference Tank system as a breaking wave analogue for the production of foam and sea-spray aerosols.* Atmospheric Measurement Techniques, 2013. **6**(4): p. 1085-1094.

81.   Schill, S.R., D.B. Collins, C. Lee, H.S. Morris, G.A. Novak, K.A. Prather, P.K. Quinn, C.M. Sultana, A.V. Tivanski, K. Zimmermann, C.D. Cappa, and T.H. Bertram, *The Impact of Aerosol Particle Mixing State on the Hygroscopicity of Sea Spray Aerosol.* Acs Central Science, 2015. **1**(3): p. 132-141.

82.   Farmer, D.K., C.D. Cappa, and S.M. Kreidenweis, *Atmospheric Processes and Their Controlling Influence on Cloud Condensation Nuclei Activity.* Chemical Reviews, 2015. **115**(10): p. 4199-4217.

83.   Petters, M.D. and S.M. Kreidenweis, *A single parameter representation of hygroscopic growth and cloud condensation nucleus activity.* Atmospheric Chemistry and Physics, 2007. **7**(8): p. 1961-1971.

84.   Kreidenweis, S.M. and A. Asa-Awuku, *Aerosol Hygroscopicity: Particle Water Content and Its Role in Atmospheric Processes*, in *Treatise on Geochemistry*, H.D. Holland and K.K. Turekian, Editors. 2014, Elsevier: Oxford. p. 331-361.

85.   Sullivan, R.C., M.J.K. Moore, M.D. Petters, S.M. Kreidenweis, G.C. Roberts, and K.A. Prather, *Effect of chemical mixing state on the hygroscopicity and cloud nucleation properties of calcium mineral dust particles.* Atmospheric Chemistry and Physics, 2009. **9**(10): p. 3303-3316.

86.   Drozd, G., J. Woo, S.A.K. Hakkinen, A. Nenes, and V.F. McNeill, *Inorganic salts interact with oxalic acid in submicron particles to form material with low hygroscopicity and volatility.* Atmospheric Chemistry and Physics, 2014. **14**(10): p. 5205-5215.

87.   Zobrist, B., V. Soonsin, B.P. Luo, U.K. Krieger, C. Marcolli, T. Peter, and T. Koop, *Ultra-slow water diffusion in aqueous sucrose glasses.* Physical Chemistry Chemical Physics, 2011. **13**(8): p. 3514-3526.

88. Tong, H.J., J.P. Reid, D.L. Bones, B.P. Luo, and U.K. Krieger, *Measurements of the timescales for the mass transfer of water in glassy aerosol at low relative humidity and ambient temperature.* Atmospheric Chemistry and Physics, 2011. **11**(10): p. 4739-4754.

89. Bones, D.L., J.P. Reid, D.M. Lienhard, and U.K. Krieger, *Comparing the mechanism of water condensation and evaporation in glassy aerosol.* Proceedings of the National Academy of Sciences of the United States of America, 2012. **109**(29): p. 11613-11618.

90. Bhattacharyya, L.R., J. S., *Applications of Ion Chromatography for Pharmaceutical and Biological Products.* 2012: John Wiley & Sons, Inc.

91. Tang, C.Y., Z.S.A. Huang, and H.C. Allen, *Binding of Mg2+ and Ca2+ to Palmitic Acid and Deprotonation of the COOH Headgroup Studied by Vibrational Sum Frequency Generation Spectroscopy.* Journal of Physical Chemistry B, 2010. **114**(51): p. 17068-17076.

Chapter 5   Summary and Future Directions

5.1   Summary

This dissertation presents a body of work that encompasses the development of a new sampling methodology for SR-CCN aerosol hygroscopicity measurements and the utility for SR-CCN measurements to extract composition and mixing state information on small (< 50 nm) aerosols.

Chapter 2 introduced the development of a basis set analysis whereby direct (SR-CCN) measurements of aerosol hygroscopicity were used to quantify chemical heterogeneity with the hygroscopicity parameter, κ. This is an important shift from the current standard technique, which assigns one population average value for what is commonly a very diverse and often externally mixed sample. This analysis also provides a benchmark for handling externally mixed aerosols, which were previously excluded in the κ mixing rule from Petters and Kreidenweis.[1]

In Chapter 3, the κ basis set analysis was validated and constrained with direct measurements of pure model compounds in a laboratory setting. This provided proof of concept for identification of multiple distinct populations (externally mixed) via SR-CCN hygroscopicity measurements, and established this technique as a high throughput, robust method for extracting aerosol mixing state information for small (< 50 nm) aerosol particles in real time. The basis set analysis was applied to complex model, highly representative laboratory, and ambient field experimental data to quantify chemically complex systems by means of hygroscopicity measurements. Importantly, the impact of accounting for external mixing relative to the internal mixing assumption was assessed and showed that while the greatest disparity between the two assumptions is relevant under a narrow range of atmospheric conditions, these conditions account for a large fraction of cloud formation conditions.

While the κ basis set analysis is well suited for high-resolution SR-CCN measurements, traditional analysis can also be used to extract aerosol composition information for well

constrained systems. Chapter 4 demonstrated the utility of traditional SR-CCN measurements to identify a potential mechanism by which soluble organics are highly enriched in marine sea-spray aerosol (SSA). This addressed an important and heretofore unexplained phenomenon of an abundance of soluble organics in SSA, specifically for small (< 50 nm) particles that are exceedingly difficult to characterize, but are high impact for cloud formation and climate properties. Moreover, the SR-CCN was able to efficiently test a model derived hypothesis for molecular interaction at the sea surface microlayer with high precision and high throughput.
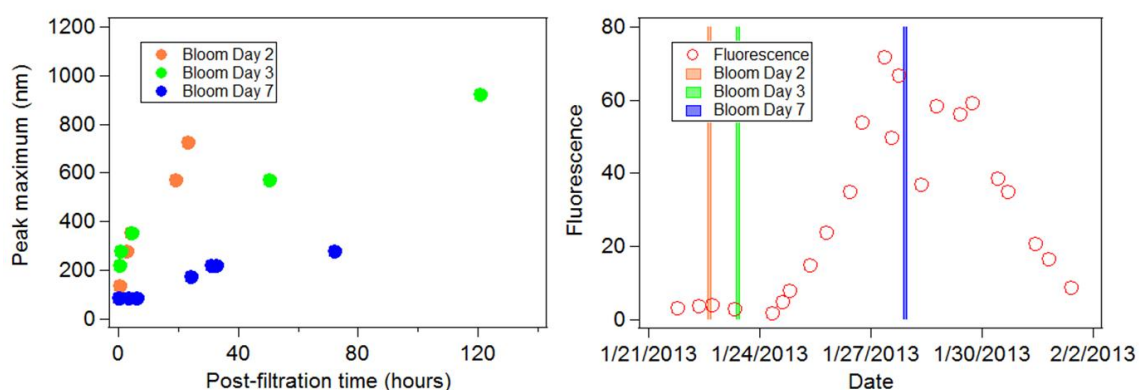
5.2   Future Directions

Having demonstrated the utility of both traditional SR-CCN and the novel κ basis set analysis methods, this dissertation concludes by presenting possible future applications of these techniques, specifically for marine relevant aerosol studies. These methods are generalizable and could also be applied to other aerosol systems, including terrestrial and/or urban populations.

5.2.1   Colloid Aggregates in Marine Environments

One outstanding question in the marine aerosol community is on the role of colloid particles in the ocean and whether they impact SSA climate properties. Spontaneous, self-assembled exudate polymer particles are known to be present in ocean environments, resultant from biological activity, and span a size range of several nanometers to tens of microns.[2-4] Ambient measurements of colloid particles in the ocean have been made for decades,[5] and Verdugo et al.[2] demonstrated that divalent metal cations play a critical role in the assembly of these particles, further supporting a role of biology on colloid particle production. The occurrence of these particles at sizes ideal for CCN active aerosols makes them a hot topic in the marine SSA community, as they may directly impact CCN number concentrations,[6] but could also explain the detection of almost entirely organic particles coming out of the ocean.[7-10] Despite this, the

extent to which these particles are ejected as marine SSA remains poorly understood. The statistical probability of intact colloid particles ejected as SSA via bubble bursting production mechanisms at the ocean's surface requires extremely high concentration of these particles based on the bubble size distribution characteristic of breaking waves, and these high concentrations have indeed been observed,[5] providing motivation for their study. To this end, dynamic light scattering (DLS) has been used to monitor particle size distributions of liquid samples,[11, 12] and previous experiments by Chin et al.[3] showed that filtration of ambient ocean water and subsequent monitoring via DLS observed spontaneous self-assembly and growth of what are thought to be colloid exudate particles. This experiment was replicated by the dissertation author with water collected from an induced phytoplankton bloom in a mesocosm experiment carried out in a Marine Aerosol Reference Tank (MART).[13] The collected seawater was filtered with 200 nm teflon filters and left at room temperature, from which small (< 60 μL) aliquots of the filtered sample were collected for DLS measurements where apparent self-assembly and growth of presumably colloid exudate particles were observed, as shown in Fig. 5.1A.

Figure 5.1: (left) DLS-derived peak maxima as a function of post-filtration time for 200 nm-filtered seawater from, and (right) fluorescence measurements of Chl-a as a function of time for a phytoplankton bloom mesocosm experiment carried out in a MART.

Particles grew to greater than 600 nm within 24 or 48 hours for bloom days 2 or 3, respectively, with the maximum detectable size of the DLS being 1000 nm. Figure 5.1B shows measured fluorescence from Chl-a as a function of time for the induced phytoplankton bloom in the MART system, in addition to collection periods for the DLS filtration experiments. Interestingly, the growth rate of these particles appears to be dependent on when they were extracted from the phytoplankton bloom, with earlier extractions yielding faster particle assembly, and vice versa. This could be explained in one of two ways: i) the compounds necessary for aggregate formation are consumed by the microbial loop such that by the end of the bloom there is little self-assembling material remaining, or ii) the assembly kinetics of these particles are affected by overall concentration, which also diminishes as the bloom proceeds, meaning the growth rate is dependent on concentration more than on composition.

This represents a potential application for high-resolution SR-CCN measurements of aerosols generated from this system, since the occurrence of colloid particles as SSA would be detected with SR-CCN hygroscopicity measurements. Because these colloids are composed of saturated hydrocarbon polymers, their corresponding hygroscopicty as SSA is expected to be dramatically less than salt-like aerosols from the same population. In this manner, the SR-CCN can be used to identify the occurrence of the new population (mixing state) as the aggregates self-assemble and, to some extent, their composition given the inherent differences in hygroscopicity. It is important to note that while occurrence of self-assembled particles from filtered seawater has been observed via DLS, it is unclear whether upon aerosolization these particles are ejected intact as colloid SSA particles. This represents a complex, outstanding question about the transfer properties from bulk to aerosol phase, and highlights the potential contributions of high-resolution SR-CCN analysis to this field.

5.2.2   A Miniature Marine Aerosol Reference Tank (miniMART)

Recent studies have shown that traditional aerosol generation techniques for laboratory studies do not adequately reproduce SSA with the correct chemicophysical properties.[14] Because the production mechanism relies on bubbles bursting at the surface of the ocean, the ability to reproduce sea-spray in the lab is tied to the ability to correctly reproduce the bubble size distribution in the bulk.[10, 13, 15, 16] This dissertation presented data collected with a MART, which is a novel aerosol generation system that accurately reproduces the bubble size distribution of the ambient ocean and the corresponding SSA size distribution.[13] One artifact of using the MART is that the production mechanism specific to this system is harsh on biologically active samples. This limits the application of the MART with biologically productive systems and is problematic for assessing the climate impacts of chemical species, i.e. for those present in the early stages of a phytoplankton bloom.

To account for this, a miniature Marine Aerosol Reference Tank (miniMART) was developed[17] and was designed with a different generation scheme, which allowed a more gentle handling of biological samples. The miniMART uses a rotating water wheel that gently creates a very small plunging sheet to produce representative SSA, whereas the MART circulated the sample through a centrifugal pump. This allows for the study of biological systems early in the microbial loop, but severely limits the available number concentration of generated SSA due to the small size of the tank and the generated plunging sheet. For example, the submicron- and supermicron-sized particle number in MART were approximately 5000 and 345 cm^{-3} at a flow rate of 3 slpm,[17] while for the miniMART these numbers were approximately 90 and 60 cm^{-3} at a flow rate of 2.6 slpm, necessitating longer sample integration times for some instrumentation.

The reduced particle number concentrations in miniMART, in comparison to MART, can present a challenge for particle instrumentation (e.g. SR-CCN measurements). For instruments where the noise is dominated by counting statistics, signal-to-noise ratios can theoretically be

improved by signal averaging. An important consideration, with respect to miniMART, is the stability of the particle source and air delivery as a function of instrument integration time. Allan variance was used by the dissertation author to determine the timescale for which signal averaging in the miniMART will no longer improve instrument signal-to-noise ratio.[18] Twelve continuous hours of 1 s CPC measurements from a miniMART containing a 500 mM NaCl solution are shown in Fig. 5.2A. The Allan variance was calculated from these data and is shown in Fig. 5.2B. The analysis indicates that improvement in signal-to-noise ratio will be achieved for averaging times up to 100 s, after which further signal averaging will result in a decrease in the signal-to-noise ratio. Further work is required to establish the experimental factors that control this optimum averaging time.
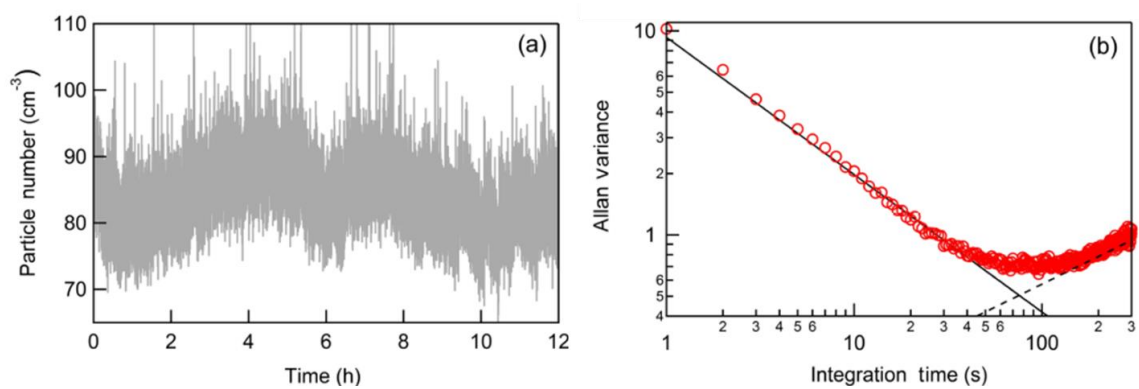
Figure 5.2: (left) Twelve continuous hours of 1 s CPC measurements from a miniMART containing a 500 mM NaCl solution and (right) corresponding Allan Variance as a function of integration time.

The development of the miniMART and characterization of its application for number-counting experiments, such as the SR-CCN, represent important advances for extending the application of hygroscopicity measurements to characterize aerosol particles, specifically SSA resulting from early phytoplankton bloom conditions. The utility of SR-CCN measurements for extracting mixing state and composition information from early-bloom SSA makes the

miniMART well-suited for laboratory mesocosm experiments, particularly where small volumes are ideal.

5.3 Acknowledgements

5.4 References

1.   Petters, M.D. and S.M. Kreidenweis, *A single parameter representation of hygroscopic growth and cloud condensation nucleus activity.* Atmospheric Chemistry and Physics, 2007. **7**(8): p. 1961-1971.

2.   Verdugo, P., *Marine Microgels.* Annual Review of Marine Science, Vol 4, 2012. **4**: p. 375-400.

3.   Chin, W.C., M.V. Orellana, and P. Verdugo, *Spontaneous assembly of marine dissolved organic matter into polymer gels.* Nature, 1998. **391**(6667): p. 568-572.

4.   Facchini, M.C., M. Rinaldi, S. Decesari, C. Carbone, E. Finessi, M. Mircea, S. Fuzzi, D. Ceburnis, R. Flanagan, E.D. Nilsson, G. de Leeuw, M. Martino, J. Woeltjen, and C.D. O'Dowd, *Primary submicron marine aerosol dominated by insoluble organic colloids and aggregates.* Geophysical Research Letters, 2008. **35**(17).

5.   Wells, M.L. and E.D. Goldberg, *Occurrence of Small Colloids in Sea-Water.* Nature, 1991. **353**(6342): p. 342-344.

6.   Orellana, M.V., P.A. Matrai, C. Leck, C.D. Rauschenberg, A.M. Lee, and E. Coz, *Marine microgels as a source of cloud condensation nuclei in the high Arctic.* Proceedings of the National Academy of Sciences of the United States of America, 2011. **108**(33): p. 13612-13617.

7.   Russell, L.M., L.N. Hawkins, A.A. Frossard, P.K. Quinn, and T.S. Bates, *Carbohydrate-like composition of submicron atmospheric particles and their production from ocean*

bubble bursting. Proceedings of the National Academy of Sciences of the United States of America, 2010. **107**(15): p. 6652-6657.

8. Quinn, P.K., T.S. Bates, K.S. Schulz, D.J. Coffman, A.A. Frossard, L.M. Russell, W.C. Keene, and D.J. Kieber, *Contribution of sea surface carbon pool to organic matter enrichment in sea spray aerosol.* Nature Geoscience, 2014. **7**(3): p. 228-232.

9. Ault, A.P., R.C. Moffet, J. Baltrusaitis, D.B. Collins, M.J. Ruppel, L.A. Cuadra-Rodriguez, D.F. Zhao, T.L. Guasco, C.J. Ebben, F.M. Geiger, T.H. Bertram, K.A. Prather, and V.H. Grassian, *Size-Dependent Changes in Sea Spray Aerosol Composition and Properties with Different Seawater Conditions.* Environmental Science & Technology, 2013. **47**(11): p. 5603-5612.

10. Prather, K.A., T.H. Bertram, V.H. Grassian, G.B. Deane, M.D. Stokes, P.J. DeMott, L.I. Aluwihare, B.P. Palenik, F. Azam, J.H. Seinfeld, R.C. Moffet, M.J. Molina, C.D. Cappa, F.M. Geiger, G.C. Roberts, L.M. Russell, A.P. Ault, J. Baltrusaitis, D.B. Collins, C.E. Corrigan, L.A. Cuadra-Rodriguez, C.J. Ebben, S.D. Forestieri, T.L. Guasco, S.P. Hersey, M.J. Kim, W.F. Lambert, R.L. Modini, W. Mui, B.E. Pedler, M.J. Ruppel, O.S. Ryder, N.G. Schoepp, R.C. Sullivan, and D.F. Zhao, *Bringing the ocean into the laboratory to probe the chemical complexity of sea spray aerosol.* Proceedings of the National Academy of Sciences of the United States of America, 2013. **110**(19): p. 7550-7555.

11. Stramski, D., M. Sedlak, D. Tsai, E.J. Amis, and D.A. Kiefer, *Dynamic Light-Scattering by Cultures of Heterotrophic Marine-Bacteria.* Ocean Optics Xi, 1992. **1750**: p. 73-85.

12. Stramski, D. and M. Sedlak, *Application of Dynamic Light-Scattering to the Study of Small Marine Particles.* Applied Optics, 1994. **33**(21): p. 4825-+.

13. Stokes, M.D., G.B. Deane, K. Prather, T.H. Bertram, M.J. Ruppel, O.S. Ryder, J.M. Brady, and D. Zhao, *A Marine Aerosol Reference Tank system as a breaking wave analogue for the production of foam and sea-spray aerosols.* Atmospheric Measurement Techniques, 2013. **6**(4): p. 1085-1094.

14. Collins, D.B., D.F. Zhao, M.J. Ruppel, O. Laskina, J.R. Grandquist, R.L. Modini, M.D. Stokes, L.M. Russell, T.H. Bertram, V.H. Grassian, G.B. Deane, and K.A. Prather, *Direct aerosol chemical composition measurements to evaluate the physicochemical differences between controlled sea spray aerosol generation schemes.* Atmospheric Measurement Techniques, 2014. **7**(11): p. 3667-3683.

15. Collins, D.B., D.F. Zhao, M.J. Ruppel, G.B. Deane, M.D. Stokes, P.J. DeMott, C. Lee, R.L. Modini, L.M. Russell, and K.A. Prather, *Evaluating the Properties of Sea Spray Aerosols Produced in the Laboratory: Comparisons with Controlled Breaking Waves.* Nucleation and Atmospheric Aerosols, 2013. **1527**: p. 551-554.

16. Quinn, P.K., D.B. Collins, V.H. Grassian, K.A. Prather, and T.S. Bates, *Chemistry and Related Properties of Freshly Emitted Sea Spray Aerosol.* Chemical Reviews, 2015. **115**(10): p. 4383-4399.

17.   Stokes, M.D., G. Deane, D.B. Collins, C. Cappa, T. Bertram, A. Dommer, S. Schill, S. Forestieri, and M. Survilo, *A miniature Marine Aerosol Reference Tank (miniMART) as a compact breaking wave analogue.* Atmospheric Measurement Techniques, 2016. **9**(9): p. 4257-4267.

18.   Werle, P., R. Mucke, and F. Slemr, *The Limits of Signal Averaging in Atmospheric Trace-Gas Monitoring by Tunable Diode-Laser Absorption-Spectroscopy (Tdlas).* Applied Physics B-Photophysics and Laser Chemistry, 1993. **57**(2): p. 131-139.